1994

An experimental evaluation of capillary tube-suction line heat exchanger performance with alternative refrigerants HFC-134a and HFC-152a

Robert Rudolph Bittle
Iowa State University

INFORMATION TO USERS

This manuscript has been reproduced from the microfilm master. UMI films the text directly from the original or copy submitted. Thus, some thesis and dissertation copies are in typewriter face, while others may be from any type of computer printer.

The quality of this reproduction is dependent upon the quality of the copy submitted. Broken or indistinct print, colored or poor quality illustrations and photographs, print bleedthrough, substandard margins, and improper alignment can adversely affect reproduction.

In the unlikely event that the author did not send UMI a complete manuscript and there are missing pages, these will be noted. Also, if unauthorized copyright material had to be removed, a note will indicate the deletion.

Oversize materials (e.g., maps, drawings, charts) are reproduced by sectioning the original, beginning at the upper left-hand corner and continuing from left to right in equal sections with small overlaps. Each original is also photographed in one exposure and is included in reduced form at the back of the book.

Photographs included in the original manuscript have been reproduced xerographically in this copy. Higher quality 6" x 9" black and white photographic prints are available for any photographs or illustrations appearing in this copy for an additional charge. Contact UMI directly to order.

UMI

A Bell & Howell Information Company
300 North Zeeb Road, Ann Arbor MI 48106-1346 USA
313/761-4700 800/521-0600

An experimental evaluation of capillary tube-suction line heat exchanger performance with alternative refrigerants HFC-134a and HFC-152a

by

Robert Rudolph Bittle

A Dissertation Submitted to the

Graduate Faculty in Partial Fulfillment of the

Requirements for the Degree of

DOCTOR OF PHILOSOPHY

Department: Mechanical Engineering
Major: Mechanical Engineering

Approved:

Signature was redacted for privacy.

In Charge of Major Work

Signature was redacted for privacy.

For the Major Department

Signature was redacted for privacy.

For the Graduate College

Iowa State University
Ames, Iowa

1994

TABLE OF CONTENTS

LIST OF TABLES

LIST OF FIGURES

NOMENCLATURE

A	flow area
$A_{h/t}$	heat transfer area
Cp_f	liquid phase specific heat
Cp_g	vapor phase specific heat
C_r	ratio of suction line specific heat to capillary tube specific heat
dc	capillary tube inner diameter (in)
df_{error}	degrees of freedom for error
ds	suction line inner diameter (in)
DTsc	capillary tube inlet subcooled level (°F)
DTsh	suction line inlet superheat level (°F)
EFFsc	effective subcooling (°F)
f	friction factor
h_{fg}	enthalpy of vaporization
k	thermal conductivity
Lc	capillary tube-suction line heat exchanger length (in)
Lhx	heat exchanger length (in)
Linlet	capillary tube adiabatic entrance length (in)
LP	evaporator pressure (psia)
$\dot{m}$	mass flow rate (lbm/hr)
Nu	Nusselt number
NTU	number of transfer units
%oil	oil concentration (by mass)
P	pressure

Pr	Prandtl number
Q	quality (%)
$\dot{q}_{gross}$	power supplied to the pre-heater
$\dot{q}_{loss}$	heat loss from the refrigerant flow between the preheater inlet and the capillary tube inlet
$\dot{q}_{net}$	net heat transfer rate to the refrigerant flow
Re	flow Reynolds number
std err pred	standard error of the predicted mean
t	t statistic
T_{c1}	capillary tube inlet temperature
Tcond	condenser temperature (°F)
T_{evap}	saturation temperature corresponding to the evaporator pressure
$T_{prehtr\text{-}in}$	refrigerant temperature entering the preheater
T_{sat}	saturation temperature
T_{s1}	suction line inlet temperature (°F)
T_{s2}	suction line outlet temperature
$T_{suct\text{-}avg}$	average suction line vapor temperature
$\overline{V}$	average flow velocity
x	thermodynamic equilibrium quality (mass fraction)

Greek symbols

ε	heat exchanger effectiveness
μ	viscosity
ρ	density

ACKNOWLEDGMENTS

First, I would like to acknowledge Dr. Michael B. Pate for his patience and guidance throughout my degree program. A significant portion of this study was sponsored by Admiral Company/Division of Maytag Corporation, and the advice of their engineering staff is gratefully acknowledged.

Throughout this effort, Dr. W. Robert Stephenson has been very generous with his time, and I extend to him my sincerest gratitude. Also, Dr. Robert C. Brown has been very supportive, and his time and advice are appreciated. Thanks also to my colleagues in the Heat Transfer Laboratory who have made my stay at Iowa State University more enjoyable than they could ever know.

My family has been a very strong force behind my work. My parents and grandparents were very supportive of my decision to return to school, and I felt that support always. My children Joshua Andrew, Elspeth Louise, and James Robert gave me encouragement each day, through the smiles on their faces, that they will someday understand. And finally, my wife and best friend, Becky Ann, has made this effort possible through her love and support.

ABSTRACT

Worldwide environmental concerns have resulted in mandates that CFC refrigerants be replaced with alternative refrigerants. The most common refrigerant used in household refrigerators is CFC-12, and alternative refrigerants HFC-134a and HFC-152a are potential replacements.

The capillary tube is the predominant expansion device found in household refrigerators. It is usually soldered to the suction line for three to five feet of length, thus, creating a simple counter-flow heat exchanger. Heat exchanger performance is characterized by both the refrigerant mass flow rate and a heat transfer effect, commonly referred to as effective subcooling.

Capillary tube-suction line heat exchanger performance was experimentally evaluated with alternative refrigerants HFC-134a and HFC-152a. In accomplishing this task, a test facility simulating a household refrigerator was designed and constructed with the capability of controlling the appropriate operating conditions. Next, efficient experimental test plans were designed using statistical methods. Performance databases were then obtained with each refrigerant of an applicable range of heat exchanger geometries and operating conditions including; capillary tube inner diameter (0.026 to 0.031 in), capillary tube length (96 to 130 in), heat exchanger length (30 to 70 in), condenser temperature (85 to 132 °F), evaporator pressure (16 to 26 psia), capillary tube inlet condition (15 °F subcooled to 5% quality), and oil concentration level (0% to 3%).

Measured mass flow rate ranged between 6 and 21 lbm/hr. Variables having the greatest effect on mass flow rate included condenser temperature,

capillary tube inner diameter, capillary tube length, and inlet quality level. Measured effective subcooling level ranged between 25 and 60 °F. Variables having the greatest effect on effective subcooling level included condenser temperature, heat exchanger length, suction line diameter, and suction inlet temperature.

Heat exchanger performance prediction equations were developed for HFC-134a and HFC-152a, which were based on their respective databases. A general performance prediction procedure was also developed based on the HFC-134a results, and by considering the fundamental processes affecting mass flow rate and effective subcooling. Using the procedure, measured performance was successfully predicted for HFC-152a and CFC-12.

CHAPTER 1. INTRODUCTION

Background

In response to large scale reductions in CFC's as called for in the Montreal Protocol (1987) and current environmental politics, many refrigeration equipment manufacturers are replacing CFC refrigerants with alternative refrigerants that have no potential impact on the stratospheric ozone level. The most common refrigerant used in household refrigerators is CFC-12, and alternative refrigerants HFC-134a and HFC-152a are potential replacements.

Refrigeration equipment design practices have evolved over time. These are based on past R&D efforts using the common refrigerants of the time, including CFC-12. As the next generation of equipment is designed for use with the alternative refrigerants, existing design practices have to be re-evaluated. In response, industry wide R&D efforts have commenced to develop the necessary databases to properly assess system performance, as well as component performance, with the alternative refrigerants.

A critical component in household refrigerators is the capillary tube-suction line heat exchanger. Refrigerator system performance models used in the design process require accurate component models. The current ASHRAE sanctioned procedure for predicting capillary tube-suction line heat exchanger performance is applicable to CFC-12 and HCFC-22. Alternative refrigerants have different thermodynamic and thermophysical properties, so the ASHRAE design procedures do not apply. Therefore, capillary tube-suction line heat exchanger performance prediction methods are needed that are applicable to the alternative refrigerants.

Capillary tube description

In refrigeration system terminology, a capillary tube refers to a length of drawn tubing with an inner diameter range of 0.025 to 0.090 in. The term "capillary tube" is actually a misnomer since the bore is much too large to allow capillary action (Stoeker, 1958). A capillary tube is the predominant expansion device found in household refrigerators, freezers, and many window air conditioners. Its major advantage over more complicated expansion devices is its simplicity. In addition, a capillary tube allows the system pressure to equalize during the "off cycle", thus allowing the compressor to be driven by a small, low torque motor (Staebler, 1948).

In a refrigeration unit, the capillary tube connects the condenser and evaporator (Figure 1.1). As the expansion device, its diameter and length combination provides the necessary system restriction for operating at design conditions. Refrigerant usually enters the capillary tube as a subcooled liquid, and initially experiences a constant pressure drop in the tube due to friction alone. After the pressure falls below the saturation pressure, the liquid refrigerant will begin to vaporize, or flash. The location corresponding to initial vaporization is commonly called the flash point.

Downstream of the flash point, the pressure drop increases rapidly as a result of both two-phase friction and vapor acceleration. Accompanying the rapid pressure drop is a corresponding reduction in saturation temperature, and therefore, a reduction in refrigerant temperature. As the pressure continues to drop, liquid refrigerant continues to flash, the refrigerant temperature continues

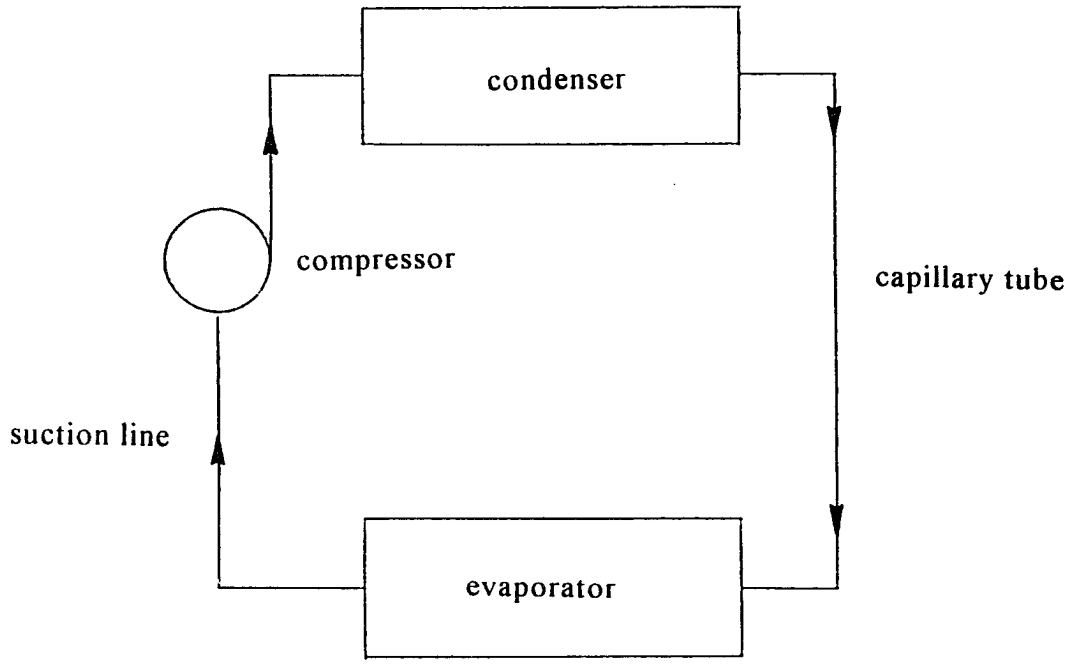

Figure 1.1: Capillary tube position in a refrigeration system

to decrease, and the quality continues to increase. A choked flow condition generally exists at the exit.

A typical pressure and temperature profile through an adiabatic capillary tube is given in Figure 1.2. In a adiabatic capillary tube, the refrigerant temperature remains constant until the flash point is reached. For the case shown, the flash point occurs at a pressure below the saturation pressure. Downstream of the saturation pressure point and prior to the flash point, superheated liquid exists at a pressure less than saturation. This is a non-equilibrium, or metastable, condition, and only occurs in adiabatic capillary tubes (Pate and Tree, 1984a).

Refrigeration system design parameters include the evaporator capacity and the evaporating and condensing temperatures. The key to a successful system design is sizing the capillary tube properly (diameter and length) so that system balance is achieved at design conditions. System balance simply refers to the "steady" condition that exists when the compressor mass flow rate equals the capillary tube mass flow rate.

Even though sized for a specified design condition, a capillary tube has self-compensating characteristics that allow the system to rebalance during off-design operation. As an example, consider a household refrigerator operating in a kitchen where the ambient air temperature remains relatively constant. If several gallons of warm milk are suddenly placed inside the refrigerator, the air temperature inside the refrigerator will increase. This warmer air passing over the evaporator will cause the pressure and temperature of the refrigerant in the evaporator to increase. The increase in evaporator pressure will result in the compressor drawing more refrigerant out of the evaporator than can be supplied by the capillary tube. An unbalanced condition exists, and the resulting

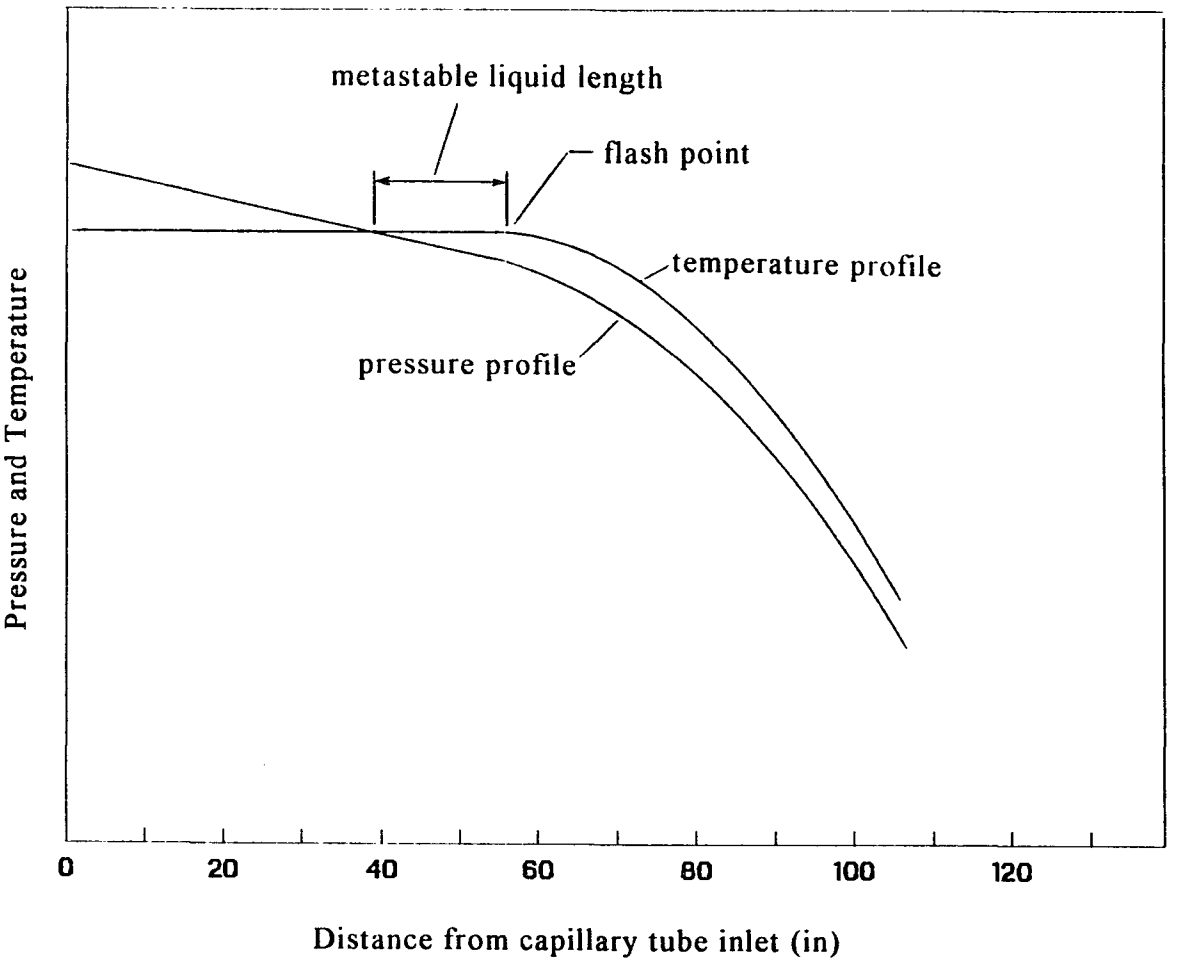

Figure 1.2: Pressure and temperature profile through an adiabatic capillary tube

refrigerant accumulation in the condenser causes an increase in the condenser pressure. This, in turn, forces more refrigerant through the capillary tube, and the system condition moves back toward a balanced point. Over time, the milk's temperature decreases, and the system returns to the design condition.

Capillary tube-suction line heat exchangers

In the household refrigerator application, the capillary tube is soldered on to three to five feet of the compressor suction line, thereby creating a simple counter-flow heat exchanger (Figure 1.3). This has two main advantages over an adiabatic configuration. First, heat transfer from the capillary tube increases the refrigeration capacity of the system for a given mass flow rate. Second, heat transfer to the suction line prevents slugging of the system compressor. These effects are illustrated in the P-h diagram shown in Figure 1.4 for an ideal refrigeration cycle.

Capillary tube-suction line heat exchanger performance is characterized by both the refrigerant mass flow rate and a heat transfer effect, commonly referred to as effective subcooling. Effective subcooling, EFFsc, is a calculated quantity based on the heat transferred from the capillary tube flow to the suction line flow and is given by

$$EFFsc = \frac{Cp_{gs}}{Cp_{fc}} \cdot (T_{s2} - T_{s1}) \qquad (1.1)$$

In Equation 1.1, Cp_{gs} is the suction line vapor specific heat at the vapor pressure and average vapor temperature, Cp_{fc} is the capillary tube liquid specific heat at

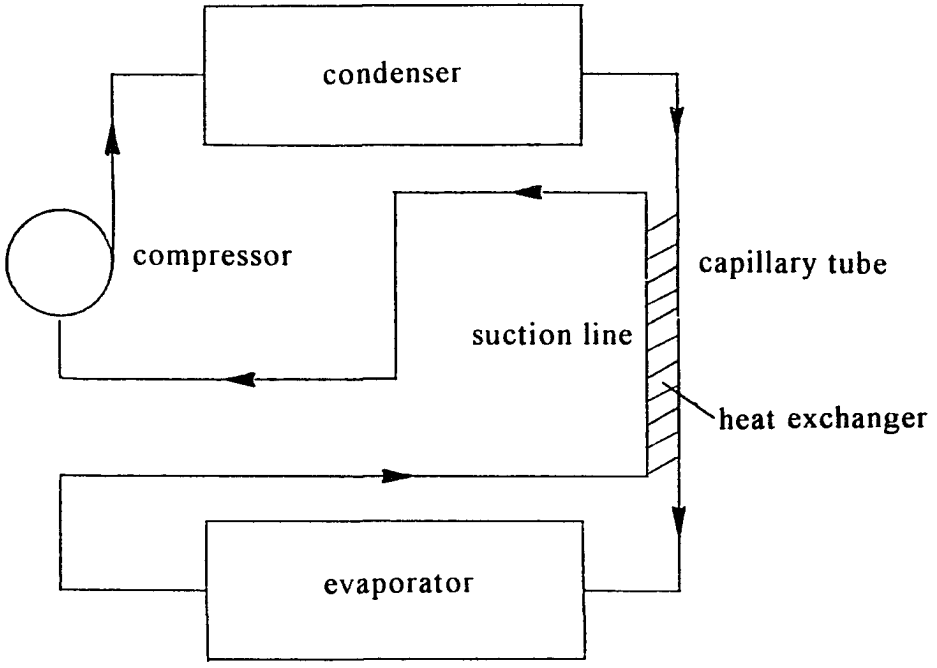

Figure 1.3: Capillary tube-suction line heat exchanger arrangement

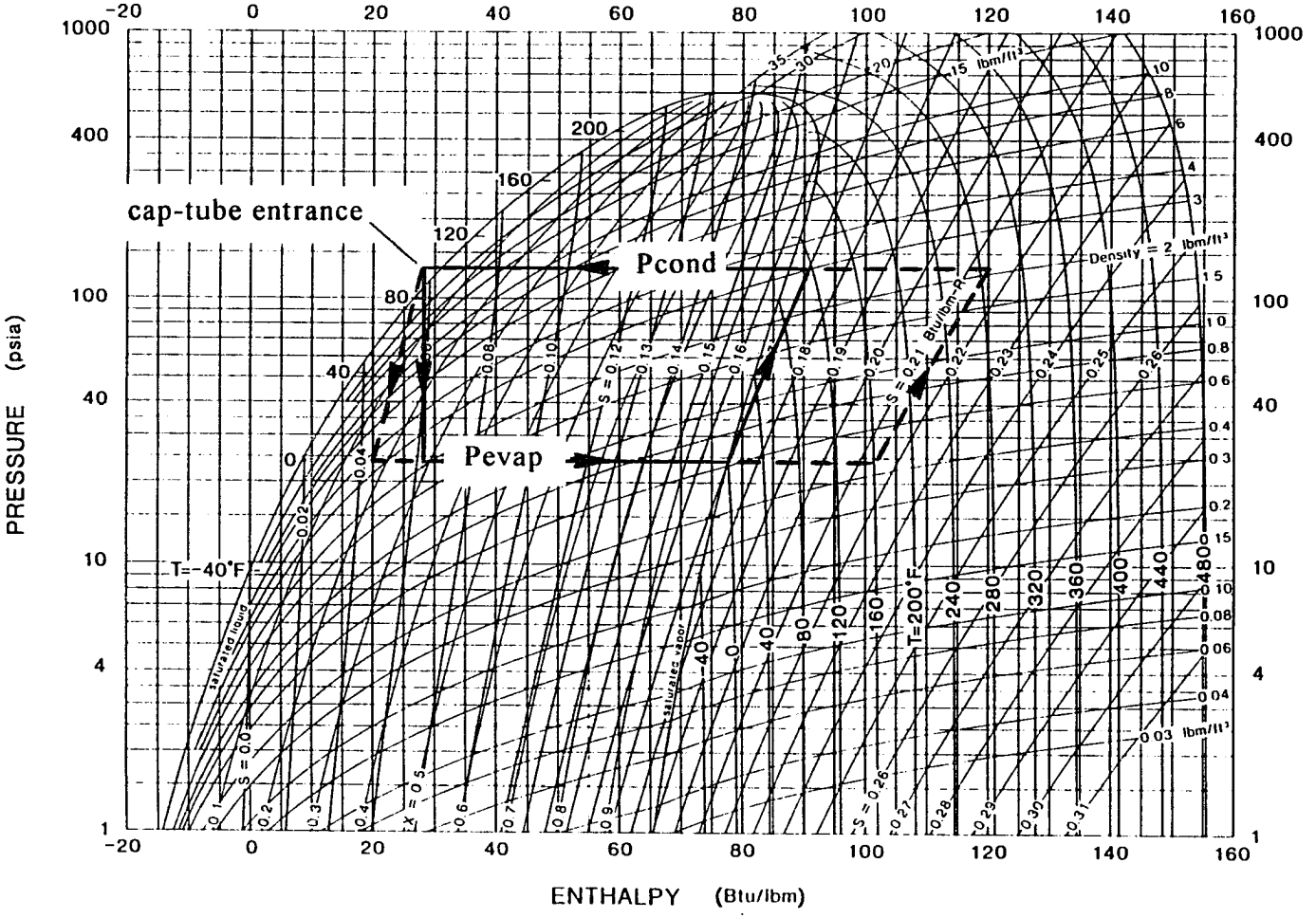

——— w/o suction line heat exchange — — — — — w/ suction line heat exchange

Figure 1.4: P-h diagram illustrating the effect of the capillary tube-suction line heat exchanger (ASHRAE, 1989)

the average liquid temperature through the heat exchange region, and T_{s1} and T_{s2} are the suction line inlet and exit measured vapor temperature, respectively.

The increase in suction line vapor temperature through the heat exchanger will result in an increase in the specific volume. The compressor work required for the heat exchanger configuration is, therefore, greater than for the adiabatic configuration, since work is $\int vdP$ (ignoring kinetic and potential energy effects.) In the heat exchanger configuration, the increase in required work to the system is generally greater than the improvement in refrigeration capacity.

Based on thermodynamic performance considerations alone, refrigeration units incorporating the adiabatic capillary tube configuration would be preferable to those with the heat exchanger configuration. However, the heat exchanger improves compressor reliability, which is a more important consideration to the household appliance customer.

Literature review

During the past 50 years, adiabatic capillary tube performance has been studied extensively. A representative group of these researchers include Bolstad and Jordan (1948), Hopkins (1950), Whitesel (1957), Cooper et.al. (1957), Mikol (1963), Koizumi and Yokohama (1980), Kuijpers and Janssen (1983), Kuehl and Goldschmidt (1990,1991), Li et. al. (1990), Chen et. al. (1990), and Wijaya (1991). In comparison, capillary tube-suction line heat exchanger performance, or nonadiabatic capillary tube performance, has been the focus of only a small number of studies. This is somewhat surprising since the capillary tube-suction line heat exchanger configuration has been used in household refrigerators for

years. The research efforts that have been reported in the literature are reviewed in the following paragraphs.

Swart (1946) discussed the fundamentals of refrigeration system design using a capillary tube-suction line heat exchanger. The major emphasis of the work was to show the increase in system capacity realized by employing a heat exchanger. Experimental testing was done with CFC-12, and conducted on a capillary tube of diameter 0.042 in, lengths of 84 and 108 in, and heat exchange lengths of 60 and 72 in. No information on the test facility was given, even though measured pressure profiles along the capillary tube with and without heat exchange are shown.

Staebler (1948) also gave a thorough discussion of the basics of refrigeration system design using a capillary tube. He states that the refrigeration capacity can be increased 35% by soldering the capillary tube to the suction line, and recommends a heat exchange length of at least 48 in. Test data for CFC-12 are presented for a number of capillary tube diameters and lengths, all soldered to 48 in of suction line. Condenser temperatures were 86 and 108 °F, and evaporator temperature ranged between -15 and 30 °F. No information about the suction line or the capillary tube inlet temperature is given.

Boldstad and Jordan (1949) reported experimental results for capillary tube-suction line heat exchanger analysis. Compared to the earlier efforts, their test apparatus is described thoroughly. A relatively wide range of capillary tube diameters, lengths, and inlet pressures were tested, but only with a heat exchanger length of four feet. The suction line inlet temperature was varied, but is not reported as an independent variable. Mass flow rate data are presented in plots for the different inlet pressures, capillary tube diameters, and capillary tube

lengths. This information is useful to the designer after considering the heat exchanger effectiveness. Sample calculations are given.

Christensen and Jorgensen (1967) looked at a single heat exchanger made up of a 0.028 in diameter and 197 in long capillary tube, and a 3/8 in diameter suction line in thermal contact for 39.4 in. The only independent geometry variable was the position of the 39.4 in long heat exchange region. The independent boundary variables were condenser temperature (inlet pressure), inlet subcool level, and evaporator temperature. As in the earlier efforts, it was shown that condenser temperature (or pressure) has a large effect on mass flow rate. Also, the presence of heat exchange with the suction line increased the capillary tube mass flow rate beyond what was measured for the corresponding adiabatic case. In several of the configurations, there was very little or no effect of evaporator temperature on mass flow rate. This was contrary to the Bolstad and Jordan (1949) results which demonstrated a consistent increase in flow rate with decreasing evaporator temperature for all test configurations. A possible explanation may be that Christensen and Jorgensen used brine as the thermal contact medium, while Bolstad and Jordan soldered the capillary tube to the suction line.

Pate and Tree (1984a) reported on experimental results from a capillary tube-suction line heat exchanger study with application to household refrigerators using CFC-12. A single 0.028 in diameter capillary tube was instrumented such that pressures and wall temperatures were measured along the tube length. In addition, suction line gas temperatures were measured. Inlet conditions and suction line conditions were varied, as well as heat exchanger length and position. Using their experimental data base, Pate and Tree (1984b) also developed a two-

phase flow model for the capillary tube flow. This is the only capillary tube two-phase flow model including suction line heat exchanger that has been reported in the literature to date.

In summarizing the earlier research into capillary tube-suction line heat exchanger performance, the following points can be made. First, all previous work was done with CFC-12, which has been the common refrigerant used in household refrigerators during the past 45 years. Second, the majority of the earlier studies certainly expanded the understanding of capillary tube-suction line heat exchangers; however, the results are not readily applicable to designing refrigerators. And third, all past efforts have been limited in scope to three or four variables due to the complexity of the non-adiabatic capillary tube flow phenomenon. In reality, capillary tube-suction line heat exchanger performance is potentially affected by up to 10 design variables.

Objective and scope of the study

The primary objective of this study was to experimentally evaluate the capillary tube-suction line heat exchanger performance with alternative refrigerants HFC-134a and HFC-152a. Since capillary tube-suction line heat exchangers are used mainly in household refrigerators, a test facility was first constructed simulating this application. A database, which incorporated the effects on performance of ten heat exchanger design variables, was then obtained for each alternative refrigerant. This experimental effort greatly exceeds the scope of any previously reported study.

Based on their respective databases, heat exchanger performance prediction equations were developed for HFC-134a and HFC-152a. These can be considered design tools that are readily usable by engineers, and that are also much more accurate than the tools previously available for use.

General heat exchanger performance prediction procedures were also developed that enable performance predictions to be made for other pure HFC and CFC refrigerants. The procedures were developed by considering the fundamental processes influencing mass flow rate and effective subcooling, and involve scaling the predicted performance for HFC-134a through thermodynamic and thermophysical properties.

An underlying focus of this study was on the application of statistical methods in designing the experimental test plan. Statistical methods applied to experimentation insure balance and efficiency in testing, which, for this study, translated into a thorough coverage of all ten variable effects with a minimum of experimental test points.

Overall, this study will have a major impact on the design of the next generation of household refrigerators. The improved accuracy of the design tools will mean more efficient unit operation. The use of alternative refrigerants will mean no potential for depleting the stratospheric ozone level.

CHAPTER 2. EXPERIMENTAL TEST FACILITY

The test facility was designed to represent an actual refrigerator for the region bounded by the capillary tube inlet and exit, and the suction line inlet and exit. A one-pass-through design concept was used that has several advantages when compared to a compressor driven system. These advantages include a faster time to reach steady conditions, and better control of capillary tube inlet pressure. In addition, it has the capability of running either pure refrigerant or oil/refrigerant mixtures. A schematic of the test facility is shown in Figure 2.1.

Heat exchanger assemblies were installed into the test stand by making connections to four attachment platforms that slid laterally along a horizontal track (Figure 2.2). Upon each attachment platform was a fixed 12 in long, 3/8 in copper tube that included a pressure and fluid temperature measurement location at the test section connection point. Attachment platforms were connected to the preheater, evaporator, and condenser/receiver through 3/8 in flexible plastic tubing.

Heat exchanger assemblies were tested in a horizontal and straight configuration. A typical capillary tube connection is shown in Figure 2.3. This connection was made by first drilling a slightly oversized hole in the center of a compression fitting plug. Next, the capillary tube was pushed through the hole and soldered in place. The capillary tube/plug assembly was then screwed into the corresponding compression fitting nut fixed to the 3/8 in tubing on the attachment platform. The suction line connections were simply made using compression fitting unions.

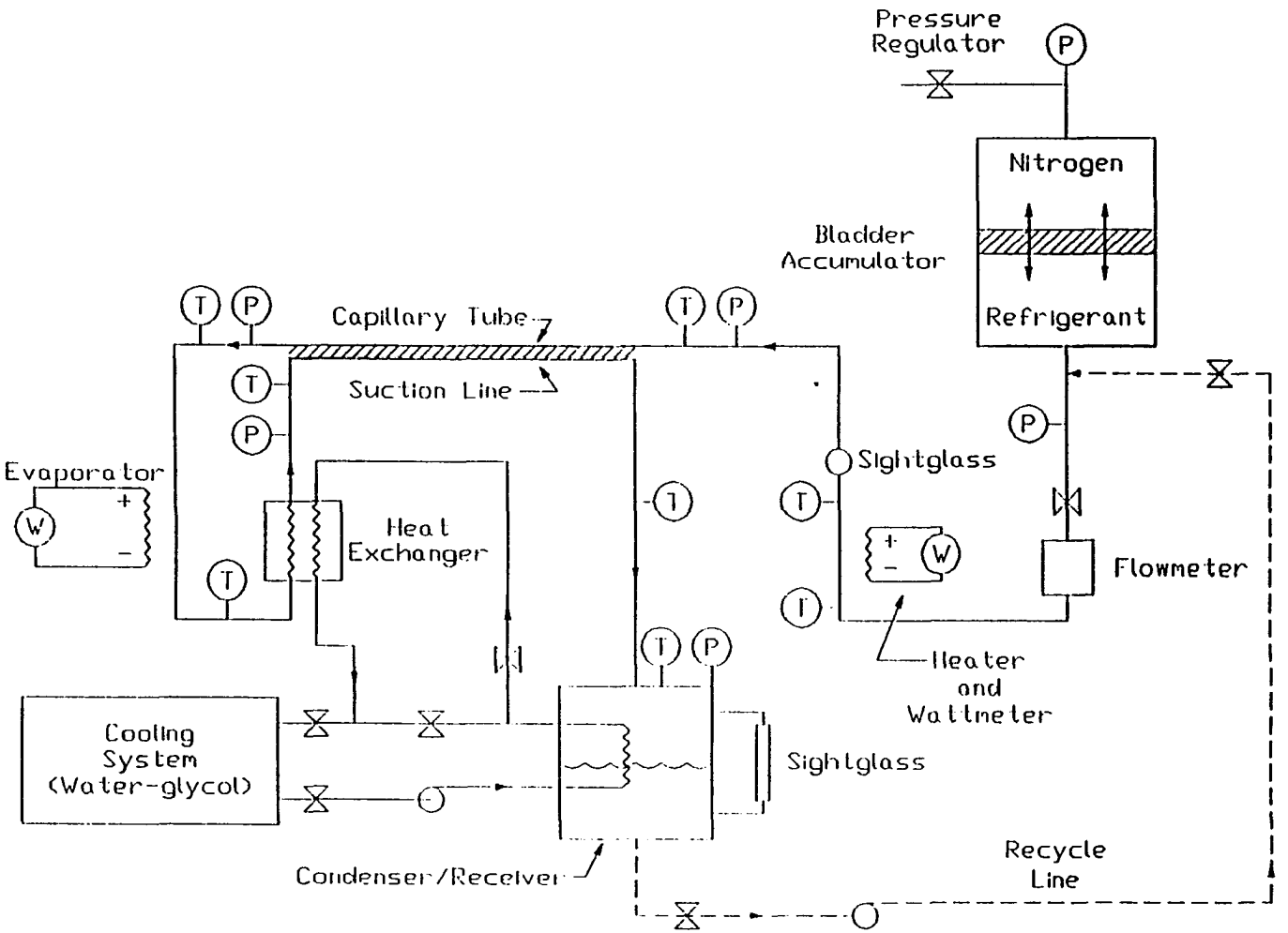

Figure 2.1: Test facility schematic

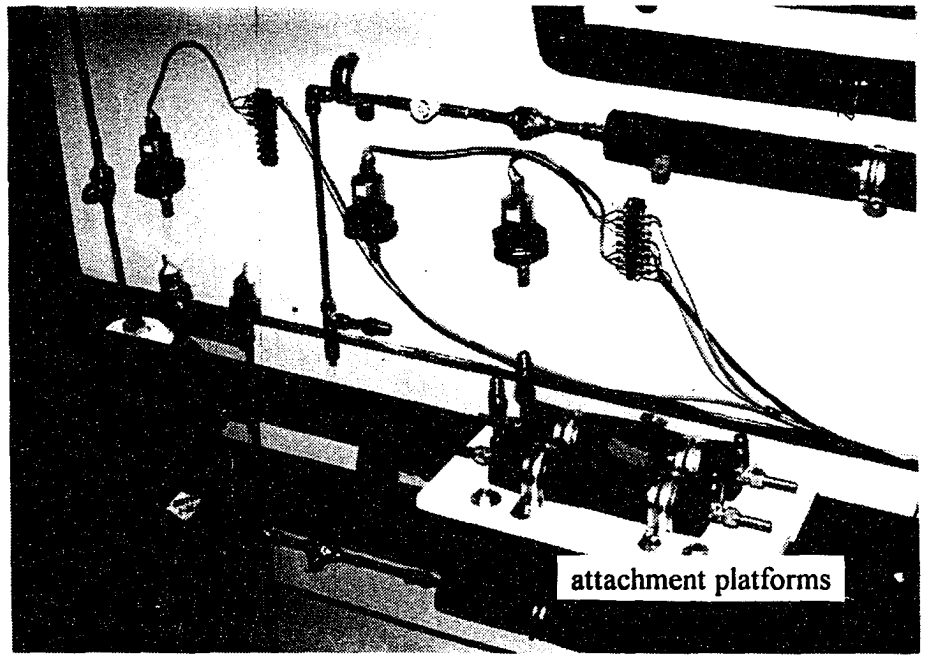

Figure 2.2: Attachment platforms

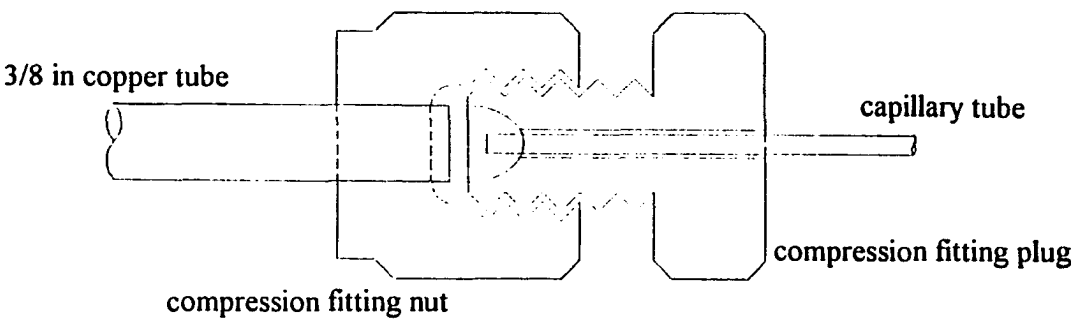

Figure 2.3: Capillary tube connection

Capillary tube inlet pressure was controlled by using a bladder accumulator. Due to compatibility considerations, the accumulator bladder material was butyl rubber during operation with both HFC-134a and HFC-152a. The bladder material was buna N during operation with CFC-12. Evaporator pressure was set in the receiver since there was a relatively small pressure drop between the capillary tube exit and the condenser/receiver for the range of flow rates tested. The operating temperature (and, therefore the saturation pressure) of the receiver was controlled by using a water-glycol supply from the I.S.U. Refrigeration Laboratory's 40 ton chiller.

The capillary tube inlet condition, either subcooled or quality, was established with an electric preheater. The preheater power level was controlled manually with a rheostat and measured with a wattmeter. The preheater consisted of electric heating tape wrapped around eight feet of 3/8 in copper tubing that had an enhanced inner surface. Inlet quality was determined from knowledge of the measured flow rate and power to the preheater. It is important to note that the capillary tube inlet temperature and pressure were measured two inches prior to the capillary tube inlet, which insured a known inlet condition.

The evaporator exit temperature was established with an electric heater of similar construction to the preheater, and also controlled manually by a rheostat. During most test point runs, the evaporator exit temperature was 50 to 70 °F above the saturation temperature associated with the evaporator pressure. The suction inlet temperature was controlled by using a refrigerant/water-glycol coaxial heat exchanger positioned between the evaporator exit and suction inlet (Figure 2.1). The water-glycol supplied to the heat exchanger was the water-glycol exiting the condenser/receiver. Refrigerant entered the heat exchanger at

the relatively warm evaporator exit temperature, and was reduced to the desired suction line inlet temperature. The suction line inlet temperature level was controlled by varying the water-glycol flow rate to the heat exchanger by using a valve located just upstream of the heat exchanger.

System temperatures were measured with type-T thermocouple probes immersed in the refrigerant flow stream at several key points in the system. Key points included the preheater inlet, capillary tube inlet, and the suction line inlet and exit. Measured thermocouple accuracy was ±0.5 °F for the test facility.

System pressures were measured with pressure transducers at the capillary tube inlet and exit, and suction line inlet. Evaporator pressure was taken as an average of measured values at the capillary tube exit and suction line inlet. The accuracy of the capillary tube inlet pressure transducer was ±0.25 psia, and the accuracy of the evaporator transducer was ±0.10 psia. A calibration check was performed on the critical instrumentation before testing commenced and midway through the testing. Pressure and temperature measurements were shown to be within specification for both calibration checks.

The mass flow rate though the capillary tube-suction line heat exchanger was measured just upstream from the preheater by using a coriolis-type true mass flow meter that was claimed accurate to within 1% by the manufacturer. A calibration check was made on the unit by using water flow rates comparable to the refrigerant flow rates tested, and confirmed the manufacturer's accuracy claim.

Since the system is a one-pass-through design, after each test it was necessary to recycle the refrigerant in the receiver back to the bladder accumulator. This was accomplished with a magnetically driven gear pump. The pump's gears

were made of Ryton which has been proven to be compatible with many refrigerants, including HFC-134a, HFC-152a, and CFC-12.

The data acquisition was controlled by a Zenith Z-386 computer and incorporates a National Instruments AT-MIO-16L board with 2 AMUX-64 multiplexer boards. During testing a data acquisition program ran continuously and collected system data every 30 seconds, providing a continuous visual update. After a test point was completed, the data was downloaded to a spreadsheet template where basic manipulations of the data were carried out and plots generated.

CHAPTER 3. EXPERIMENTAL DESIGN AND METHODOLOGY

Background

Based on previously reported research and engineering experience, it was determined that up to ten independent design variables have a potential effect on capillary tube-suction line heat exchanger performance (Table 3.1). Using more

Table 3.1: Design variables

Design Variable	Design Variable Description
Tcond	condenser temperature
dc	capillary tube i.d.
Lc	capillary tube length
Lhx	heat exchanger length
ds	suction line i.d.
Linlet	capillary tube adiabatic entrance length
DTsc, Q	capillary tube inlet condition subcooled or quality
DTsh	refrigerant vapor superheat level at the suction line inlet
LP	evaporator pressure
%oil	%oil concentration

common approaches to experimental design, the amount of testing suggested in order to examine all ten effects was overwhelming. For example, any thorough evaluation of independent variable effects on performance would have to include the investigation of combined variable effects, referred to as interaction effects.

If each of the ten variables were tested at three different levels, the combination of all possible variable levels would require a total of 3^{10}, or 59049 test points. This was obviously unrealistic, and is one reason why past efforts have been relatively limited in scope.

Considering the time and resource constraint, the need was apparent for an alternate approach to more common practices in designing the most efficient test plan. At this point, it was decided that incorporating statistical methods in the experimental design process would offer the best solution.

Statistical methods applied to experimentation are well established tools in areas where governing fundamental equations do not exist. In fields such as agriculture and biological sciences, most analyses are empirically based. Here, the attributes of statistical methods are recognized, including efficient experimental design and objective data collection methodology. However, in many engineering R&D efforts, statistical methods are not commonly employed. This is surprising since engineers frequently use empirically based design correlations.

Statistical methods benefit an experimental effort in terms of efficiency. In other words, the application of statistical methods can maximize the amount of information obtained from a minimum number of experimental test points. This improvement in efficiency comes from an investment of time in the design of the experimental plan prior to the beginning of experimentation. The approach also insures that the resulting data is easily reduced and analyzed by using common statistical analysis techniques.

Application of statistical methods also includes the incorporation of testing procedures which help insure the highest degree of quality and objectivity in the

data. Experimental error is the random "noise" in data that cannot be explained by the independent variables being varied, and is commonly characterized as precision. In order to reduce experimental error, statistical methods emphasize the importance of a methodical testing process.

Another major emphasis of statistical methods in experimental work is randomized data procurement. In many experiments, data is not taken in a random manner, but based on convenience. The advantage of randomizing the order in which test points within a test matrix are run is that the possibility of an unexplained bias occurring in the collected data is reduced. Randomized data procurement is not always the most time expedient data collection plan. However, the gain in overall data integrity far outweighs the relatively minor time sacrifice.

Two-level factorial designs

Before proceeding, some basic statistics terminology needs to be made clear. The independent heat exchanger design variables are referred to as factors, main effects, or explanatory variables. The dependent variables (mass flow rate and effective subcooling) are referred to as the response variables. An interaction between two or more factors implies that the effect of the combination of factors on the response variable is different from what would be predicted given the individual effects of each factor separately. An interaction effect can be synergistic by adding to the individual effects of the factors, or antagonistic by subtracting from the individual effects of the factors. In this study, the calculated

interaction effect on mass flow rate between the factors condenser temperature (Tcond) and capillary tube diameter (dc) was statistically significant. An exaggerated plot of this phenomenon is given in Figure 3.1. If the calculated interaction effect was insignificant, then the two lines representing the mass flow response in Figure 3.1 would be parallel. Interaction effects involving three factors or more are routinely assumed to be insignificant. In addition, these higher level interactions are very difficult to visualize or explain physically.

In applying statistical methods in this study, the core experimental test matrices were constructed based on a two-level factorial design. With a two-level factorial design, each independent variable is tested at a low and high "level" (hence, the term two-level), corresponding to the variable's specific application range. Within the two-level factorial design test matrix, testing is balanced such that each independent variable is tested at its two levels the same number of times. A full two-level factorial design test matrix would require experimental test points for all possible variable level combinations. For example, a full two-level factorial design with three variables would require 2^3, or eight experimental test points. In the case of ten variables, a full two-level factorial design would require 2^{10}, or 1024 experimental points. This large number of test points can be reduced by using a fractional factorial design approach.

Fractional factorial designs require only a fraction of the total number of test points associated with a full factorial design. A fractional design allows for a broad based experimental evaluation of a relatively large number of independent variables (such as ten), with a relatively small number of runs. Testing is still balanced, as in the full factorial design. By first taking a superficial look at the linear response relationships of all independent variables (based on the two

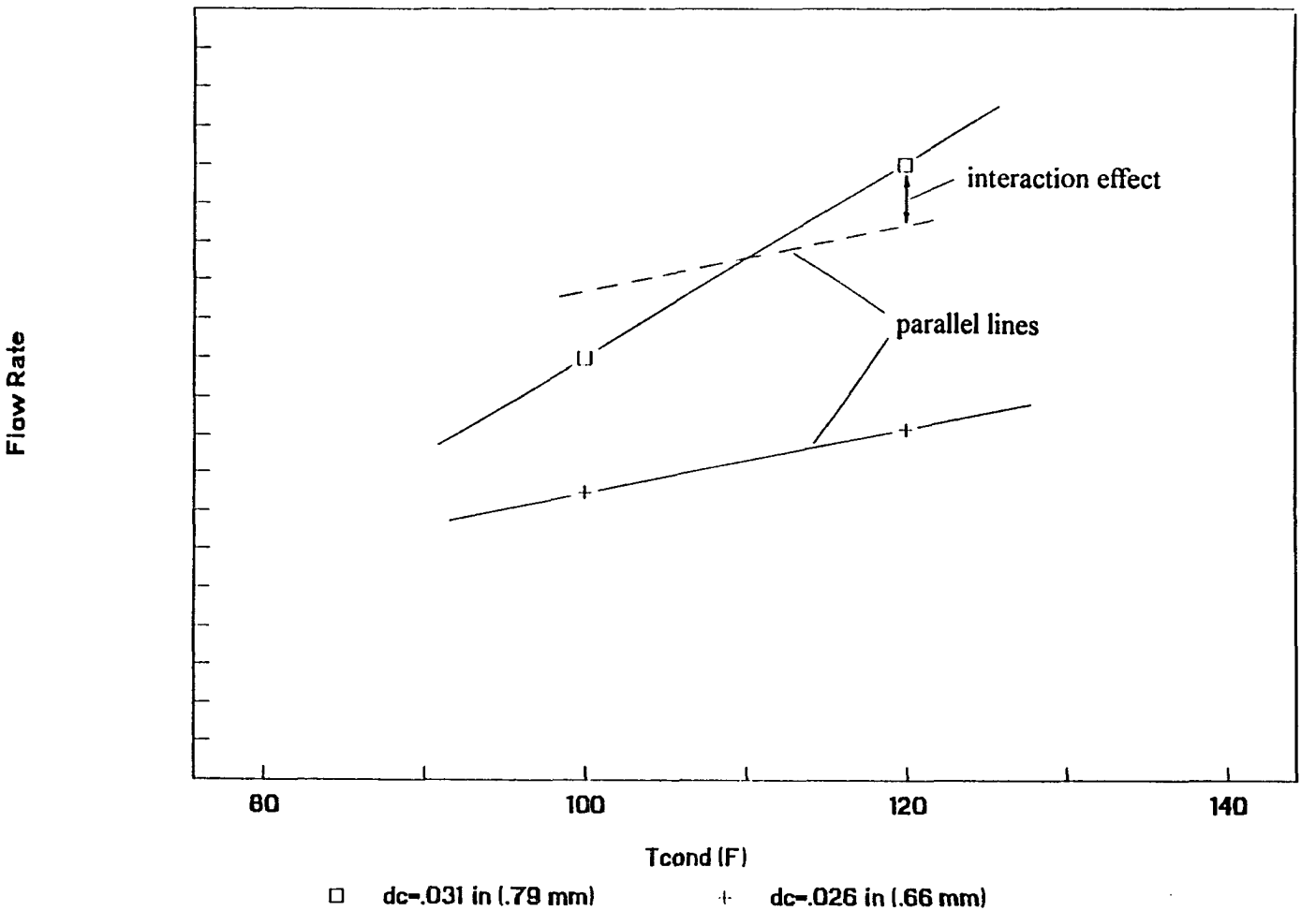

Figure 3.1: An exaggerated plot of the condenser temperature and capillary tube diameter interaction effect

levels), the variables having a major effect on the response variable can be identified. If necessary, additional experimental test points can then be focused on the important variables, while variables having little or no effect can be eliminated from the analysis. In this way, fractional factorial designs allow for a methodical, "building block" approach to data collection, and thus, are a very efficient experimental tool.

A disadvantage of fractional factorial designs is that even though interaction effects can be calculated, it may be impossible to differentiate between some of the interactions. These interactions are termed confounded. Main effects can also be confounded with interactions, so experiments are usually designed such that main effects are confounded with three factor and higher interactions (routinely assumed insignificant). These are referred to as designs with resolution IV or higher (V, VI, etc.). Both the HFC-134a and HFC-152a core test matrices are resolution IV designs. Resolution IV designs also mean that two-factor interactions will be confounded with other two-factor interactions. This could have caused problems with identifying the legitimate interaction effects. However, a general sense of the relative variable effects on performance provided some guidance in defining the test matrices, and problems were avoided. Confounding patterns for all test matrices are included in Appendix D.

Testing methodology

To achieve the highest possible level of precision, consistent testing methods were essential. Each of the heat exchanger assemblies was prepared for

testing in the same manner. Capillary tubes were rinsed internally with isopropyl alcohol twice and dried using nitrogen prior to being installed in the test stand. After installation, the evaporator and test section portion of the circuit were evacuated for a minimum of one hour to remove any non-condensable gases and moisture. All heat exchanger assemblies were thoroughly insulated prior to testing.

The test points within a given test matrix were run in random order, and all test points were run using identical procedures. Before refrigerant flowed through the test section, the evaporator pressure was pre-set at the desired level. The temperature of the chiller's water-glycol delivered to the condenser/receiver (which sets evaporator pressure) was maintained at the pre-set level throughout a test point run. Also prior to the test run, the mass flow meter's "zero flow" calibration was verified. The capillary tube inlet condition would initially be set at 100 psia and near room temperature (a subcooled condition). As the refrigerant began to flow through the test section, the capillary tube inlet pressure was increased to the saturation pressure value corresponding to the condenser temperature test point level. After establishing the pressure, the capillary tube inlet temperature was controlled by adjusting the power supplied to the preheater. Similarly, evaporator exit conditions were controlled by adjusting power to the evaporator heater.

The capillary tube quality inlet condition test points were more difficult to obtain. The thermodynamic equilibrium quality, x, at the capillary tube inlet was calculated from an energy balance on the refrigerant flow as follows,

$$x = \frac{\dot{q}_{net} - \dot{m}Cp_{fc}(T_{sat} - T_{prehtr\text{-}in})}{\dot{m}h_{fg}} \qquad (3.1)$$

where $\dot{q}_{net}$ was the net heat transferred to the refrigerant between the preheater inlet and the capillary tube inlet. The value of $\dot{q}_{net}$ is given by

$$\dot{q}_{net} = \dot{q}_{gross} - \dot{q}_{loss} \qquad (3.2)$$

The gross preheater power level, $\dot{q}_{gross}$, was measured by the wattmeter. The heat loss to the surroundings, $\dot{q}_{loss}$, was calculated from an energy balance on the refrigerant flow when the capillary tube inlet temperature just reaches the saturation point, T_{sat}, for the inlet pressure.

$$\dot{q}_{loss} = \dot{q}_{gross} - \dot{m}Cp_{fc}(T_{sat} - T_{prehtr\text{-}in}) \qquad (3.3)$$

Once the steady saturated inlet condition was established, the power to the preheater was increased slightly by 3 to 4%. At this point, instead of "searching" for the appropriate preheater level and mass flow rate balance to achieve steady flow, the preheater power level was held constant. This allowed the inlet quality to increase, which in turn caused a decrease in mass flow rate. The mass flow response was generally slow enough so that all important parameters except the increasing quality were maintained at a steady level. Quality level was then determined from Equation 3.2.

The key to a stable capillary tube flow rate throughout a test point was in maintaining the suction line inlet temperature at a relatively stable level. This was accomplished with the refrigerant/water-glycol heat exchanger. A relatively

stable refrigerant flow rate resulted in only minor power level changes to the preheater and evaporator heater as the target test condition was approached. Steady system conditions were generally reached in 15 to 30 minutes.

CHAPTER 4. EXPERIMENTAL RESULTS FOR HFC-134a

HFC-134a has already been accepted as the replacement refrigerant for CFC-12 by many domestic refrigeration equipment manufacturers. In response, the bulk of this study's experimental evaluation of heat exchanger performance was done with HFC-134a.

Performance testing with HFC-134a was accomplished in three phases. Phase 1 test points were run with a subcooled condition at the capillary tube inlet, which is the most common refrigerator design condition. Phase 2 test points were run with a quality condition (i.e., two-phase) at the capillary tube inlet, since occasionally a low quality condition ranging from 0 to 5% exists during a refrigerator's off-design operation. Phase 3 testing focused on determining the effect of a typical range of refrigerant/oil mixture concentration levels on heat exchanger performance.

The details of each phase are discussed in the chapter sections that follow.

Phase 1: Subcooled inlet

Test matrix

Phase 1 testing was the most comprehensive of the phases since it represents the most common design condition in household refrigerators. The core HFC-134a subcooled inlet test matrix was a 1/16 fraction of a full two level factorial design with nine independent design variables (resolution IV.) A full factorial design with nine variables would include 512 (or 2^9) test points, while a

1/16 fraction includes 32 (1/16 of 512) test points. The nine variables and their respective low (-) and high (+) test levels are given in Table 4.1. All Phase 1 testing was done at the 1% oil concentration level.

The complete Phase 1 core test matrix with all variable level settings is presented in Table 4.2. Each independent variable was tested 16 times at the low (-) and high (+) level, providing balance in the testing. The test matrix used 32 different heat exchanger assemblies, one for each of the five geometric variable combinations ($2^5 = 32$). The added benefit of testing 32 different assemblies was that production variability was included in the testing, and appeared as part of the data scatter. In this way, there was empirical evidence of the potential production variability. In keeping with the requirements of a statistical design, the 32 test points were run in random order.

Table 4.1: HFC-134a Phase 1 variables and test ranges

Variable	"-" level	"+" level
Tcond	85 F	132 F
dc	0.026 in	0.031 in
ds	0.201 in	0.319 in
Lc	96 in	130 in
Lhx	40 in	70 in
Linlet	6 in	20 in
DTsc	5 F	10 F
DTsh	5 F	20 F
LP	19 psia	24 psia

Table 4.2: HFC-134a Phase 1 test matrix ("-" and "+" levels are given in Table 4.1)

Run(HX)	d_c	L_c	L_{hx}	d_s	L_{inlet}	T_{cond}	LP	DT_{sc}	DT_{sh}
1	-	-	+	+	-	-	+	+	+
2	+	+	-	-	+	+	+	-	-
3	+	-	-	-	+	-	+	+	+
4	-	+	+	+	-	+	+	-	-
5	+	-	-	-	-	+	-	+	+
6	+	+	-	-	-	-	-	-	-
7	-	+	+	+	+	-	-	-	-
8	-	-	+	+	+	+	-	+	+
9	+	-	-	+	-	+	+	-	+
10	+	+	-	+	-	-	+	+	-
11	-	+	+	-	+	-	+	+	-
12	-	-	+	-	+	+	+	-	+
13	-	+	-	+	-	+	-	-	+
14	+	-	+	-	+	-	-	+	-
15	+	+	+	-	+	+	-	-	+
16	-	-	-	+	-	-	-	+	-
17	-	-	-	-	-	-	+	-	-
18	+	-	+	+	+	-	+	-	-
19	-	+	-	-	-	+	+	+	+
20	+	+	+	+	+	+	+	+	+
21	-	+	-	+	+	-	+	-	+
22	-	-	-	+	+	+	+	+	-
23	+	-	+	-	-	+	+	+	-
24	+	+	+	-	-	-	+	-	+
25	-	+	+	-	-	+	-	+	-
26	-	-	+	-	-	-	-	-	+
27	+	+	-	+	+	+	-	+	-
28	+	-	-	+	+	-	-	-	+
29	-	-	-	-	+	+	-	-	-
30	+	-	+	+	-	+	-	-	-
31	+	+	+	+	-	-	-	+	+
32	-	+	-	-	+	-	-	+	+

Mass flow data reduction

Calculated variable effects

Measured mass flow rate data from the core test matrix was analyzed using a standard statistical analysis package, SAS (SAS, 1989). Individual variable effects, or main effects, and interaction effects were calculated within SAS using Yates' algorithm (Box, et.al., 1978). All nine main effects, plus the two factor interactions between the dominant main effects, are presented in Table 4.3 and Figure 4.1. A preliminary mass flow rate prediction equation, Equation 4.1, was constructed including the calculated effects given in Table 4.3.

Table 4.3: HFC-134a Phase 1 calculated variable effects on mass flow rate

Main effects and interactions	Calculated effect (lbm/hr)
Tcond	+ 3.24
dc	+ 2.53
Lc	- 0.90
DTsh	- 0.28
LP	- 0.20
DTsc	+ 0.12
Lhx	+ 0.10
Linlet	- 0.07
ds	+ 0.04
dc x Tcond	+ 0.71
Lc x Tcond	- 0.29
dc x Lc	- 0.10

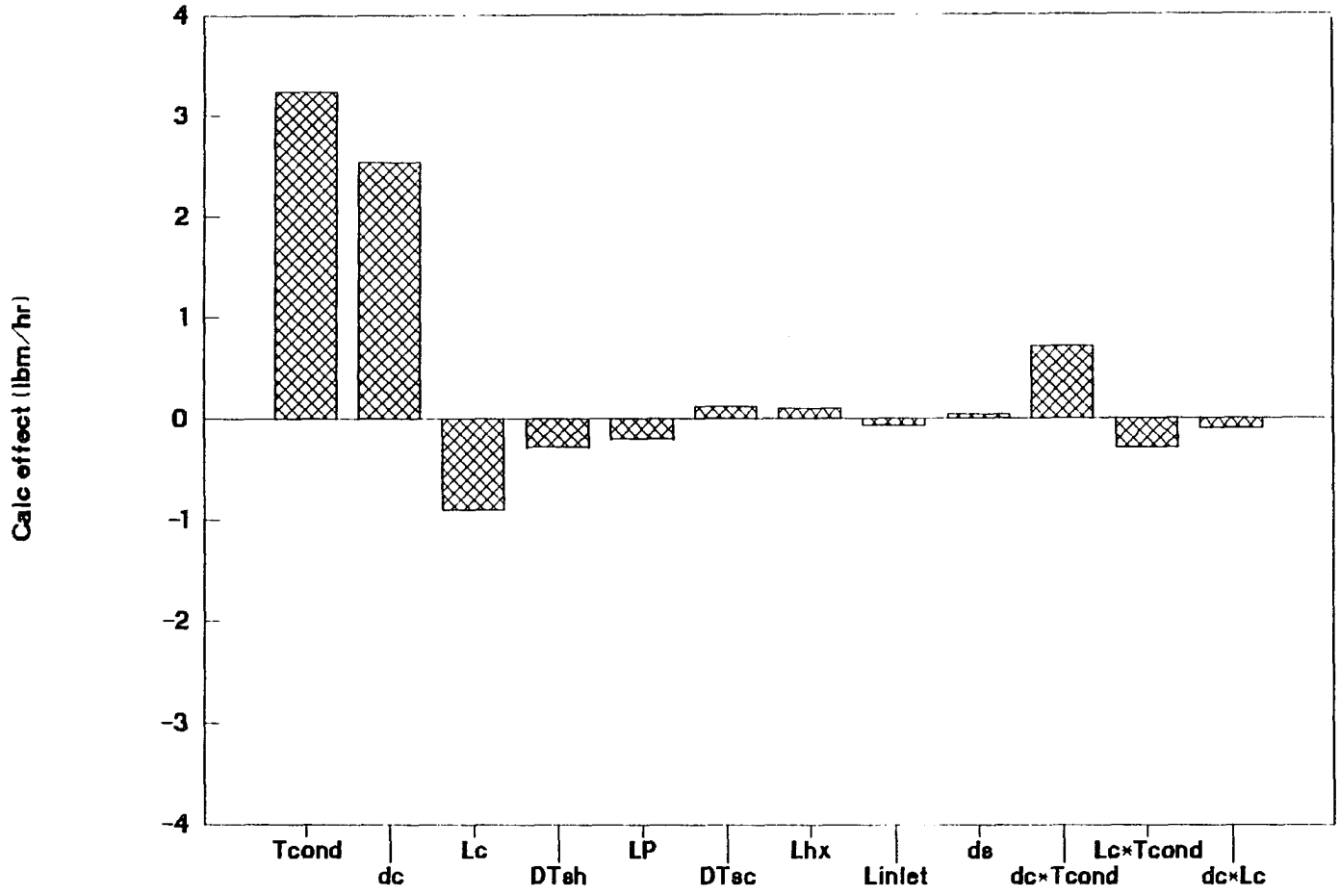

Figure 4.1: HFC-134a Phase 1 variable effects on mass flow rate

$$\dot{m}_{prelim}(lbm/hr) = 12.57 + 3.24X_{Tcond} + 2.53X_{dc} - 0.90X_{Lc} - 0.28X_{DTsh} - 0.20X_{LP} + 0.12X_{DTsc} + 0.10X_{Lhx} - 0.07X_{Linlet} + 0.04X_{ds} + 0.71X_{dc*Tcond} - 0.29X_{Lc*Tcond} - 0.10X_{dc*Lc} \quad (4.1)$$

Equation 4.1 was designated "preliminary" because the statistical significance of each variable effect had not yet been established.

The interpretation of Equation 4.1, which is of a convenient form for the statistical analysis of the data, is based on the nature of the two level factorial design. The value 12.57 is the mean mass flow rate for the 32 test points. Each X parameter corresponds to a subscripted main effect or two level interaction, and has values of -1 and +1. The -1 and +1 values correspond to the variable's low and high test level. The X parameter coefficients are the calculated effects given in Table 4.3. For example, the calculated effect of evaporator pressure (LP) on mass flow rate is -0.20 lbm/hr. This means that a change in evaporator pressure (LP) between its low (-1) and high (+1) level will be reflected in a predicted change in mass flow rate ($\dot{m}_{pred}$) of +0.20 to -0.20 lbm/hr, for a total decrease of 0.40 lbm/hr.

Significance limit

The statistical significance of a main effect or interaction effect was determined by comparing the calculated effect to a function of the experimental error, or random "noise" associated with the test facility and methodology. Experimental error was quantified by the repeatability of the measured data. In

order to be deemed statistically significant, a calculated effect had to be larger than what could be attributed to random "noise" alone.

Eight test points were selected at random from the core test matrix for replication testing and were run in a random order. By analyzing the data scatter surrounding the predicted mean response using Equation 4.1 and including the replicate test points, the mass flow rate significance limit was determined to be 0.12 lbm/hr. Calculated main effects and interaction effects beyond 0.12 lbm/hr were included in the final prediction equation. Supporting SAS analysis output is included in Appendix E.

Prediction equation

The final mass flow rate prediction equation is given in Equation 4.2, and includes all calculated effects greater than 0.12 lbm/hr.

$$\begin{aligned}\dot{m}_{pred}(\text{lbm/hr}) = {} & 12.57 + 0.1373(\text{Tcond}-108.6) + 1010(\text{dc}-.0285) \\ & - 0.0531(\text{Lc}-113) - 0.04078(\text{DTsh}-12.85) \\ & - 0.0737(\text{LP}-21.4) + 0.0464(\text{DTsc}-8.2) + 0.0064(\text{Lhx}-55) \\ & + 12.034(\text{dc}-.0285)(\text{Tcond}-108.6) \\ & - 7.228\text{x}10^{-4}(\text{Tcond}-108.6)(\text{Lc}-113) \\ & + 5.867(\text{dc}-.0285)(\text{Lhx}-55) \end{aligned} \qquad (4.2)$$

In using Equation 4.2, variable units must be consistent with the units specified in the nomenclature listing.

In comparing Equation 4.2 with its preliminary form, Equation 4.1, the Linlet and ds variables, and the dc*Lc interaction do not appear in the final equation because these effects do not meet the test for significance. The dc*Lhx interaction was added to the final equation since its calculated effect of 0.22 lbm/hr was greater than the significance limit. Finally, the final equation retained the Lhx effect (0.10 lbm/hr) due to its importance to the heat exchanger design process, even though it did not quite meet the significance limit.

A plot of measured versus predicted mass flow rate using Equation 4.2 is given in Figure 4.2, and shows good agreement. The 95% confidence interval for Equation 4.2 is ±0.40 lbm/hr, and the 95% prediction interval (shown in Figure 4.2) is ±0.85 lbm/hr. The 95% confidence interval means that with 95% confidence, the stated interval bounding the predicted performance value will include the true mean performance value. The 95% prediction interval means that with 95% confidence, the stated interval bounding the predicted performance value will include the actual measured performance value for an individual heat exchanger. These intervals were calculated based on a statistical analysis of the scatter in the data around the predicted mean value. The implicit assumption of a normal distribution of residuals in the data around the predicted mean values was verified.

A plot of the measured versus predicted mass flow rate using Equation 4.2 for the eight replicate test points is given in Figure 4.3, and verifies the excellent repeatability in the test facility and methodology.

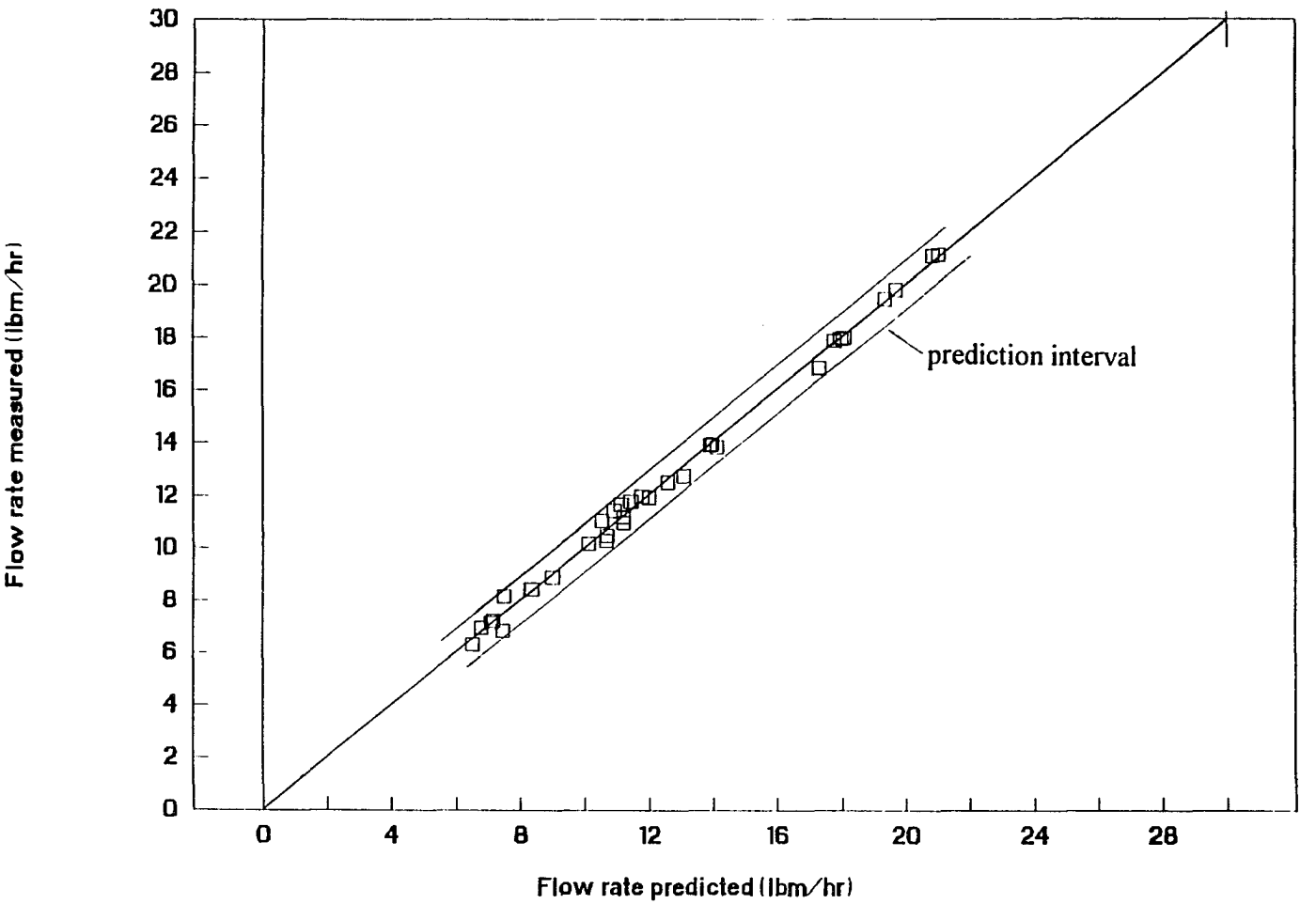

Figure 4.2: Phase 1 measured versus predicted flow rate (Equation 4.2)

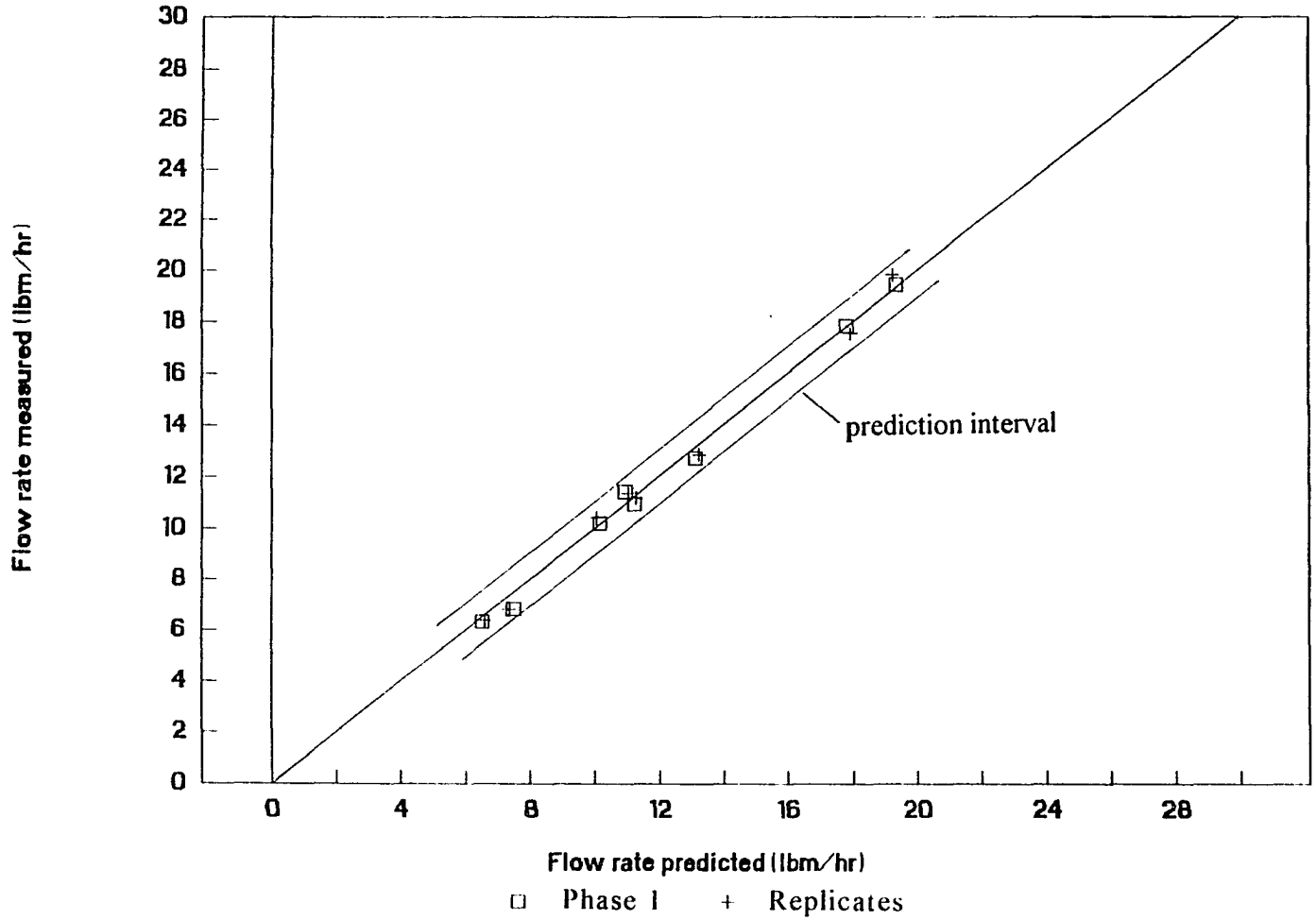

Figure 4.3: Phase I replicate test points, measured versus predicted flow (Equation 4.2)

Analysis of mass flow variable effects

Tcond effect

One of the most significant variables affecting mass flow rate was condenser temperature (Tcond), with a calculated effect of 3.24 lbm/hr. This effect is presented graphically in Figures 4.4 and 4.5, where mass flow rate is shown to increase with condenser temperature for a fixed capillary tube geometry. This response is more readily understood in terms of condenser pressure. Figure 4.6 shows the liquid-vapor saturation curve for HFC-134a. Condenser pressure is the saturation pressure corresponding to the condenser temperature. As condenser temperature increases, the condenser pressure increases, which is the capillary tube inlet pressure. Hence, the mass flow rate increases with the inlet pressure, as would be expected.

dc and Lc effects

The two other most significant variables affecting mass flow rate were capillary tube diameter (dc) and length (Lc), with calculated effects of 2.53 and -0.90 lbm/hr, respectively. These effects are shown in Figures 4.4, 4.5, and 4.7. The mass flow response for any flow restriction device with a fixed upstream and downstream condition is inversely related to the resistance provided by the restriction device. In other words, an increase in flow resistance means a decrease in flow rate, and visa versa. For a capillary tube, flow resistance is inversely related to the flow area, or diameter, and is directly related to length.

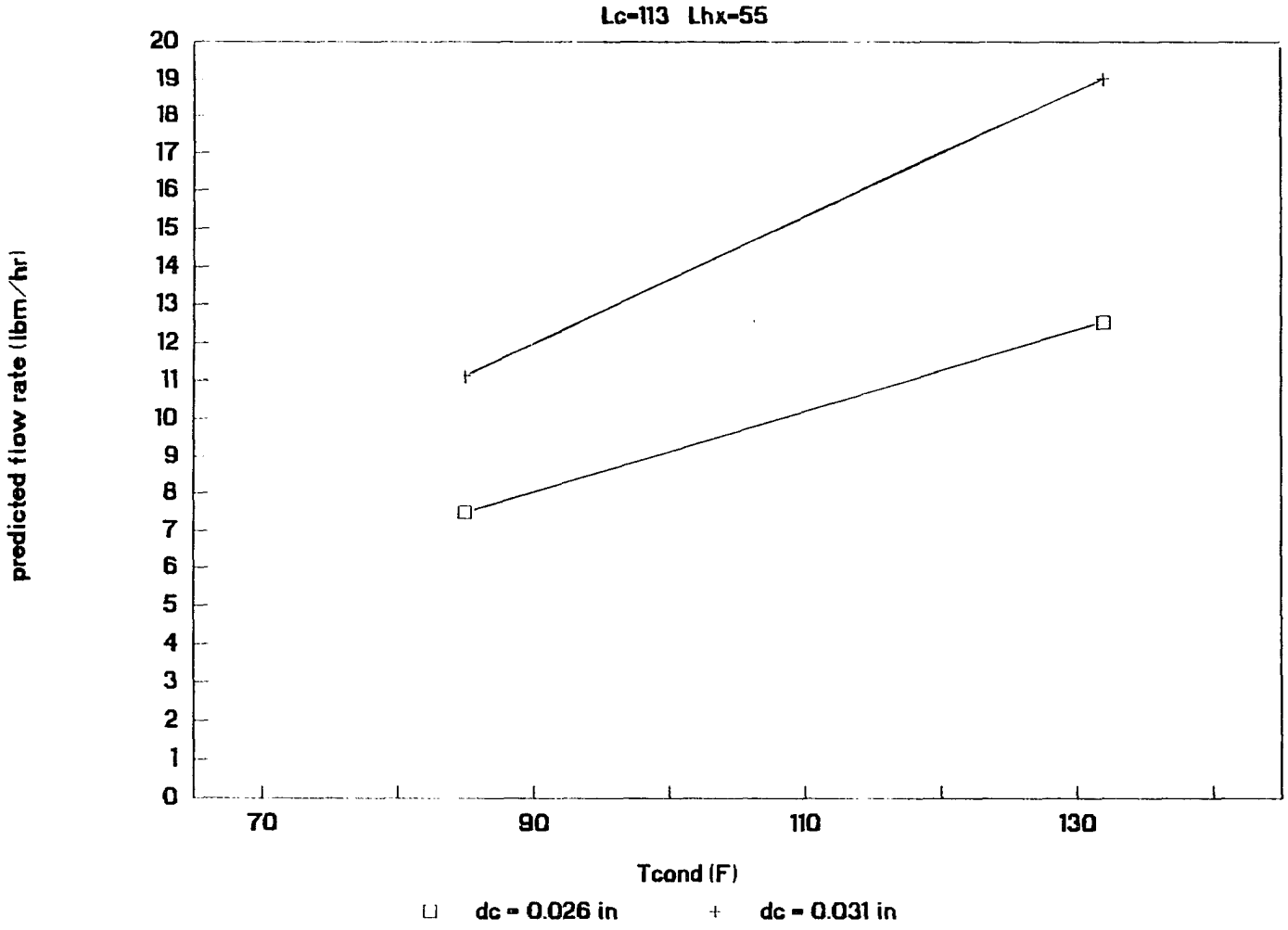

Figure 4.4: Condenser temperature effect on mass flow rate

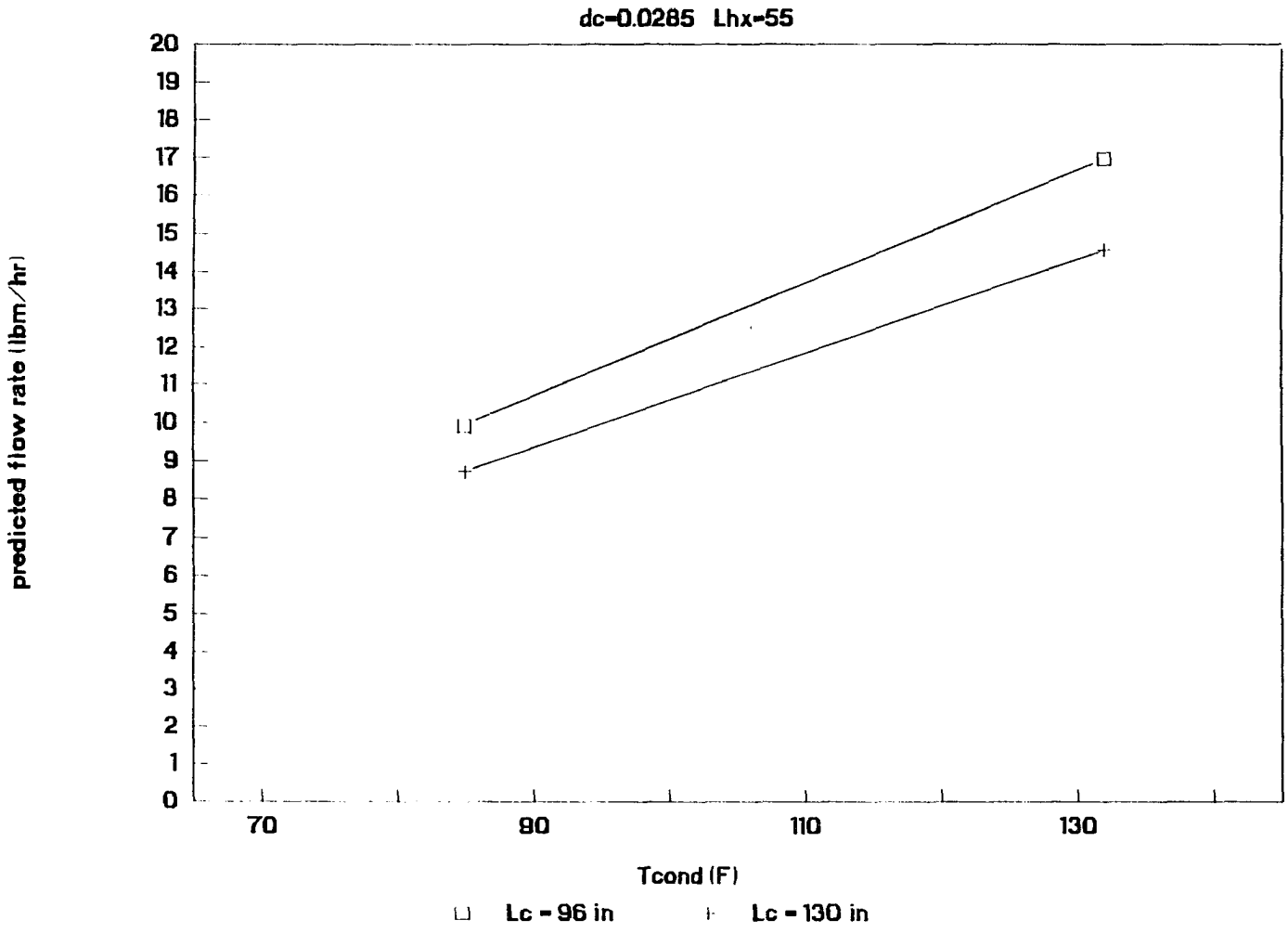

Figure 4.5: Condenser temperature effect on mass flow rate

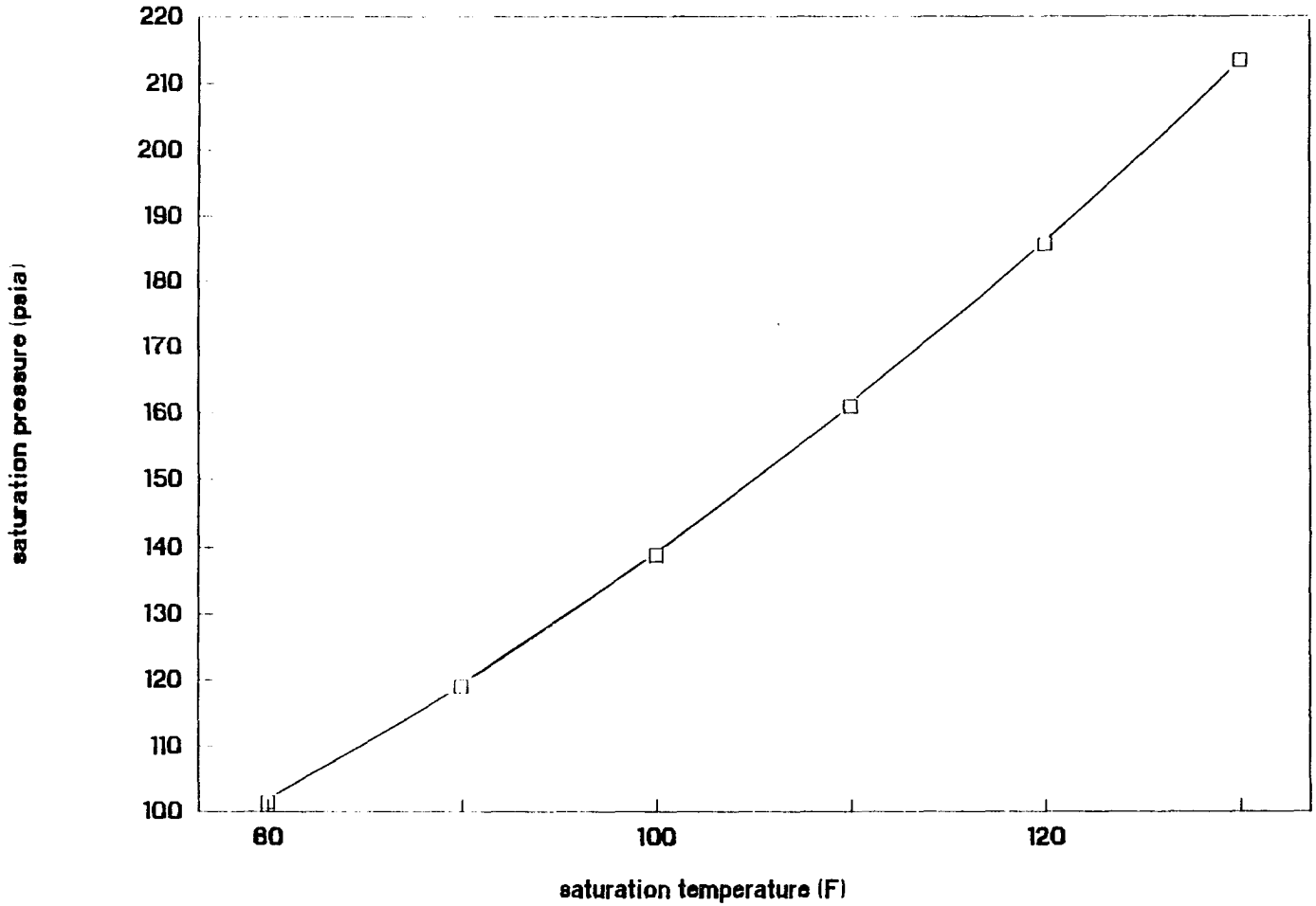

Figure 4.6: Liquid-vapor saturation curve for HFC-134a

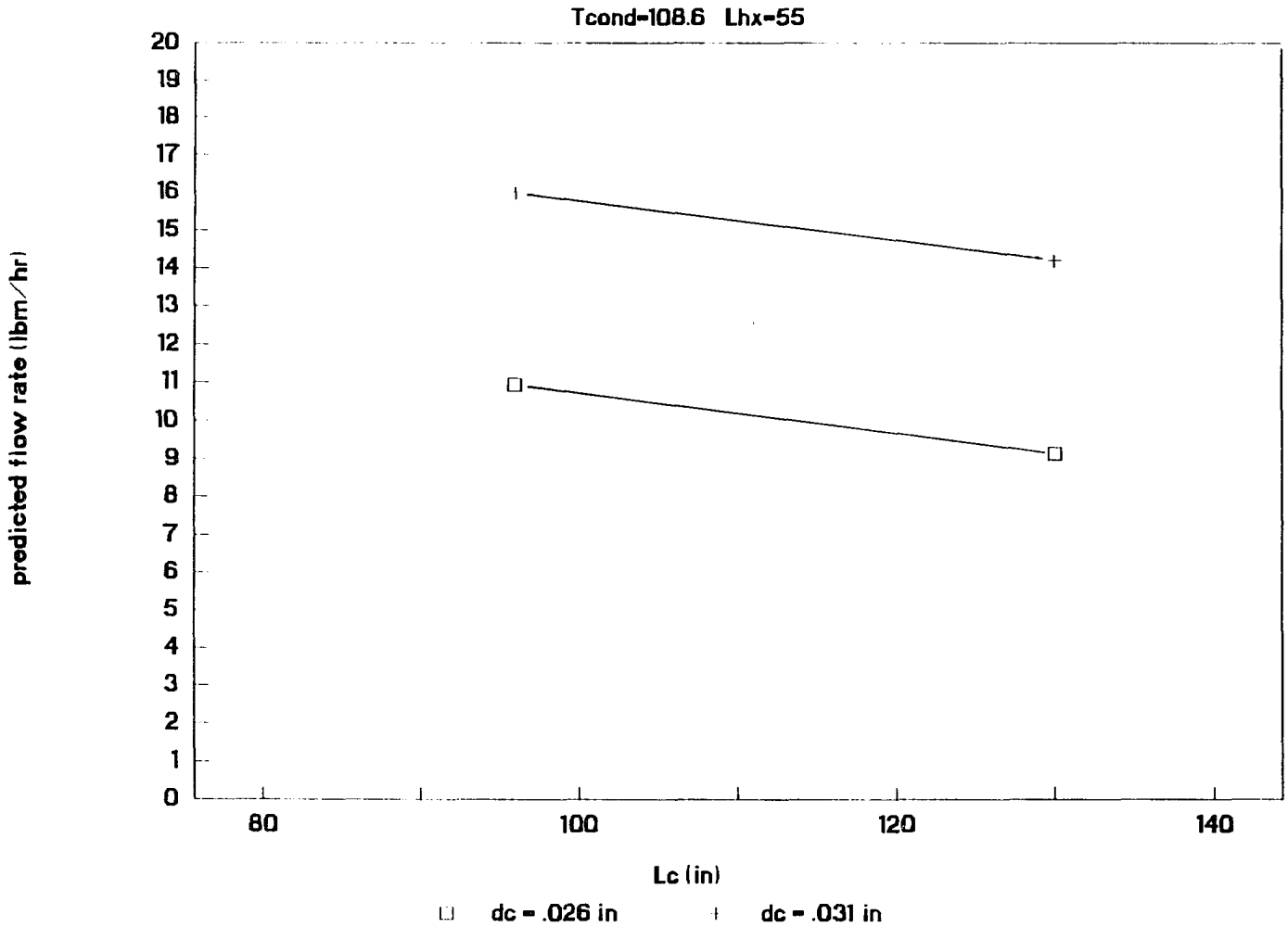

Figure 4.7: Capillary tube length effect on mass flow rate

In Figures 4.4, 4.5, and 4.7, the effects of dc and Lc are as expected. As diameter increases, the flow resistance decreases, and the mass flow rate increases (Figures 4.4 and 4.7). Conversely, as capillary tube length increases, the flow resistance increases, and the mass flow rate decreases (Figures 4.5 and 4.7).

DTsc effect

The effect on mass flow rate of inlet subcooling level (DTsc) was +0.12 lbm/hr, which means mass flow rate increases with an increase in inlet subcooling. This effect can also be explained in terms of flow resistance within the capillary tube. With a subcooled inlet condition, the refrigerant remains liquid until the onset of vaporization, or the flash point. Upstream of the flash point, the subcooled liquid experiences a constant pressure drop due to friction alone. Downstream of the flash point, the pressure drop increases rapidly as a result of both the two-phase friction and vapor acceleration. The pressure gradients in the subcooled and two-phase regions are directly related to their respective contributions to overall flow resistance. An increase in the inlet subcool level for a fixed condenser temperature will result in an increase in the length of the subcooled liquid region, and the vaporization point will be delayed. It then follows that as inlet subcool level increases, overall flow resistance will be reduced, and mass flow rate will increase.

DTsh and LP effect

For suction line inlet superheat level (DTsh) and evaporator pressure (LP), the calculated effect on mass flow rate were -0.28 and -.20 lbm/hr, respectively. This implies that an increase in superheat level or evaporator pressure results in a decrease in mass flow rate. These effects are both related to suction line temperature level, and are consistent with previously reported mass flow rate behavior in nonadiabatic capillary tubes.

All prior nonadiabatic studies have shown that the effect of heat transfer from the capillary tube is an increase in mass flow rate. It had been generally reasoned that the heat transfer effectively increased the subcool level of the liquid refrigerant, and delayed the vaporization point. As discussed previously, an increase in the subcool level decreases the overall flow resistance in the capillary tube, and the result is an increase in mass flow rate. Pate and Tree (1984a, 1984b), though, showed that heat transfer from the capillary tube to the suction line did not necessarily delay the vaporization point, but did suppress considerably the quality increase in the capillary tube. The effect is still a decrease in overall flow resistance, and an increase in flow rate.

If either the evaporator pressure or inlet superheat level is increased, the suction line temperature level will increase. This increase in suction line temperature for a fixed capillary tube inlet condition will result in a decrease in the temperature difference between the two flow streams, and thus, the heat transfer rate. Corresponding to the decrease in heat transfer rate, the mass flow rate will also decrease, which agrees with the calculated effect for both the evaporator pressure (LP) and suction line inlet superheat level (DTsh).

The effect of the evaporator pressure (LP) on mass flow rate can be separated from the suction line temperature effect described in the previous paragraph. The evaporator pressure is also the capillary tube discharge pressure. For an increase in evaporator pressure between the Phase 1 low and high levels, 19 and 24 psia, the effect on mass flow rate is -0.40 lbm/hr. For this evaporator pressure increase, the suction line inlet temperature can be maintained at a constant level by reducing the superheat level, DTsh, by 10 °F. The effect on mass flow rate of a 10 °F decrease in DTsh is +0.37 lbm/hr. The net effect on mass flow rate of an independent evaporator pressure change is -0.03 lbm/hr, which is insignificant. Therefore, for the evaporator pressure range tested, the capillary tube flow can be considered choked.

Lhx effect

The calculated effect of heat exchanger length (Lhx) on mass flow rate was +0.10 lbm/hr. The increase in heat exchange length is directly related to an increase in heat transfer area, and thus, heat transfer rate. As described previously, an increase in heat transfer rate between the flow streams will result in an increase in mass flow rate.

Effective subcooling data reduction

Calculated variable effects

Effective subcooling data from the core test matrix was analyzed using SAS. All nine main effects, plus the two factor interactions between the dominant main effects, are presented in Table 4.4 and Figure 4.8. A preliminary effective subcooling prediction equation, Equation 4.3, was constructed that included the effects given in Table 4.4.

$$\begin{aligned} EFFsc_{prelim}(F) = {} & 39.2 + 7.45X_{Tcond} - 3.29X_{DTsh} + 2.72X_{Lhx} \\ & - 2.55X_{LP} - 1.68X_{ds} - 0.55X_{DTsc} \\ & - 0.36X_{dc} + 0.02X_{Linlet} + 0.00X_{Lc} \\ & + 1.10X_{Tcond*Lhx} - 0.48X_{ds*Tcond} \\ & + 0.31X_{ds*DTsh} + 0.30X_{Tcond*DTsh} \\ & + 0.25X_{LP*DTsh} - 0.20X_{LP*Lhx} \\ & + 0.12X_{ds*Lhx} - 0.11X_{DTsh*Lhx} \\ & - 0.10X_{Tcond*LP} + 0.08X_{ds*LP} \end{aligned} \qquad (4.3)$$

The interpretation of the terms in Equation 4.3 follows the description given previously for Equation 4.1.

Table 4.4: HFC-134a Phase 1 calculated variable effects on EFFsc

Main effects and interactions	Calculated effect (°F)
Tcond	+ 7.45
DTsh	- 3.29
Lhx	+ 2.72
LP	- 2.55
ds	- 1.68
DTsc	- 0.55
dc	- 0.36
Linlet	+ 0.02
Tcond x Lhx	+ 1.10
ds x Tcond	- 0.48
ds x DTsh	+ 0.31
Tcond x DTsh	+ 0.30
LP x DTsh	+ 0.25
LP x Lhx	- 0.20
ds x Lhx	+ 0.12
DTsh x Lhx	- 0.11
Tcond x LP	- 0.10
ds x LP	+ 0.08

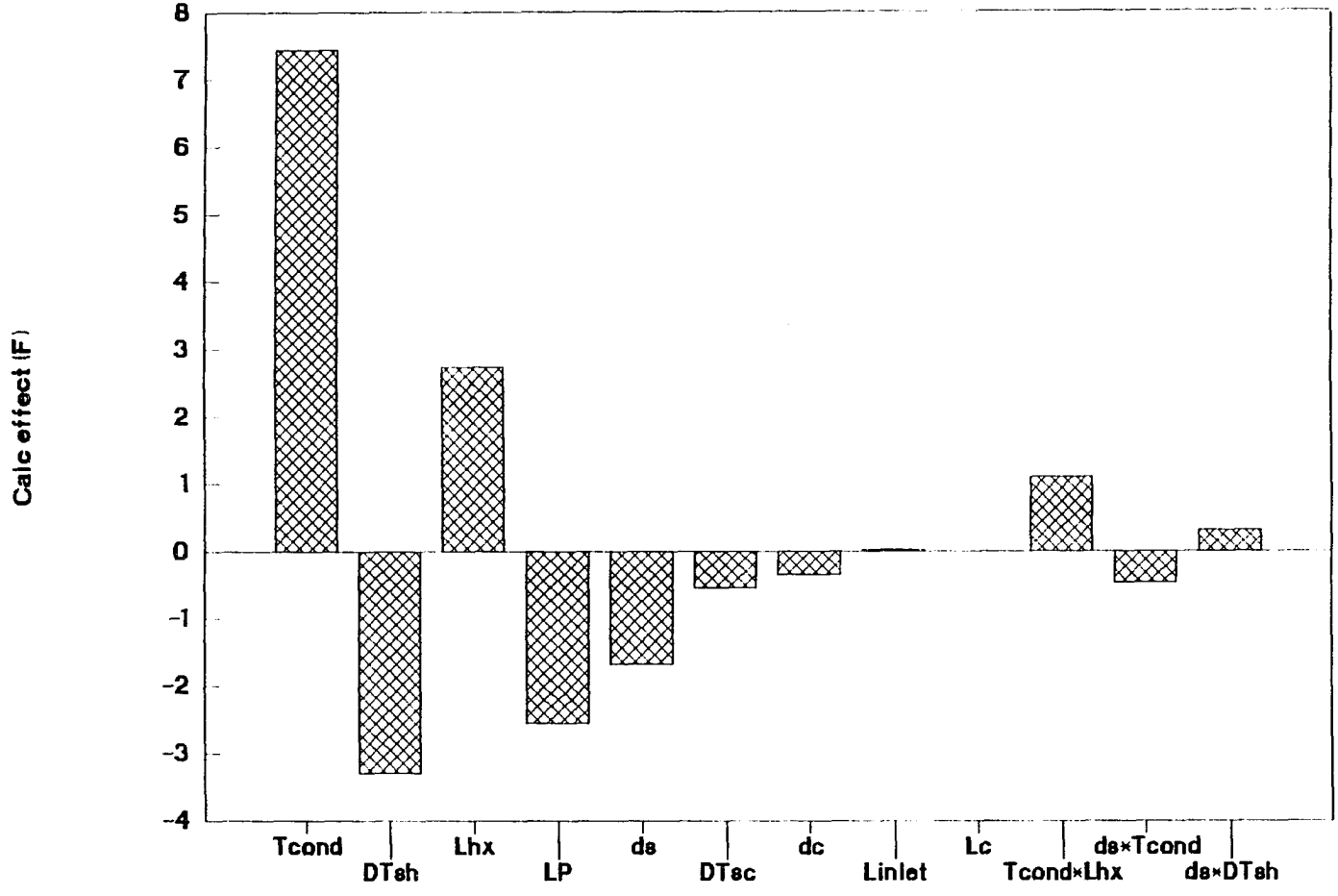

Figure 4.8: HFC-134a Phase 1 variable effects on EFFsc

Significance limit

As in the mass flow rate data analysis, the statistical significance of all calculated effects on effective subcooling was determined by comparison to a function of the experimental error. By analyzing the data scatter surrounding the predicted mean response using Equation 4.3 and by including the replicate test points, the effective subcooling significance limit was determined to be 0.26 °F. Calculated main effects and interactions effects beyond 0.26 °F were included in the final prediction equation. Supporting SAS analysis output is included in Appendix E.

Prediction equation

The final effective subcooling prediction equation is given in Equation 4.4 below, and includes effects greater than 0.26 °F.

$$\begin{aligned} EFFsc_{pred}(F) = {} & 39.2 + 0.3156(Tcond-108.6) - 0.4735(DTsh-12.85) \\ & + 0.1815(Lhx-55 - 0.9262(LP-21.4) - 28.54(ds-0.260) \\ & - 0.2188(DTsc-8.2) - 143.6(dc-0.0285) \\ & + 3.116\times10^{-3}(Lhx-55)(Tcond-108.6) \\ & - 0.343(Tcond-108.6)(ds-0.260) \\ & + 0.756(ds-0.260)(DTsh-12.85) \\ & + 1.829\times10^{-3}(Tcond-108.5)(DTsh-12.85) \end{aligned} \qquad (4.4)$$

In using Equation 4.4, variable units must be consistent with the units specified in the nomenclature listing.

In comparing Equation 4.4 with its preliminary form, Equation 4.3, the Linlet and Lc variables do not appear in the final equation. Also not appearing in Equation 4.4 are the following interactions: LP*DTsh, LP*Lhx, ds*Lhx, DTsh*Lhx, Tcond*LP, and ds*LP. These variables and interactions did not meet the test for significance.

A plot of measured versus predicted effective subcooling using Equation 4.4 is given in Figure 4.9, and shows good agreement. The 95% confidence interval for Equation 4.9 is ±0.88 °F, and the 95% prediction interval (shown in Figure 4.9) is ±1.84 °F.

A plot of measured versus predicted effective subcooling using Equation 4.4 for the eight replicate test points is given in Figure 4.10, and verifies the repeatability in the test facility and methodology.

Analysis of effective subcooling variable effects

Tcond, DTsc, LP, and DTsh effects

The calculated effects of Tcond, DTsc, LP, and DTsh were relatively large because these variables are directly related to the definition of EFFsc. EFFsc was defined in Equation 1.1 based on an energy balance between the two flow streams.

$$EFFsc = (Cp_{gs}/Cp_{fc})(T_{s2} - T_{s1}) \qquad (1.1)$$

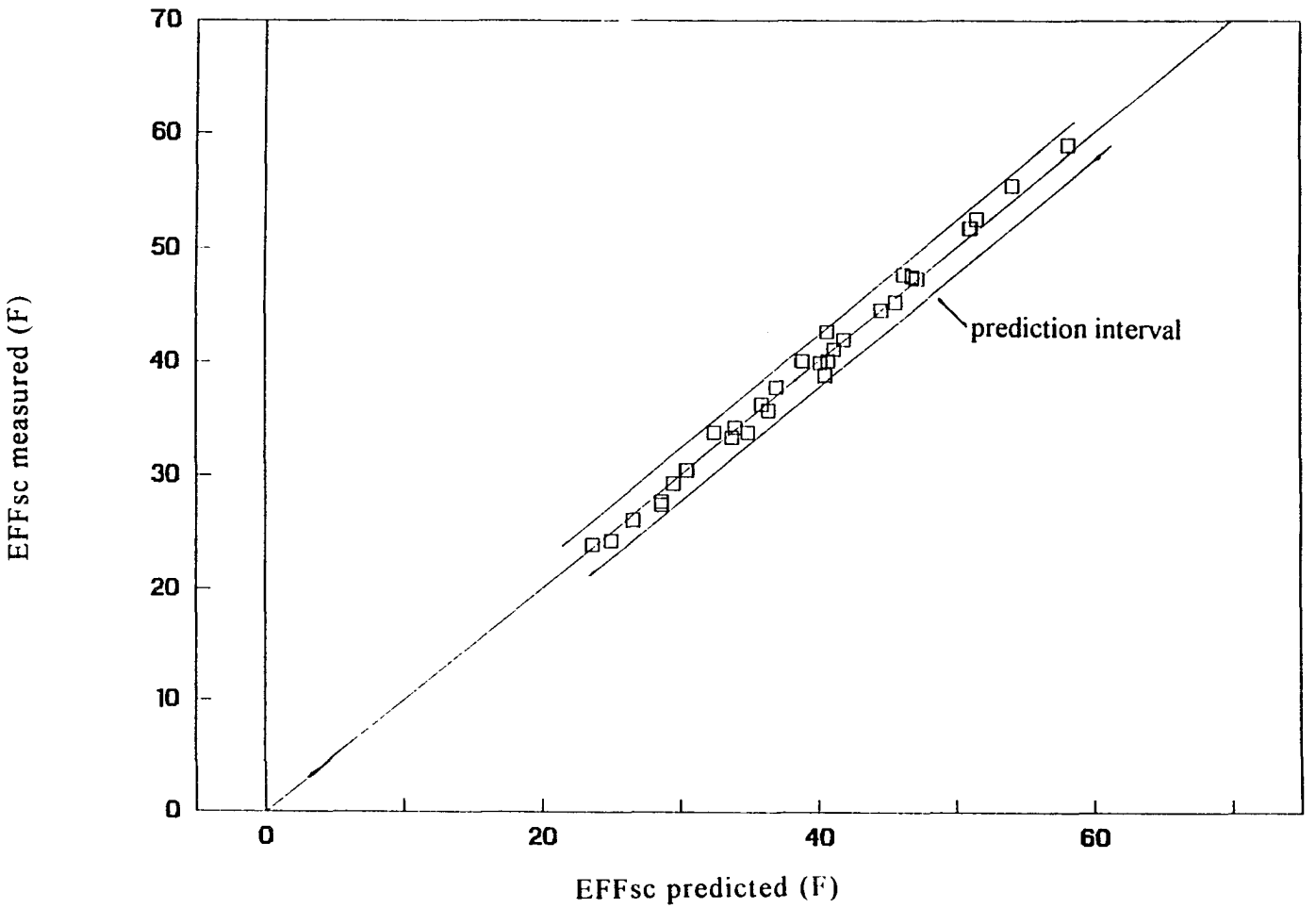

Figure 4.9: Phase 1 measured versus predicted EFFsc (Equation 4.4)

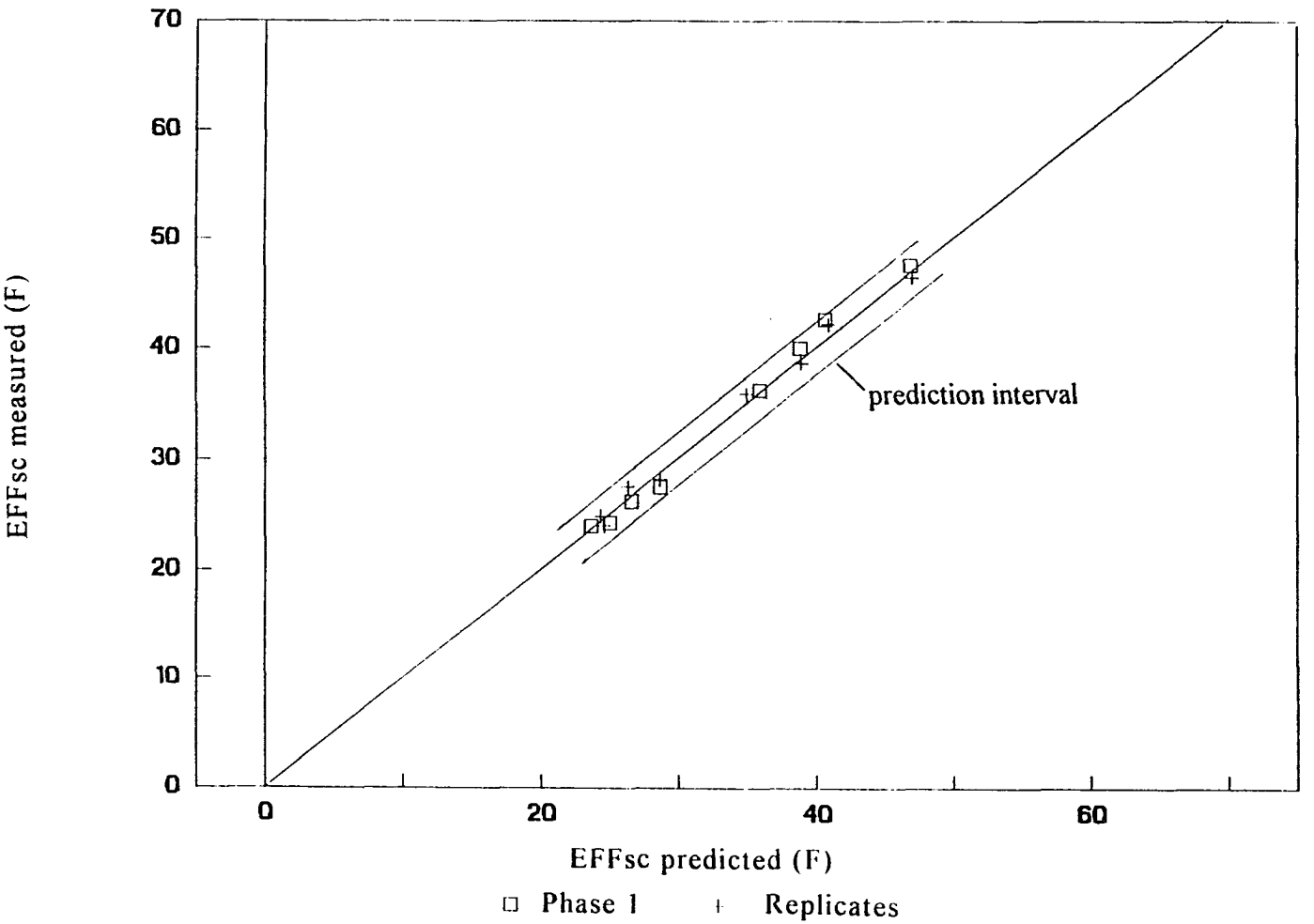

Figure 4.10: Phase 1 replicate test points, measured versus predicted EFFsc (Equation 4.4)

It is used, along with mass flow rate, to quantify the increase in refrigeration capacity for the heat exchanger configuration in comparison to an adiabatic capillary tube configuration.

By definition, EFFsc is the difference between the capillary tube inlet temperature, T_{c1} and an effective temperature exiting the heat exchanger region, T_{c2}.

$$EFFsc = T_{c1} - T_{c2} \tag{4.5}$$

The inlet temperature level, T_{c1}, is established by the condenser saturation temperature, Tcond, and the inlet subcool level, DTsc.

$$T_{c1} = Tcond - DTsc \tag{4.6}$$

Since Tcond and DTsc define T_{c1}, and thus, EFFsc, the calculated effects of Tcond and DTsc were relatively large.

The suction line inlet temperature in Equation 1.1, T_{s1}, is established by the evaporator saturation temperature, T_{evap}, at the evaporator pressure, LP, and suction line inlet superheat level, DTsh.

$$T_{s1} = T_{evap@LP} + DTsh \tag{4.7}$$

Since LP and DTsh define T_{s1}, and thus, EFFsc, the calculated effects of LP and DTsh were also large.

Lhx and ds effects

The two dominant variables in the EFFsc prediction equation (Equation 4.4) that are independent of the EFFsc definition are suction line diameter, ds, and heat exchanger length, Lhx. A graphical representation of the effect of heat exchanger length (Lhx) and condenser temperature (Tcond) on effective subcooling is given in Figure 4.11. In Figure 4.11, EFFsc increases with Lhx because the total heat transfer area between flow streams increases.

$$A_{h/t} = (\pi ds)Lhx \tag{4.8}$$

The effect of suction line diameter (ds) and condenser temperature (Tcond) on EFFsc is given in Figure 4.12, and EFFsc is shown to decrease with ds. This effect can be explained by considering that ds affects both the total heat transfer area (Equation 4.8) and the suction line heat transfer coefficient, as given below.

$$Nu_{ds} = f(Re_{ds})^{0.8} = f(1/ds)^{0.8} \tag{4.9}$$

$$h = Nu_{ds}(ks/ds) = f(1/ds)^{1.8} \tag{4.10}$$

The heat transfer rate between flow streams is a function of the product of h (Equation 4.10) and $A_{h/t}$ (Equation 4.8), and the net effect of ds is $(1/ds)^{0.8}$. Since EFFsc is an indicator of heat transfer rate, EFFsc will decrease with ds, which agrees with the measured result.

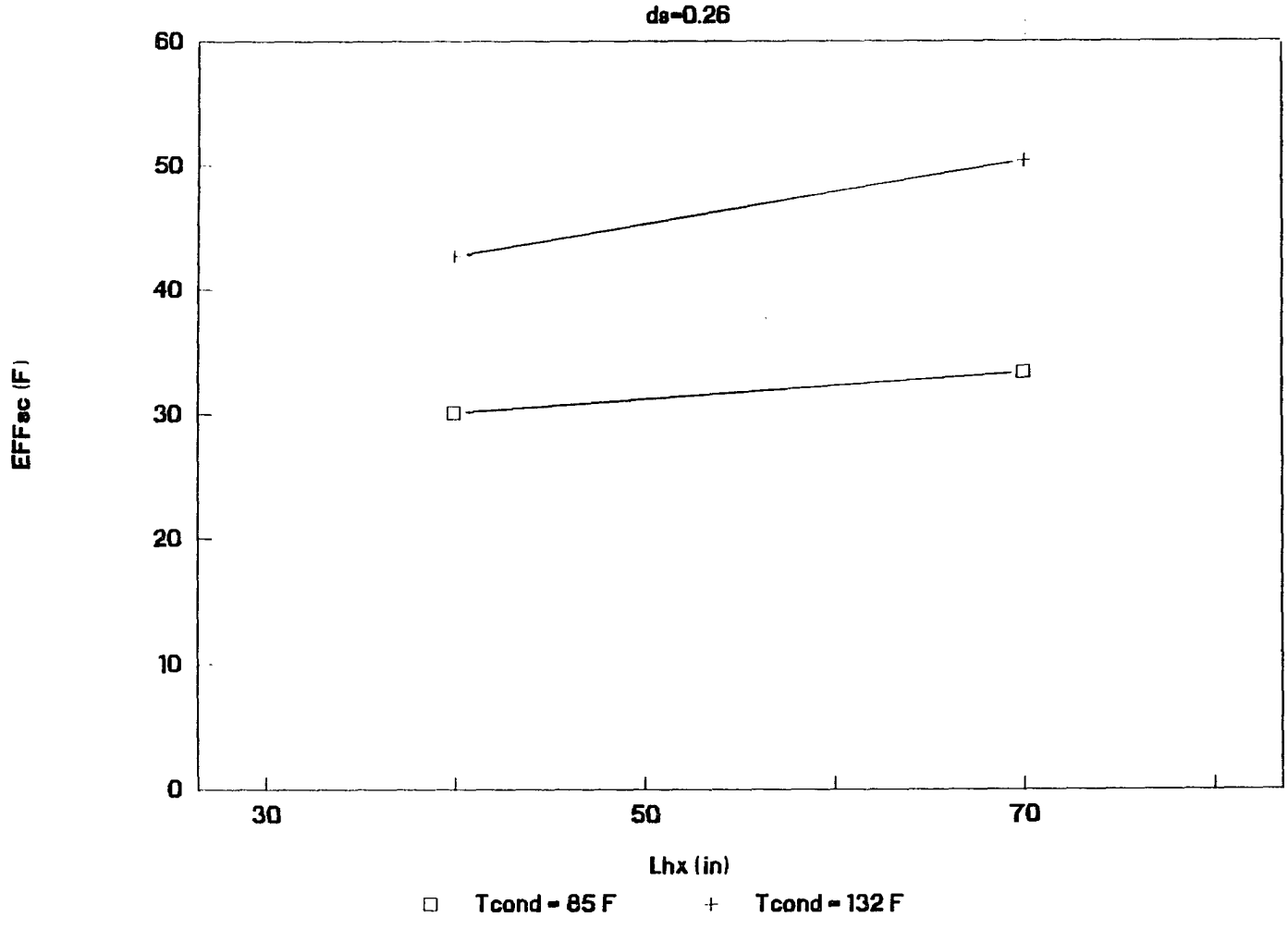

Figure 4.11: Heat exchanger length effect on EFFsc

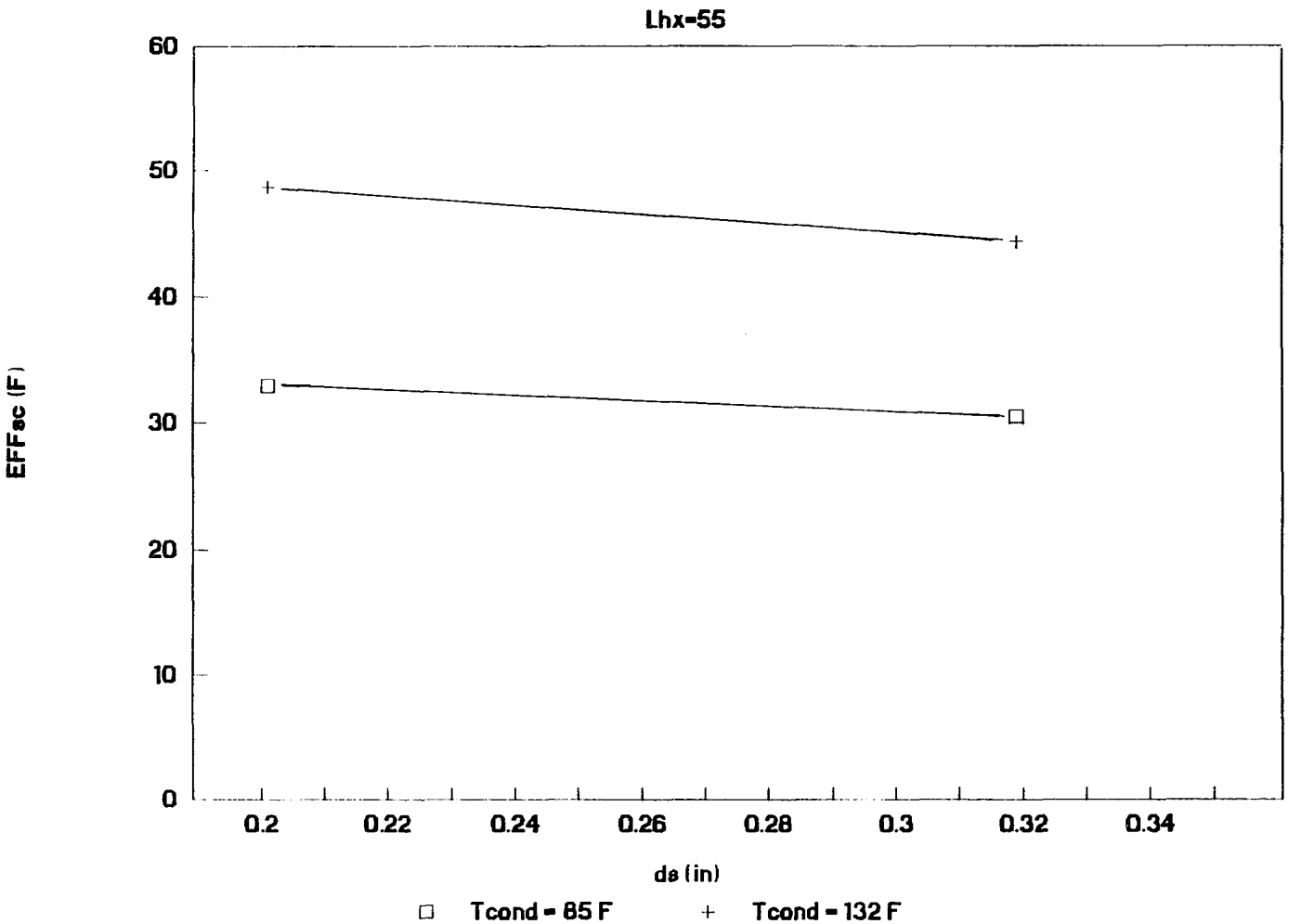

Figure 4.12: Suction line diameter effect on EFFsc

Performance prediction verification

A two level factorial design results in prediction equations linear in all independent variables. Therefore, the next experimental step was to investigate the possibility of nonlinear variable effects on both response variables, mass flow rate and effective subcooling. The simplest approach was to run additional test points at mid-range levels of the most significant variables, and make comparisons between the measured and predicted performance. If significant nonlinear effects existed, then measurements and predictions would not agree.

Seven mid-range level test points were defined for different combinations of the most significant variables affecting heat exchanger performance. These test points were run using seven production heat exchanger assemblies supplied by a refrigerator manufacturer. In Figure 4.13, measured mass flow rate is compared to predictions using Equation 4.2. All data falls within the 95% prediction interval.

Likewise, in Figure 4.14, measured effective subcooling is compared to predictions using Equation 4.4. For two of the heat exchanger assemblies, measured effective subcooling levels are greater than predicted. These two heat exchanger assemblies had suction lines with an enhanced inner surface. The enhancement had the effect of increasing the suction line heat transfer coefficient, and thereby, the heat transfer rate. Since Equation 4.4 was developed based on smooth suction line tubes, the increase in effective subcooling beyond the predicted mean value is attributed to the effect of the enhanced inner surface suction line.

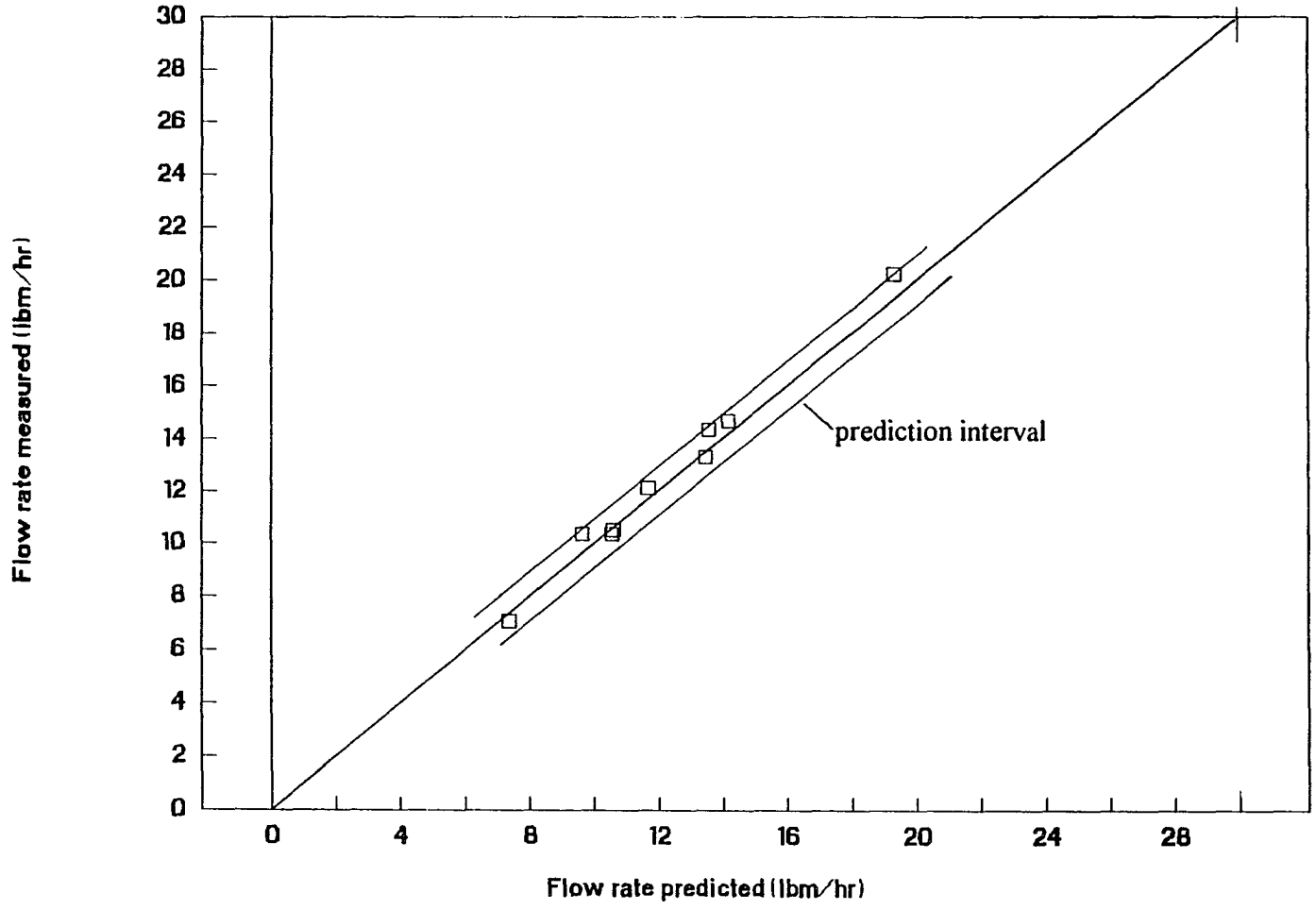

Figure 4.13: Phase I mid-range level test points, measured versus predicted mass flow (Equation 4.2)

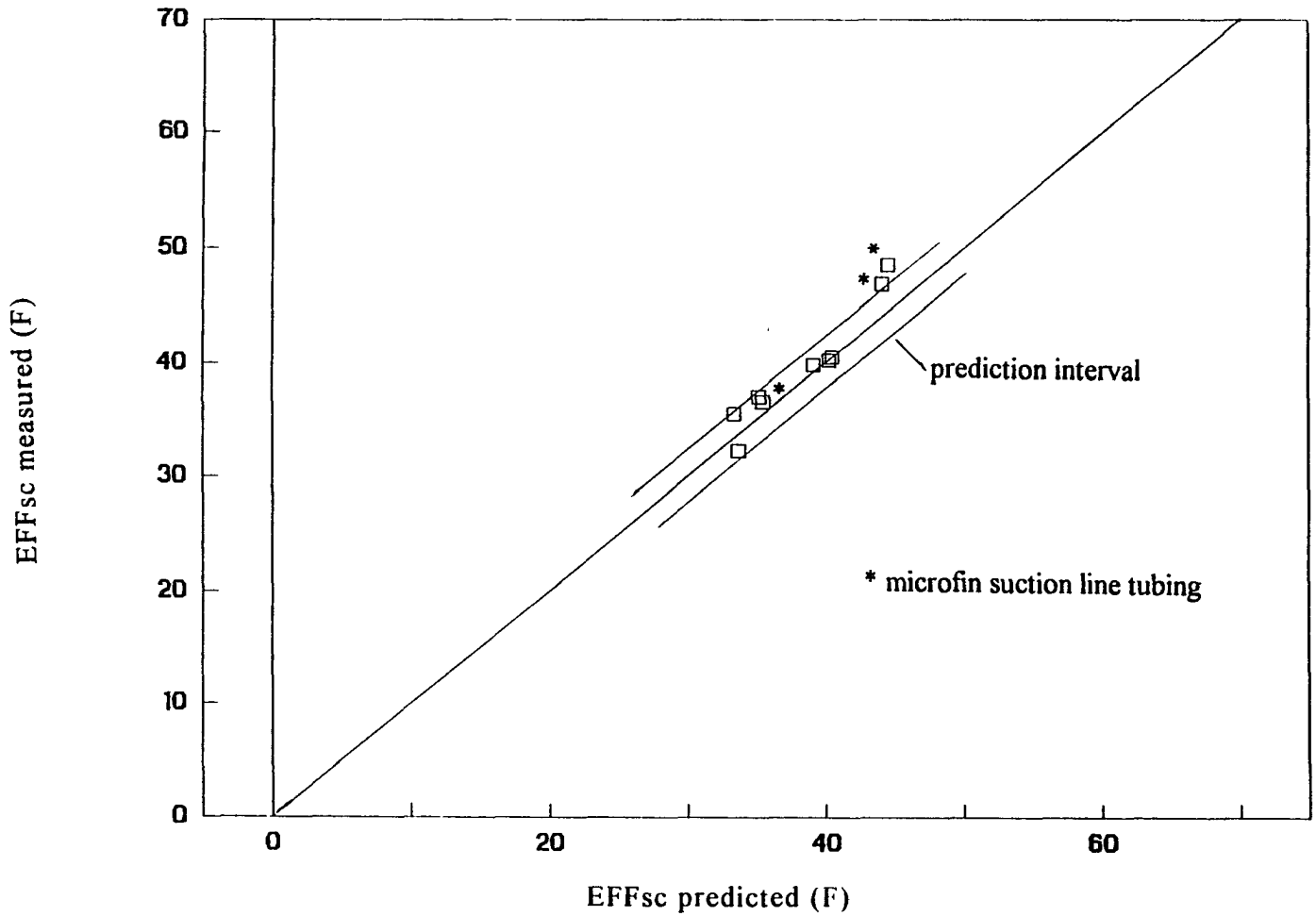

Figure 4.14: Phase 1 mid-range level test points, measured versus predicted EFFsc (Equation 4.4)

The final conclusion is that there are no significant nonlinear effects on mass flow rate and effective subcooling for the range of variable levels tested. In addition, the use of production heat exchanger assemblies provided for the irrefutable evidence that verified the prediction accuracy of Equations 4.2 and 4.4.

Performance equation sensitivity

Geometry variability amongst the 32 heat exchanger assemblies and instrumentation error (as part of the experimental error) were contributing factors to the scatter in the data seen in Figures 4.2 and 4.9. Uncertainty analyses demonstrated that predicted flow rate was the most sensitive to capillary tube diameter. All other factor variabilities had a relatively small effect on predicted mass flow rate and effective subcooling. The 32 capillary tubes tested were from the same manufacturer's lots of capillary tubes with nominal inner diameters of 0.026 and 0.031 in. The result was a very small tube-to-tube variation in actual capillary tube diameter, quoted to be ±0.0001 in. Manufacturing tolerance on capillary tube diameter can be on the order of ±0.0005 in. If a refrigerator manufacturer's stock of capillary tubes have a similar variability in actual tube diameter, then this can result in flow rate variation within the nominal size. For example, the predicted flow variation for Phase 1 test points 5 and 8 with a capillary tube diameter variation of ±0.0005 in is ±0.33 and ±0.5 lbm/hr, respectively, which would be deemed a significant effect in the current study.

Production stock capillary tube diameter variability can be reduced through standardized flow capacity measurements such as the referenced ASHRAE

standard (ASHRAE Standard 1988). A tolerance on flow capacity of ±2% translates into a tolerance on a 0.026 in capillary tube of ±0.0002 in since the flow capacity is proportional to $d_c^{2.5}$. The predicted flow variation for test points 5 and 8 with a diameter tolerance of ±.0002 in is ±0.13 and ±0.25 lbm/hr, respectively.

Phase 2: Quality inlet

Test matrix

The intent of the Phase 2 testing was to determine the effect of a quality inlet condition on heat exchanger performance. The quality inlet test matrix was a 1/2 fraction of a full two level factorial design with five independent design variables (resolution V). A full factorial design with five variables would include 32 (or 2^5) test points, while a 1/2 fraction includes 16 test points. The five independent variables included quality (0 and 5% levels) and four other important design variables as determined from phase 1 test results. The four additional variables were included in order to establish the significance of potential quality interaction effects. All five variables and their respective low (-) and high (+) test levels are given in Table 4.5. Phase 2 testing was done at the 1% oil concentration level.

The complete phase 2 test matrix with all variable settings is presented in Table 4.6. Each independent variable was tested eight times at the low (-) and high (+) level. The 16 test points were run in random order.

Table 4.5: HFC-134a Phase 2 variables and test ranges

Variable	"-" level	"+" level
Tcond	95.6 F	115.7 F
dc	0.026 in	0.031 in
Lc	96 in	130 in
LP	16 psia	26 psia
Inlet quality, Q	0 %	5 %

Table 4.6: HFC-134a Phase 2 test matrix ("-" and "+" levels given in Table 4.5)

Test point	Tcond	dc	Lc	LP	Q
1	-	-	+	-	+
2	+	-	+	-	-
3	-	-	+	+	-
4	+	-	+	+	+
5	+	+	-	+	+
6	-	+	-	+	-
7	-	+	-	-	+
8	+	+	-	-	-
9	-	-	-	+	+
10	+	-	-	+	-
11	-	-	-	-	-
12	+	-	-	-	+
13	-	+	+	+	+
14	+	+	+	+	-
15	+	+	+	-	+
16	-	+	+	-	-

Mass flow data reduction

Calculated variable effects

Measured mass flow rate data was analyzed using SAS. The calculated effects of all five main effects, plus the two factor interactions between the dominant main effects, are presented in Table 4.7 and Figure 4.15.

Table 4.7: HFC-134a Phase 2 calculated variable effects on mass flow rate

Main effects and interactions	Calculated effect (lbm/hr)
dc	+ 2.24
Tcond	+ 1.37
Q	+ 1.33
Lc	- 0.91
LP	- 0.29
dc x Q	+ 0.28
dc x Tcond	+ 0.16
Tcond x Q	+ 0.02

Significance limit

Phase 2 testing did not include any replicate test points. The statistical significance of the calculated effects was determined by using the Phase 1 significance limit of 0.12 lbm/hr.

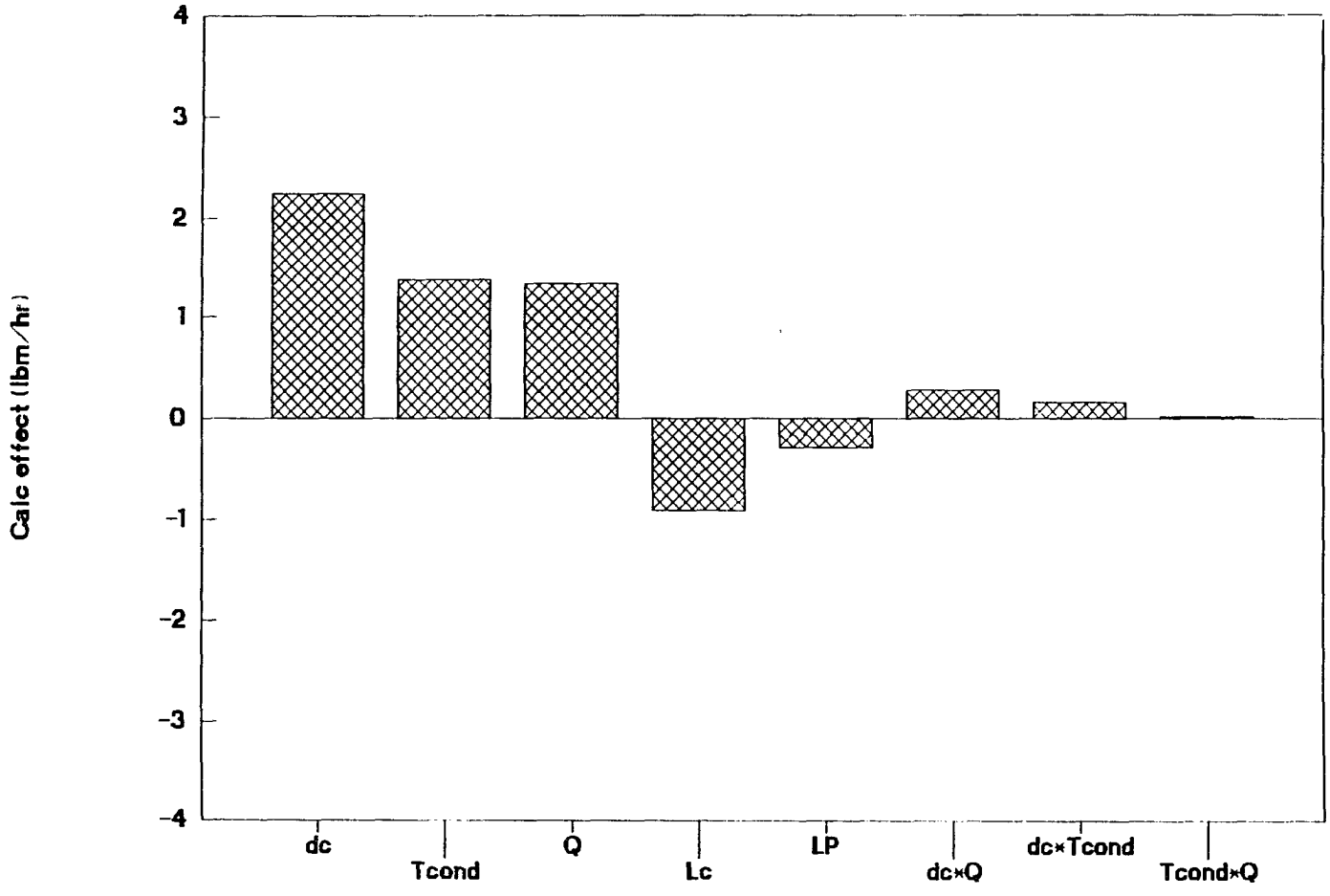

Figure 4.15: HFC-134a Phase 2 variable effects on mass flow rate

Prediction equation

The quality inlet mass flow rate prediction equation is given in Equation 4.11, and includes effects greater than 0.12 lbm/hr.

$$\dot{m}_{qual}(lbm/hr) = 10.78 + 894.4(dc-.0285) + 0.1368(Tcond-105.7) - 0.605(Q-2.2) - 0.0533(Lc-113) - 0.0576(LP-21) - 51.64(Q-2.2)(dc-.0285) + 0.00515(LP-21)(Tcond-105.7) - 5.506(dc-0.0285)(Lc-113) - 17.92(LP-21)(dc-0.0285) + 6.408(dc-0.0285)(Tcond-105.7) \quad (4.11)$$

In using Equation 4.11, variable units must be consistent with the units specified in the nomenclature listing.

A plot of measured versus predicted mass flow rate using Equation 4.11 is given in Figure 4.16. The 95% confidence interval for Equation 4.11 is ±0.47 lbm/hr, and the 95% prediction interval is ±0.73 lbm/hr. These intervals were calculated based on a statistical analysis of the scatter in the data around the predicted mean using Equation 4.11.

Equation 4.11 includes 10 effects out of the 15 possible effects calculated for the 16 run test matrix. Since Phase 2 did not include any replicate test points, a better indication of confidence in the accuracy of Equation 4.11 is the uncertainty interval, which is calculated in Appendix C to be ±1.1 lbm/hr. The inclusion of replicate test points would have certainly resulted in a more reliable statistical assessment of the measured data.

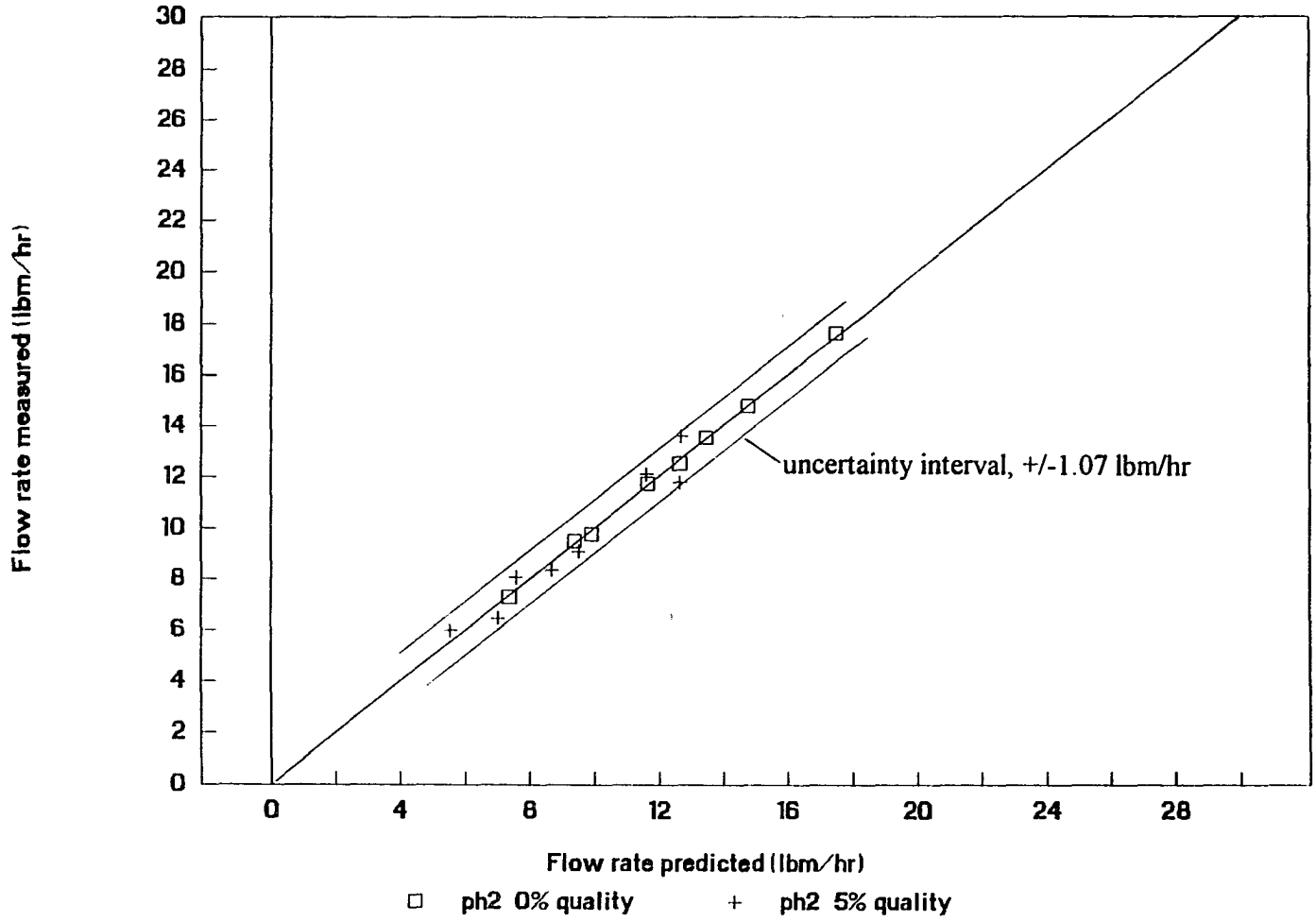

Figure 4.16: Phase 2 measured versus predicted flow rate (Equation 4.11)

In Figure 4.16, the 5% quality data points exhibit the most scatter around the correlation line. This should not be too surprising due to the inherently unstable nature of two-phase flow. This phenomena is illustrated by a measured mass flow rate plot for one of the Phase 2 test points (Figure 4.17). Early in the run, the capillary tube inlet condition was subcooled and the measured flow rate was relatively steady. At the end of the run, the quality was approaching 5% and the measured flow rate was more erratic.

Mass flow rate predictions were made for the eight test points run at 0% inlet quality using the Phase 1 subcooled inlet prediction equation, Equation 4.2, and plotted in Figure 4.18. A 0% quality inlet condition is synonymous with a 0 ° F subcool inlet condition. As can be seen, the data fall within the prediction interval associated with Equation 4.2.

Effective subcooling values were calculated for all 16 Phase 2 test points. In Figure 4.19, the calculated values are compared to predicted values by using Equation 4.4 from Phase 1, and taking the inlet subcool level, DTsc, to be 0 °F. The calculated effective subcooling values all fall within the prediction interval. Therefore, Equation 4.4 is applicable to a quality inlet condition between 0 and 5%.

Analysis of the inlet quality effect

Refrigerators are designed to operate with a slightly subcooled condition at the capillary tube inlet. Upon occasion, though, a quality inlet condition does exist. The inlet subcool level range for Phase 1 testing was 5 to 10 °F, with a calculated effect on mass flow rate of 0.12 lbm/hr. The inlet quality level range

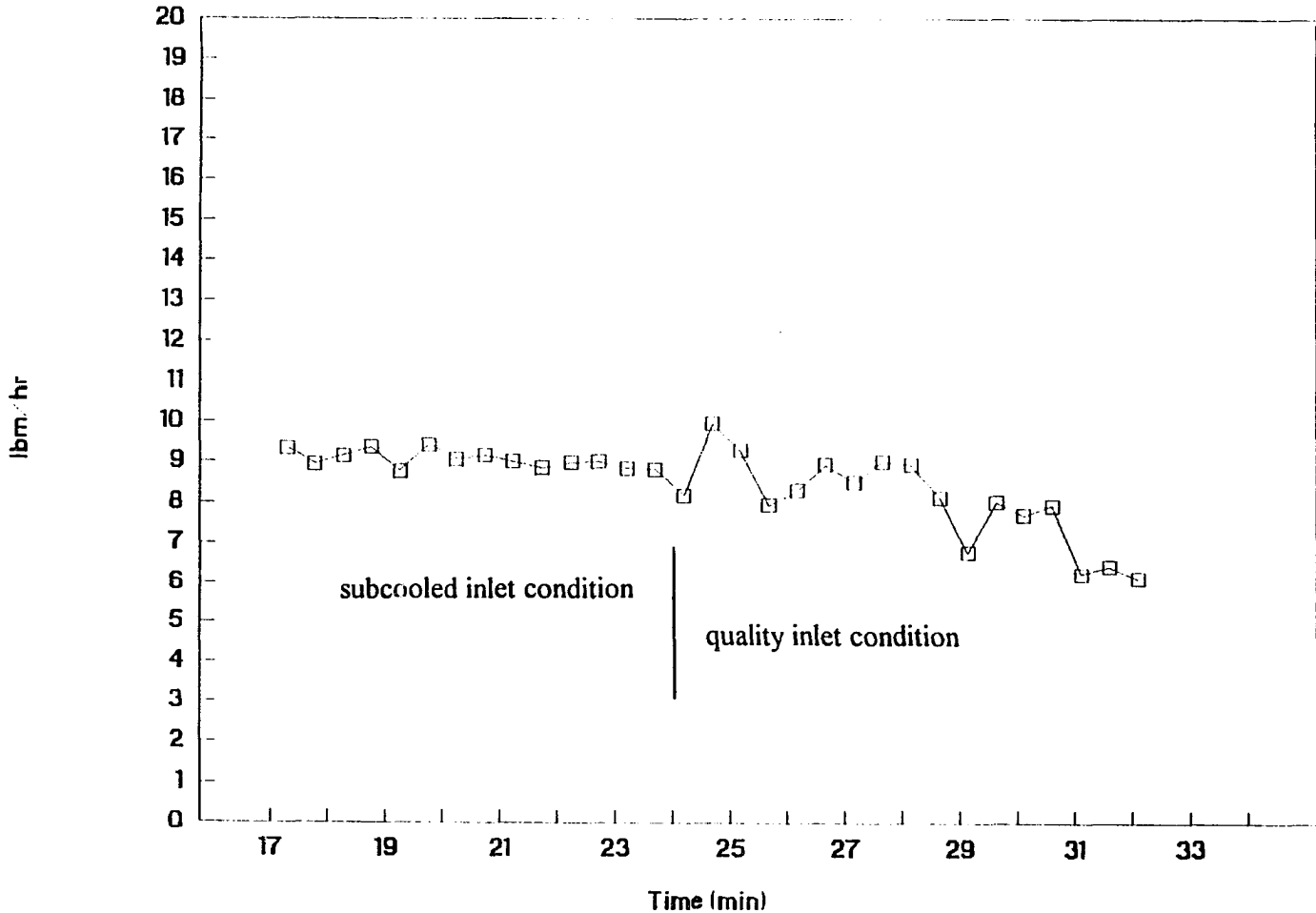

Figure 4.17: Measured flow rate during Phase 2 test point 9

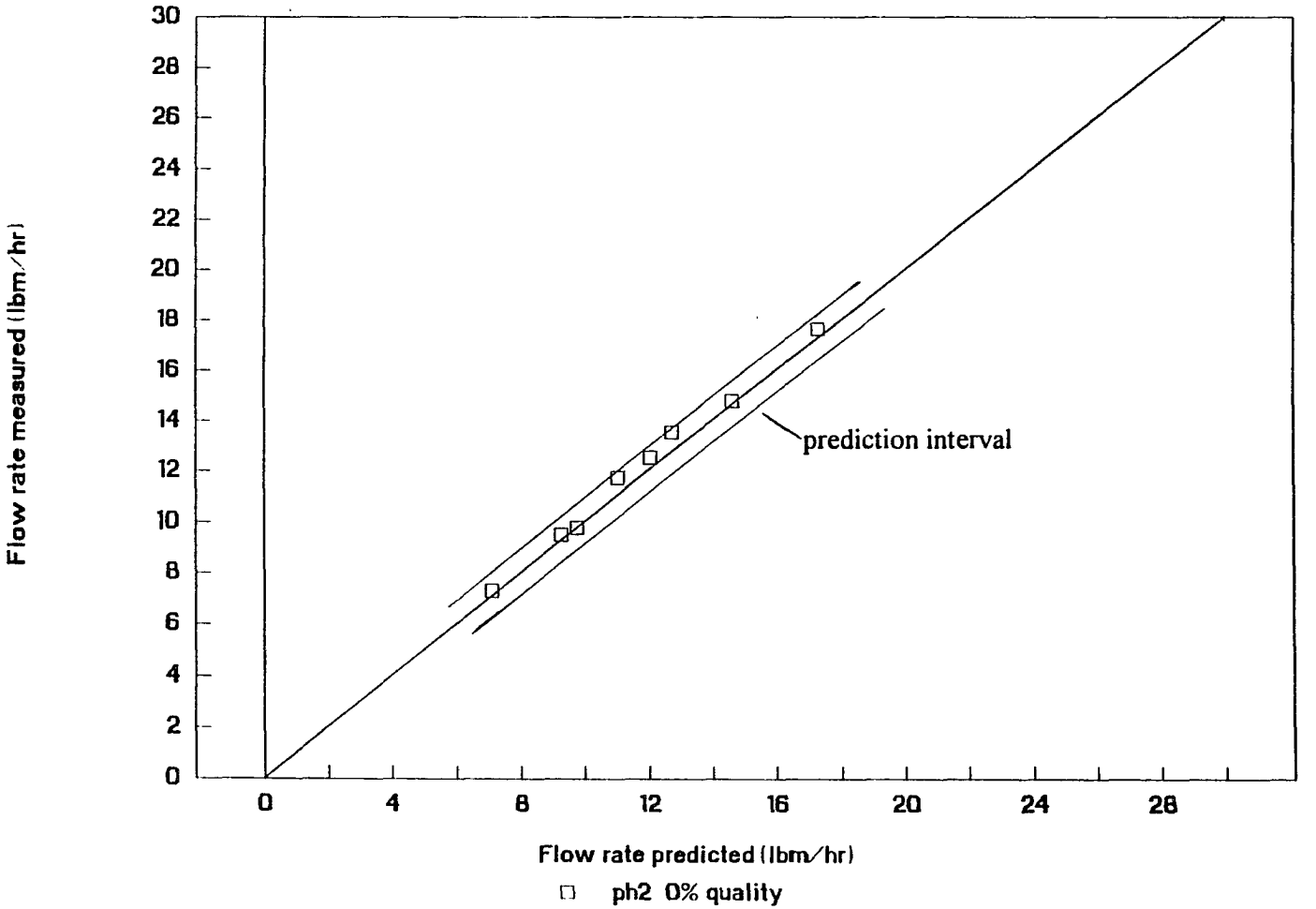

Figure 4.18: Phase 2 measured versus predicted mass flow for the 0% quality test points (Equation 4.2)

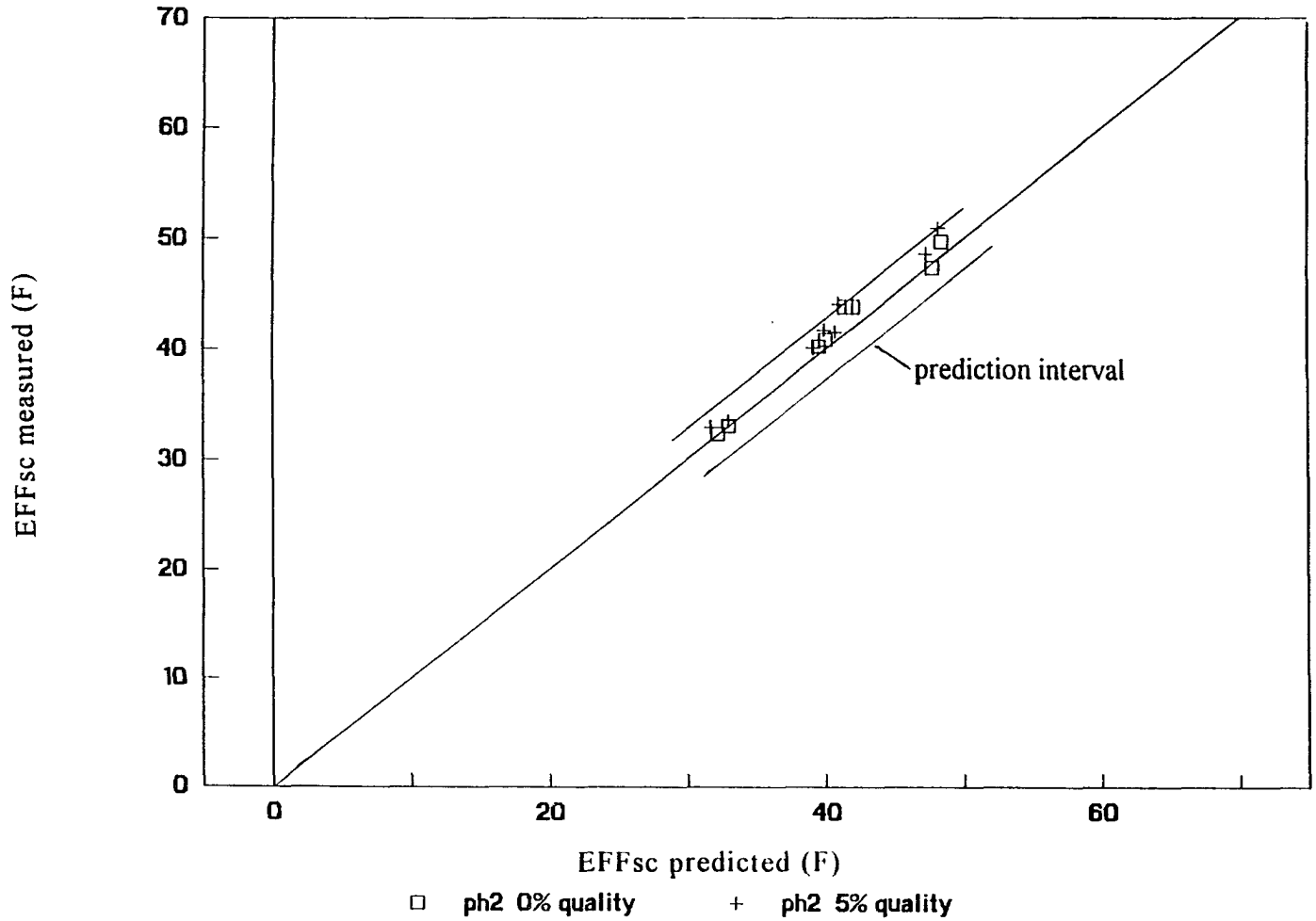

Figure 4.19: Phase 2 measured versus predicted EFFsc (Equation 4.4)

for Phase 2 testing was 0 to 5%, with an effect on mass flow rate of 1.33 lbm/hr. The comparison of effects is shown in Figure 4.20, and demonstrates that the mass flow rate can be dramatically affected when a quality condition exists at the capillary tube inlet. The difference in flow response for the two inlet regimes is, again, related to flow resistance.

The effect of an increase in inlet subcool level, DTsc, (i.e., a decrease in capillary tube inlet temperature) is an increase in mass flow rate. This is a result of a reduction in overall flow resistance caused by a delay in the vaporization point. At the 0 °F inlet subcool level, which is synonymous to the 0% quality condition, a metastable liquid length can exist within the capillary tube. If this liquid length reaches into the heat exchanger region, the heat transfer process acts to suppress the quality increase. Pate and Tree (1984b) showed maximum quality levels of less than 2% in the heat exchange region, for subcooled inlet conditions.

In comparison, no metastable liquid length can exist with a 5% inlet quality. As this liquid-vapor mixture enters the heat exchanger region, it is not known from previous research whether the heat exchanger reduces the quality level and/or suppresses the quality increase. The measured results reported herein, however, suggest that the quality condition does not disappear through the heat exchange region. The result is that the overall resistance to flow in the capillary tube is much higher relative to a subcooled inlet condition.

Analysis of effective subcooling variable effects

The effective subcooling values for all Phase 2 test points can be predicted using the Phase 1 prediction equation, Equation 4.4, even though Equation 4.4

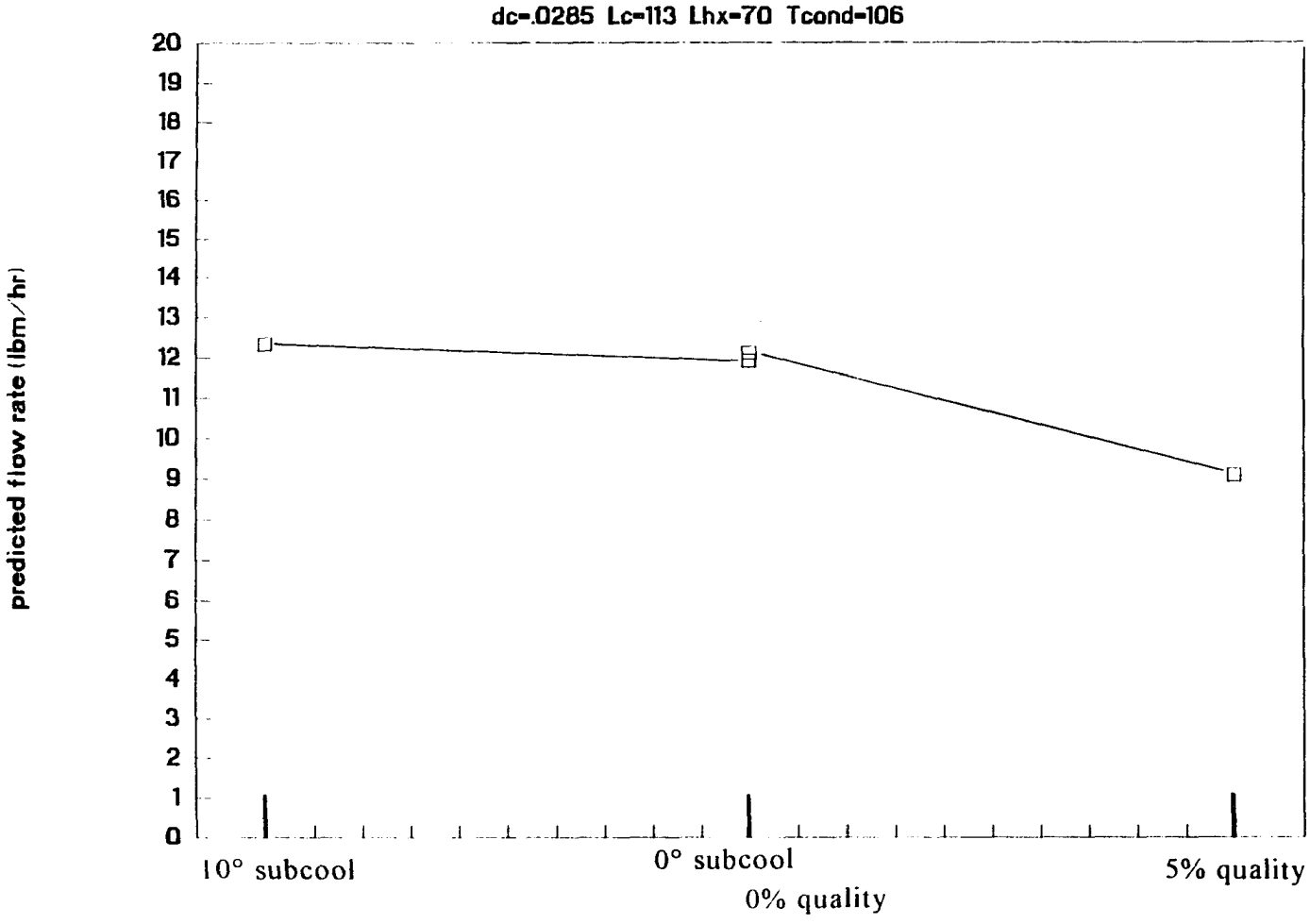

Figure 4.20: The effect of inlet condition on mass flow rate

was developed based on subcooled inlet test data (Figure 4.19). This can be explained by recalling that effective subcooling level is an indicator of the heat transfer rate between the capillary tube flow stream and the suction line flow stream. It is a function of capillary tube inlet temperature level, suction line inlet temperature level, total heat transfer area, and an overall heat transfer coefficient between the flow streams.

The overall heat transfer coefficient is controlled by the suction line heat transfer coefficient, since the capillary tube heat transfer coefficient effect is five to six times larger. For a capillary tube inlet quality change between 0% and 5%, the inlet temperature remains constant, and the capillary tube heat transfer coefficient is influenced slightly. The variables affecting effective subcooling do not change, and is why Equation 4.4 successfully predicts all Phase 2 measured effective subcooling values.

Phase 3: The oil concentration effect

Test matrix

The intent of the Phase 3 testing was to determine the effect of oil concentration on heat exchanger performance. In order to maximize experimental sensitivity to a potential oil concentration effect, Phase 3 testing was done with a subcooled inlet condition. As in Phase 2, the test matrix was a 1/2 fraction of a full two level factorial design with five independent variables. The five variables included oil concentration level (0 and 3% by weight), and four other important design variables. The four additional variables are included in order to establish

the significance of any potential oil concentration interaction effects. All five variables and their respective low (-) and high (+) test levels are given in Table 4.8.

The complete Phase 3 test matrix with all variable settings is given in Table 4.9. Each independent variable was tested eight times at the low (-) and high (+) level. A complete randomization of the run order was not possible because the oil concentration level could not be easily changed. Therefore, the first eight runs were made at the 0% concentration level, and the second eight runs were made at the 3% level.

Table 4.8: HFC-134a Phase 3 variables and test ranges

Variable	"-" level	"+" level
Tcond	95.6 F	115.7 F
dc	0.026 in	0.031 in
Lc	96 in	130 in
DTsc	0 F	5 F
%oil	0 %	3 %

Mass flow data reduction

Calculated variable effects

Measured mass flow rate data was analyzed using SAS. The calculated effects of all five main effects, plus the two factor interactions between the

Table 4.9: HFC-134a Phase 3 test matrix ("-" and "+" levels given in Table 4.8)

Test point	Tcond	dc	Lc	DT	%oil
1	-	+	+	+	-
2	+	+	+	-	-
3	+	-	+	+	-
4	-	-	+	-	-
5	+	+	-	+	-
6	-	+	-	-	-
7	-	-	-	+	-
8	+	-	-	-	-
9	-	-	+	+	+
10	+	-	+	-	+
11	+	-	-	+	+
12	-	-	-	-	+
13	+	+	-	-	+
14	-	+	-	+	+
15	+	+	+	+	+
16	-	+	+	-	+

dominant main effects, are presented in Table 4.10 and Figure 4.21. A preliminary mass flow rate prediction equation, Equation 4.12, was constructed that included the two factor interaction with a calculated effect greater than the 0.12 lbm/hr significance limit established for Phase 1 testing.

$$m_{prelim}(lbm/hr) = 12.78 + 1.38X_{Tcond} + 2.56X_{dc} - 1.08X_{Lc} + 0.12X_{\%oil} + 0.06X_{DTsc} + 0.24X_{Tcond*dc} \qquad (4.12)$$

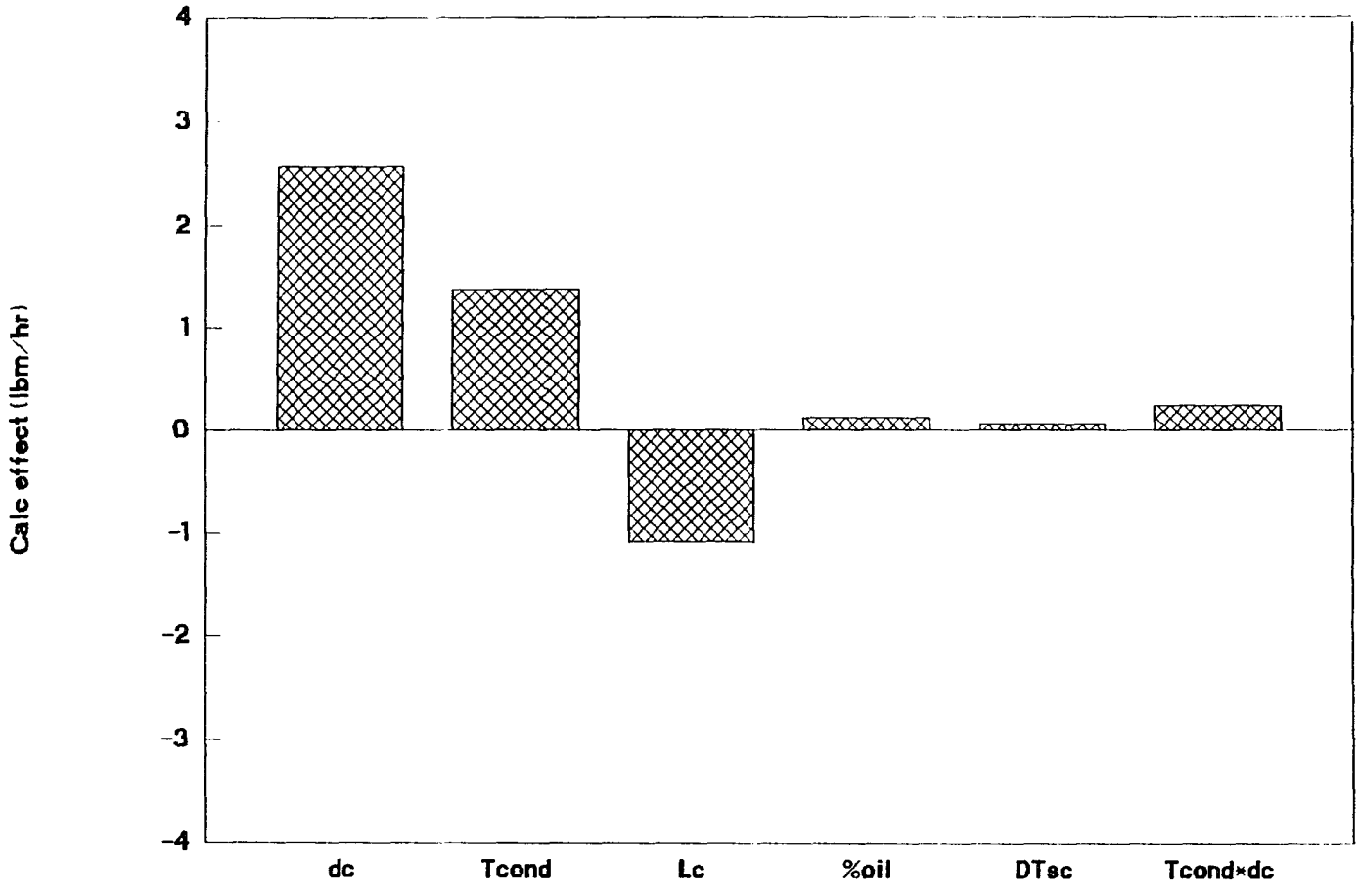

Figure 4.21: HFC-134a Phase 3 variable effects on mass flow rate

Table 4.10: HFC-134a Phase 3 calculated variable effects on mass flow rate

Main effects and interactions	Calculated effect (lbm/hr)
dc	+ 2.56
Tcond	+ 1.38
Lc	- 1.08
%oil	+ 0.12
DTsc	+ 0.06
Tcond x dc	+ 0.24

Equation 4.12 is designated "preliminary" because the statistical significance of each variable effect had not been established.

Significance limit

Phase 3 testing did not include any replicate test points. In this case, though, a significance limit could be established based on the data scatter around the predicted mean flow rate using Equation 4.12, and was calculated to be 0.16 lbm/hr. In Equation 4.12, there are only 5 potentially significant effects (excluding the DTsc effect) out of 16 test points, which allows for a reasonable estimation of a significance limit. Since the calculated effect on mass flow rate of oil concentration level was 0.12 lbm/hr, the oil effect was deemed insignificant.

Analysis of mass flow variable effects

Again, the primary purpose of Phase 3 testing was to experimentally evaluate the effect of oil concentration on heat exchanger performance. The oil concentration variable, %oil, was included with the four other important design variables in order to investigate potential interaction effects. Based on the calculated significance limit of 0.16 lbm/hr within the Phase 3 testing, oil concentration between 0% and 3% does not have a statistically significant effect on mass flow rate.

Mass flow rate predictions were made for all Phase 3 test point using the Phase 1 subcooled inlet correlation, Equation 4.2, and plotted in Figure 4.22. As can be seen, the data falls within the prediction interval associated with Equation 4.2.

Effective subcooling data reduction

Calculated variable effects

Effective subcooling data was analyzed using SAS. The calculated effects of all five independent variables are presented in Table 4.11, and Figure 4.23. A preliminary effective subcooling level prediction equation, Equation 4.13, was constructed that included only the main effects from Table 4.11. No two factor interactions had calculated effects greater than the significance limit of 0.26 °F established for the Phase 1 experimental results.

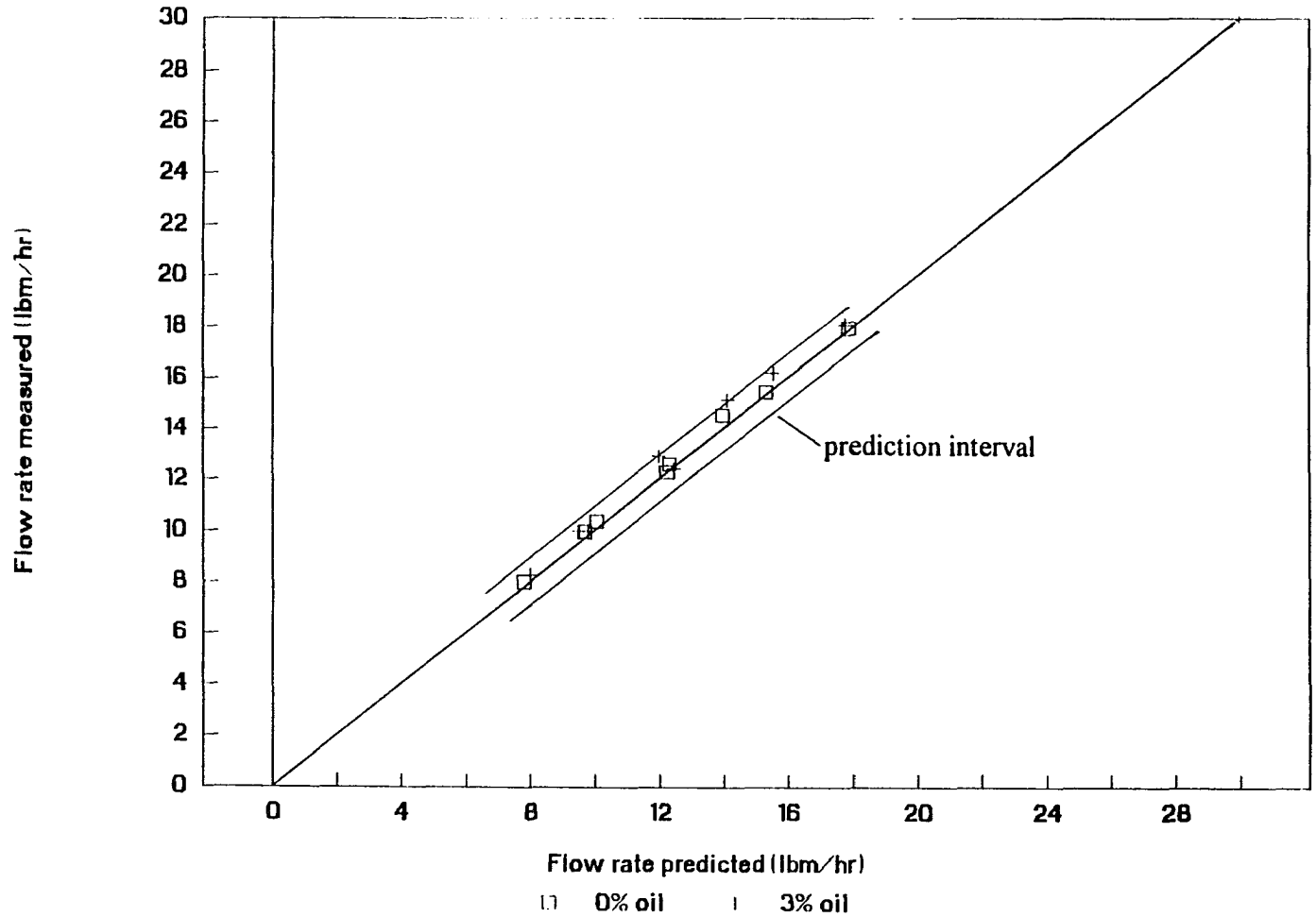

Figure 4.22: Phase 3 measured versus predicted mass flow (Equation 4.2)

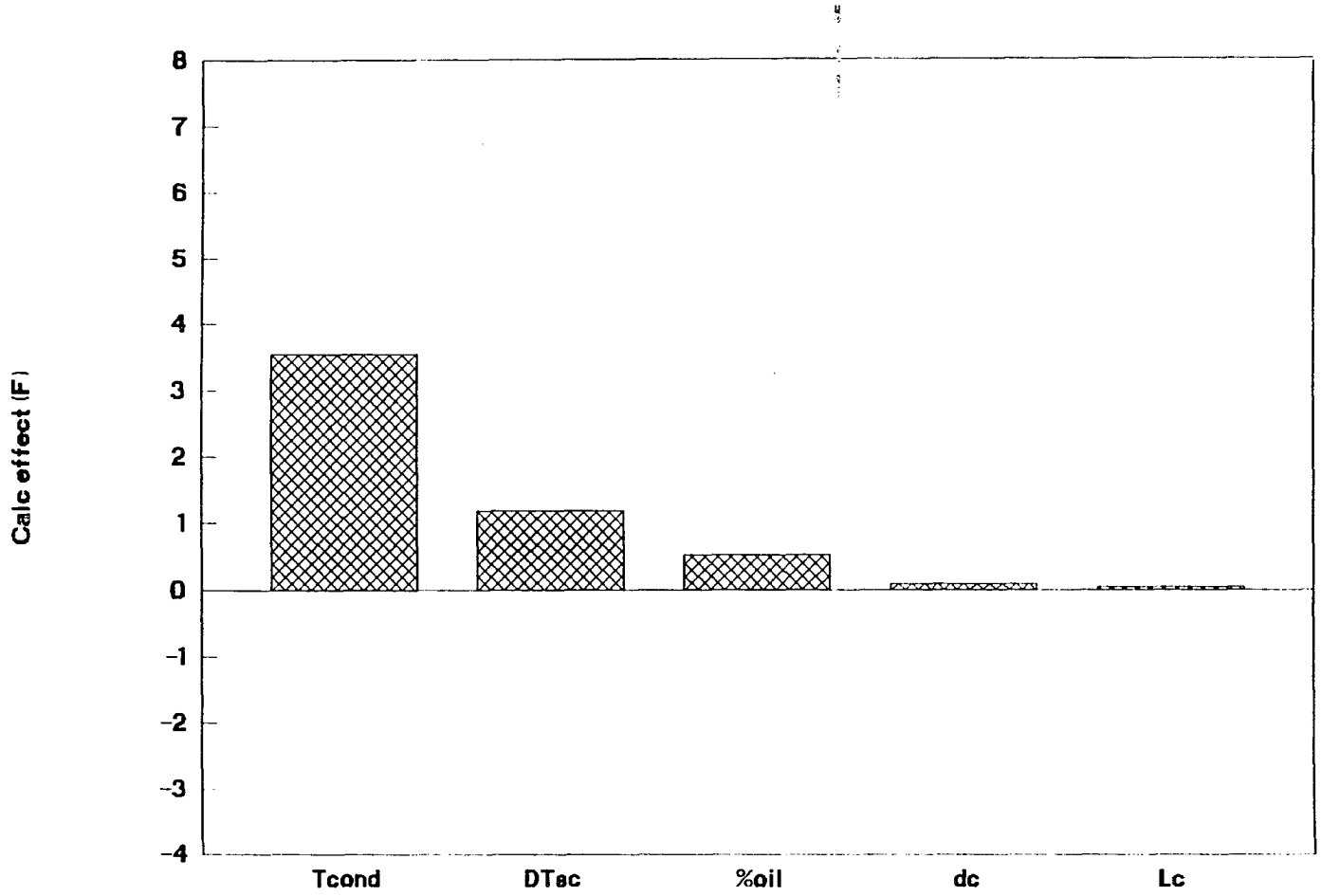

Figure 4.23: HFC-134a Phase 3 variable effects on EFFsc

Table 4.11: HFC-134a Phase 3 calculated variable effects on EFFsc

Main effects and interactions	Calculated effect (°F)
Tcond	+ 3.54
DTsc	+ 1.18
%oil	+ 0.52
dc	+ 0.08
Lc	+ 0.04

$$EFFsc_{prelim}(F) = 48.5 + 3.54X_{Tcond} - 1.18X_{DTsc} + 0.52X_{\%oil} + 0.08X_{dc} + 0.04X_{Lc} \quad (4.13)$$

Significance limit

As in the mass flow rate data analysis, the significance limit could be established based on the data scatter around the predicted mean effective subcooling level using Equation 4.13, and was calculated to be 0.31 °F. Since the calculated effect on effective subcooling of oil concentration level was 0.52 °F, the oil concentration effect was deemed statistically significant.

Analysis of effective subcooling variable effects

The variable of interest in Phase 3 testing is the oil concentration, %oil. The calculated effect of 0.52 °F means that for an oil concentration level change

between 0% and 3%, the effect on effective subcooling is an increase in 1.04 °F. Relative to effective subcooling levels of 40 to 50 °F, this is a small effect. But since it was deemed statistically significant, further explanation is in order.

There are two possible reasons for the measured behavior. The first has to do with the manner in which the testing was done. The 16 test points could not be run in completely random order, since changing the oil concentration between the 0% and 3% levels was not convenient. Therefore, the eight 0% oil concentration test points were run first, followed by the eight 3% oil concentration test points. The calculated effect could be simply a result of a bias in the data, gradually introduced while the testing progressed. Random data procurement would have reduced the possibility of a bias in the calculated effects.

In formulating a physical reason for the results, recall again that effective subcooling is an indicator of the heat transfer rate between the two flow streams. The oil concentration effect may originate in the suction line heat transfer coefficient, which controls the overall heat transfer coefficient. As the oil passes through the suction line as a film along the wall, the film alone would act to increase the resistance to heat transfer between the flow streams, thereby reducing the effective subcooling level. In order for the effective subcooling level to increase, the suction line heat transfer coefficient must be enhanced by the oil film . A possible rationale for the enhancement is that a small amount of liquid refrigerant remains within the oil film. The continuous evaporation along the suction line wall acts to enhance the suction line heat transfer coefficient, and effective subcooling increases.

An oil concentration effect term was added to the effective subcooling equation, Equation 4.4, resulting in Equation 4.14.

$$EFFsc_{pred}(F) = 39.2 + 0.3156(Tcond-108.6) - 0.4735(DTsh-12.85)$$
$$+ 0.1815(Lhx-55)- 0.9262(LP-21.4) - 28.54(ds-0.260)$$
$$- 0.2188(DTsc-8.2) - 143.6(dc-0.0285)$$
$$+ 3.116x10^{-3}(Lhx-55)(Tcond-108.6) - 0.343(Tcond-108.6)(ds-0.260)$$
$$+ 0.756(ds-0.260)(DTsh-12.85)$$
$$+ 1.829x10^{-3}(Tcond-108.5)(DTsh-12.85) + 0.347(\%oil-1.5) \quad (4.14)$$

A plot of measured versus predicted effective subcooling using Equation 4.14 is given in Figure 4.24 and shows good agreement.

Summary

The experimental results for HFC-134a testing can be summarized as follows.

1. Capillary tube-suction line heat exchanger performance was thoroughly evaluated for a wide range of design variables applicable to household refrigerator units.
2. Phase 1 testing investigated the effect of nine design variables on performance. All testing was done with a subcooled condition at the capillary tube inlet. Performance prediction equations were developed from the experimental database, and verified using production stock heat exchangers. In conclusion:

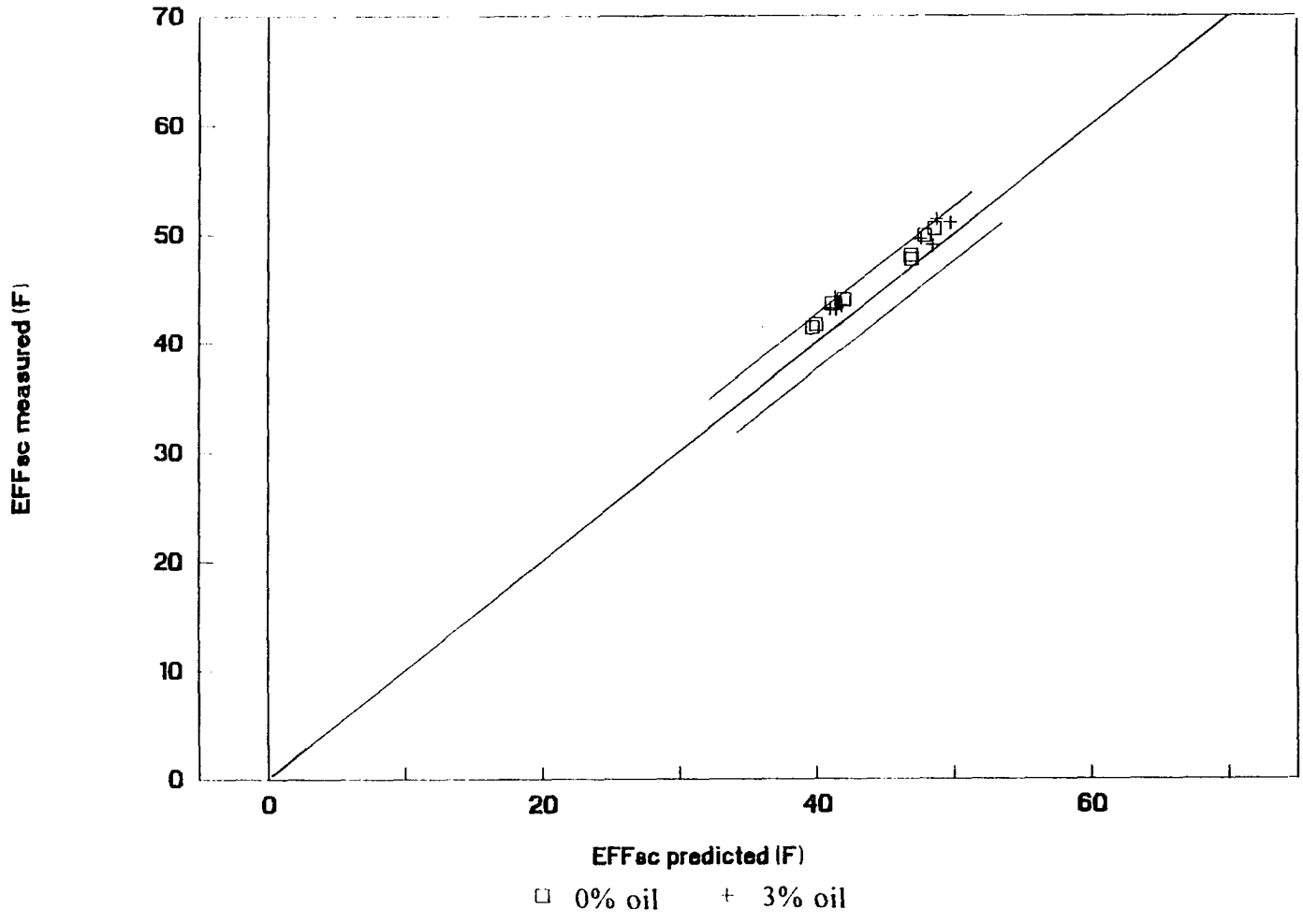

Figure 4.24: HFC-134a Phase 3 measured versus predicted EFFsc (Equation 4.14)

- o Design variables having the most significant effect on mass flow rate included the condenser temperature and capillary tube diameter and length.
- o Design variables having the most significant effect on effective subcooling level included condenser temperature, heat exchanger length, and suction line diameter.

3. Phase 2 testing investigated the effect on performance of an inlet quality between 0% and 5%. A quality inlet mass flow rate prediction equation was also developed. In conclusion:
   - o An inlet quality increase from 0% to 5% has the effect of decreasing mass flow rate.
   - o The response in mass flow rate for an inlet quality change between 0% and 5% is much greater than the response for an inlet subcool level change between 5 °F and 10 °F.
   - o An inlet quality increase from 0% to 5% has no effect on effective subcooling.
4. Phase 3 testing investigated the effect on performance of an oil concentration level change between 0% and 3%. In conclusion:
   - o Oil concentration does not have a statistically significant effect on mass flow rate.
   - o Oil concentration does have a statistically significant effect on effective subcooling.
5. The knowledge gained from the HFC-134a experimental results was used in designing test plans for HFC-152a and CFC-12.

CHAPTER 5. EXPERIMENTAL RESULTS FOR HFC-152a

HFC-152a, like HFC-134a, is a potential replacement for CFC-12 because it has similar saturation properties. HFC-152a and HFC-134a both have a zero ozone depletion potential (ODP); however, the global warming potential (GWP) for HFC-152a is only 10% of the GWP for HFC-134a, which makes it more environmentally attractive. The major hindrance to wide acceptance of HFC-152a by domestic refrigeration equipment manufacturers is its flammability, whereas HFC-134a is not flammable. Even so, there is still interest internationally in using HFC-152a in smaller refrigeration systems requiring a small charge, such as household refrigerators.

A recent investigation by Pannock, et. al. (1994) compared household refrigerator performance using HFC-152a and HFC-134a. They concluded that there was no significant difference between the two working fluids, in terms of system performance. But in terms of charge, they also reported that the HFC-152a system requires roughly 40% less refrigerant by mass, which may eventually help attenuate the flammability concerns.

For the current study, the HFC-152a heat exchanger performance testing included one 16 run matrix, plus limited replication testing. Since refrigerators are typically designed to operate with a slightly subcooled condition at the capillary tube inlet, HFC-152a testing was done with a subcooled inlet condition. In addition, all tests were run with pure HFC-152a, i.e., without oil. The details of the testing follow.

Test matrix

The HFC-152a test matrix was a 1/16 fraction of a full two level factorial design with eight independent design variables (resolution IV). A full factorial design with eight variables would include 256 (or 2^8) test points, while a 1/16 fraction includes 16 (1/16 of 256) test points. The eight variables and their respective low (-) and high (+) test levels are given in Table 5.1.

The HFC-134a data analysis concluded that the refrigerator evaporator pressure had no effect on mass flow rate. Therefore, HFC-152a testing did not include the evaporator pressure (LP) variable effect. Evaporator pressure was fixed to correspond to a 0 °F saturation pressure. The potential effect of suction line temperature on mass flow and effective subcooling would be indicated by the suction line inlet temperature, T_{s1}.

The complete test matrix with all variable settings is given in Table 5.2. Each independent variable is tested eight times at the low (-) and high (+) level, providing balance to the testing. The test matrix uses 16 different heat exchanger assemblies. In keeping with the requirements of a statistical design, the 16 test points were run in random order. Four replicate test points were also included in the testing, and the measured data was factored into calculating significance limits.

Table 5.1: HFC-152a variables and test ranges

Variable	"-" level	"+" level
Tcond	100 F	120 F
dc	0.026 in	0.031 in
ds	0.201 in	0.319 in
Lc	96 in	130 in
Lhx	30 in	70 in
Linlet	6 in	20 in
DTsc	5 F	15 F
T_{s1}	5 F	20 F

Table 5.2: HFC-152a test matrix ("-" and "+"levels in Table 5.1)

Run	Tcond	dc	Lc	DTsc	Lhx	T_{s1}	ds	Linlet
1	+	-	-	-	-	+	+	+
2	+	-	+	+	+	-	-	+
3	+	+	+	-	-	-	+	-
4	-	-	+	-	+	+	+	-
5	-	-	-	+	+	+	-	+
6	-	-	+	+	-	-	+	+
7	-	+	+	-	-	+	-	+
8	-	+	-	-	+	-	+	+
9	+	-	-	+	+	-	+	-
10	+	+	+	+	+	+	+	+
11	-	-	-	-	-	-	-	-
12	-	+	+	+	+	-	-	-
13	+	-	+	+	-	+	-	-
14	+	+	-	-	+	+	-	-
15	-	+	-	+	-	+	+	-
16	+	+	-	+	-	-	-	+

Mass flow data reduction

Calculated variable effects

Measured mass flow rate data from the core test matrix was analyzed using SAS. All eight main effects, plus the two factor interactions between the dominant main effects, are presented in Table 5.3 and Figure 5.1. A preliminary mass flow rate prediction equation, Equation 5.1, was constructed including the main effects given in Table 5.3 greater than 0.12 lbm/hr (based on HFC-134a results), plus the interactions.

Table 5.3: HFC-152a calculated variable effects on mass flow rate

Main effects and interactions	Calculated effect (lbm/hr)
dc	+ 2.07
Tcond	+ 1.08
Lc	- 0.92
Lhx	+ 0.27
DTsc	+ 0.15
ds	- 0.12
T_{s1}	+ 0.05
Linlet	- 0.03
dc x Tcond	+ 0.23
Lc x Tcond	- 0.14
dc x Lc	- 0.17

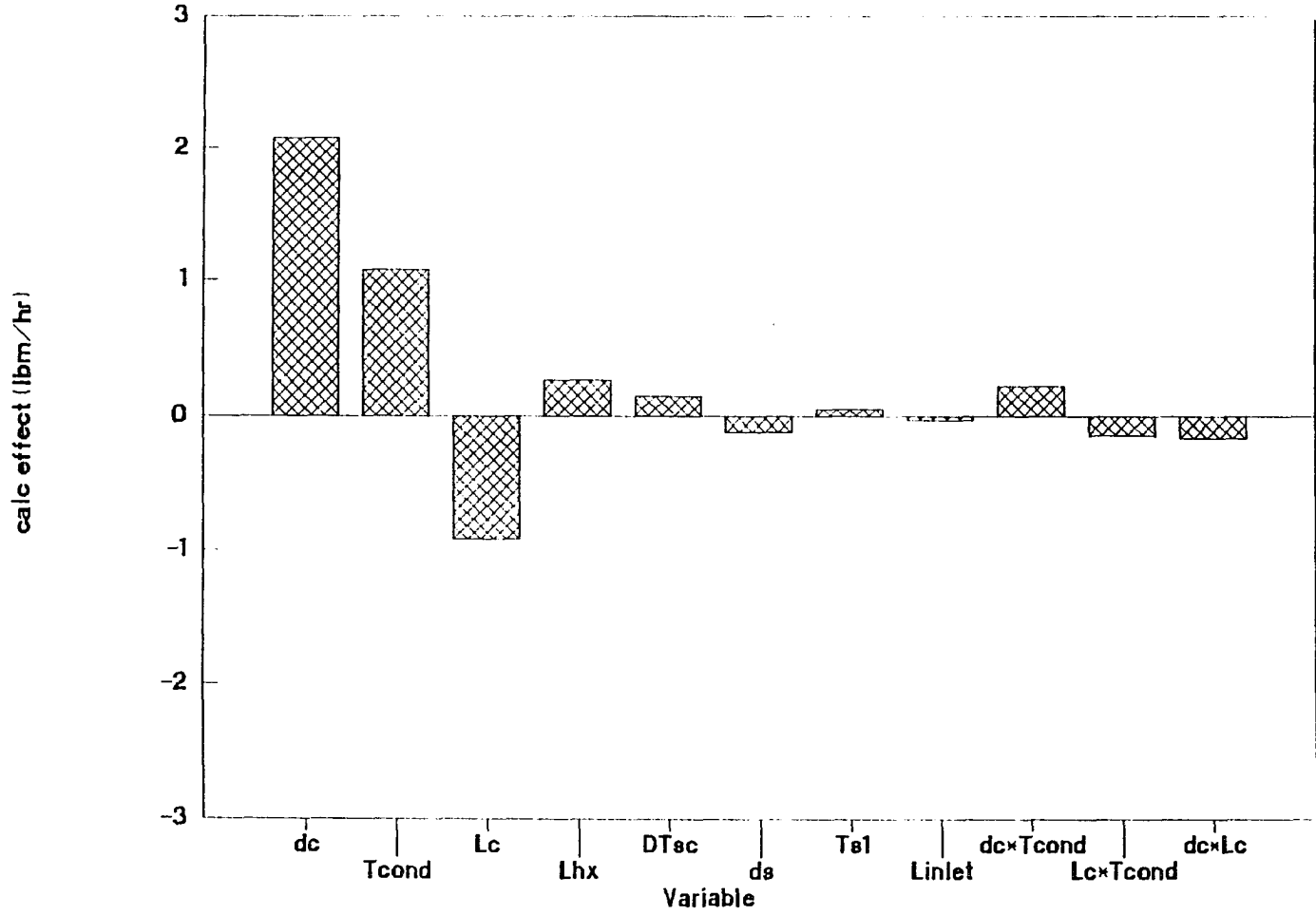

Figure 5.1: HFC-152a variable effects on mass flow rate

$$\dot{m}_{prelim}(lbm/hr) = 10.39 + 2.07X_{dc} + 1.08X_{Tcond} - 0.92X_{Lc} + 0.27X_{Lhx} + 0.15X_{DTsc} - 0.12X_{ds} + 0.23X_{dc*Tcond} - 0.14X_{Lc*Tcond} - 0.17X_{dc*Lc} \quad (5.1)$$

Equation 5.1 was designated "preliminary" because the statistical significance of each variable effect had not yet been established. The interpretation of Equation 5.1 is the same as previously given for Equation 4.1.

Significance limit

The statistical significance of the calculated effects was determined by comparison to a function of the experimental error. By analyzing the data scatter surrounding a predicted mean response using Equation 5.1 and by including the four replicate test points, the significance limit was determined to be 0.16 lbm/hr. Calculated main effects and interactions beyond 0.16 lbm/hr were included in the final prediction equation. Supporting SAS analysis output is included in Appendix E.

Prediction equation

The final mass flow rate prediction equation is given in Equation 5.2, and includes all effects greater than 0.16 lbm/hr.

$$\dot{m}_{pred}(lbm/hr) = 10.39 + 828.8(dc-.0285) + 0.1079(Tcond-110) - 0.054(Lc-113) + 0.0134(Lhx-50) + 0.030(DTsc-9.85) + 9.36(dc-.0285)(Tcond-110) - 4.024(dc-.0285)(Lc-113) \quad (5.2)$$

In using Equation 5.2, variable units must be consistent with the units specified in the nomenclature listing.

In comparing Equation 5.2 with its preliminary form, the ds variable and Lc*Tcond interaction do not appear in the final equation because these effects failed the test for significance. Although the inlet subcool level (DTsc) effect did not quite meet the significance limit, the effect was retained in the final equation due to its importance to the heat exchanger design process.

A plot of measured versus predicted mass flow rate using Equation 5.2 for all test data is given in Figure 5.2, and shows good agreement. The 95% confidence interval for Equation 5.2 is ±0.44 lbm/hr, and the 95% prediction interval (shown in Figure 5.2) is ±0.83 lbm/hr. These intervals are calculated based on a statistical analysis of the scatter in the data around the predicted mean value. The implicit assumption of a normal distribution of residuals in the data around the predicted mean values was verified.

Analysis of variable effects

The calculated effects of all the significant variables are in reasonably close agreement with those calculated for HFC-134a. Small differences are mainly associated with differences in refrigerant thermodynamic and thermophysical

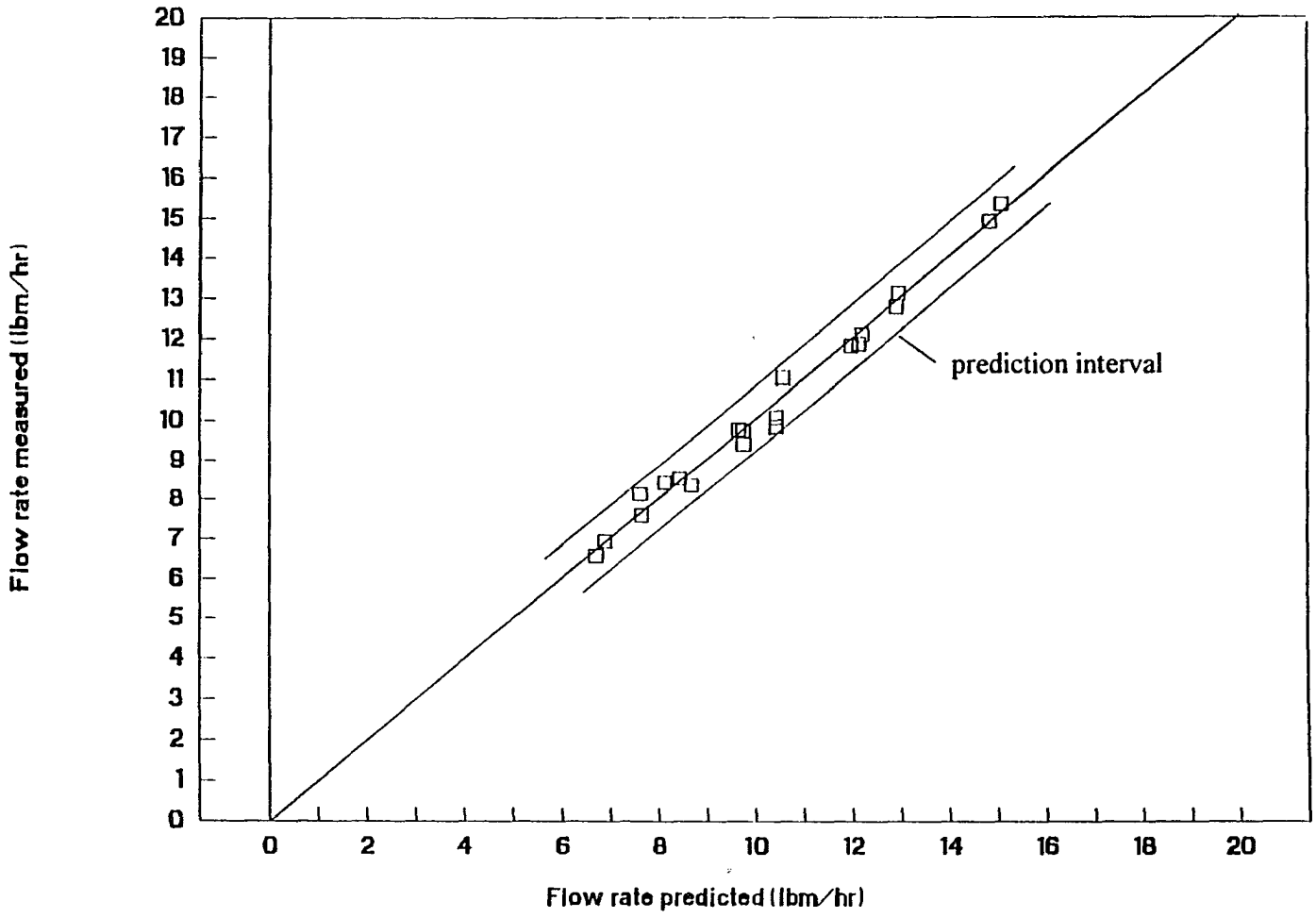

Figure 5.2: HFC-152a measured versus predicted flow rate (Equation 5.2)

properties. An evaluation of the effects of properties on mass flow rate is presented in Chapter 7 as part of the development of the general mass flow rate prediction procedure.

A noticeable exception is the calculated effect of condenser temperature on flow response. For HFC-152a, the calculated effect is 1.08 lbm/hr, while for HFC-134a, the calculated effect is 3.24 lbm/hr. Most of this difference can be attributed to a difference in condenser temperature test range. The HFC-134a test range was 85 to 132 °F, and the HFC-152a test range was 100 to 120 °F. Since the change in saturation temperature with respect to saturation pressure for both refrigerants is approximately the same, the effect on mass flow rate of a 20 °F condenser temperature range will be less than a 47 °F range. The remainder of the difference in calculated effect is associated with the property differences between the two refrigerants.

One other exception of interest is the suction line inlet temperature variable effect. In the HFC-134a Phase 1 test, the suction line inlet superheat variable, DTsh, was tested at the 5 and 20 °F levels, and the calculated effect was deemed significant at -0.28 lbm/hr. As was explained, this helped confirm the positive effect of heat transfer rate on mass flow response. The HFC-152a results also concluded that heat transfer rate has a positive effect on mass flow response, as demonstrated by the effects of capillary tube inlet subcool (DTsc) and the heat exchanger length (Lhx). In the HFC-152a test, though, the inlet temperature variable, T_{sl}, was tested at 5 and 20 °F, and was deemed insignificant at +0.05 lbm/hr.

Making the insignificant effect of T_{sl} on mass flow response even more paradoxical, its calculated effect on effective subcooling, EFFsc, is -2.90 °F,

which compares reasonably well to the 3.29 °F effect of DTsh on EFFsc for HFC-134a. This effectively eliminates the possibility of a difference in thermophysical properties being the cause of the difference in the suction line inlet condition effect on mass flow rate.

There is a possible explanation for the insignificant suction line inlet temperature effect that must be considered when using a fractional factorial design. The net T_{sl} effect may actually be buried within one or more insignificant interaction effects. In a resolution IV design like the HFC-152a test matrix, the inherent confounding amongst two factor interactions can sometimes make differentiation between two factor interactions impossible. This is a drawback of using fractional factorial designs of resolution IV. The ideal solution is to take enough data so that all two factor interactions are confounded with three factor and higher interactions, as is the case with designs of resolution V and higher. In the HFC-152a case, however, the T_{sl} effect will have to remain as an insignificant effect.

Effective subcooling data reduction

Calculated variable effects

Effective subcooling data from the test matrix were analyzed by using SAS. All eight main effects, plus the two factor interactions between the dominant main effects, are presented in Table 5.4 and Figure 5.3. A preliminary effective subcooling prediction equation, Equation 5.3, was constructed that included the

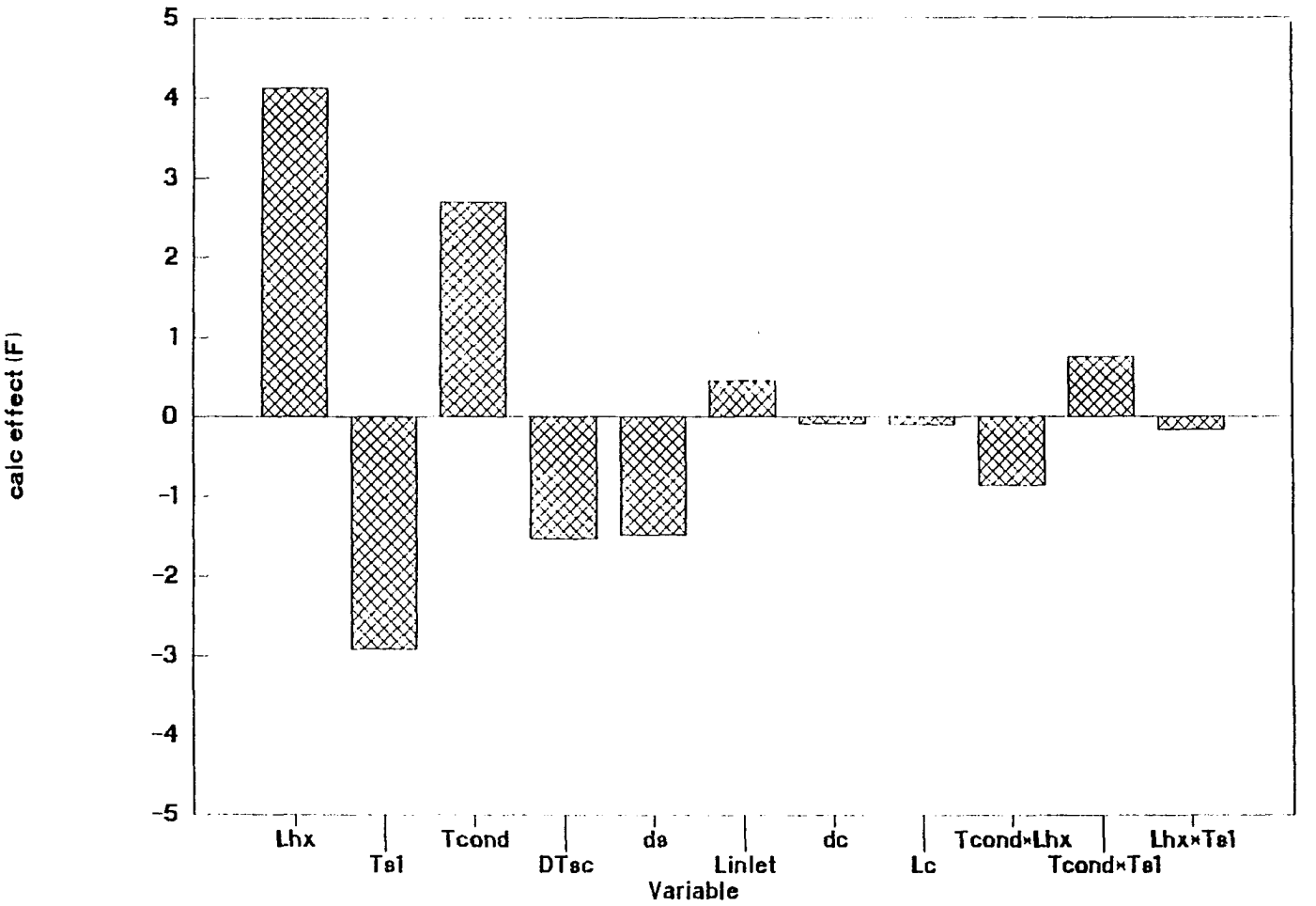

Figure 5.3: HFC-152a variable effects on EFFsc

Table 5.4: HFC-152a calculated variable effects on EFFsc

Main effects and interactions	Calculated effect (°F)
Lhx	+ 4.13
T_{s1}	- 2.90
Tcond	+ 2.70
DTsc	- 1.53
ds	- 1.48
Linlet	+ 0.45
dc	- 0.08
Lc	- 0.10
Tcond x Lhx	- 0.86
Tcond x T_{s1}	+ 0.76
Lhx x T_{s1}	- 0.16

main effects and interactions given in Table 5.4 greater than 0.26 °F (based on HFC-134a results).

$$EFFsc_{prelim}(F) = 37.6 + 4.13X_{Lhx} - 2.90X_{Ts1} + 2.70X_{Tcond} - 1.53X_{DTsc} - 1.48X_{ds} + 0.45X_{Linlet} - 0.86X_{Tcond*Lhx} + 0.76X_{Tcond*Ts1} \quad (5.3)$$

The interpretation of the terms in Equation 5.3 is the same as previously given in Chapter 4 for Equation 4.1.

Significance limit

As in the mass flow rate data analysis, the statistical significance of all calculated effects on effective subcooling was determined by comparison to a function of the experimental error. By analyzing the data scatter surrounding a predicted mean response using Equation 5.3 and by including the four replicate test points, the significance limit was determined to be 0.46 °F. Calculated main effects and interactions effects beyond 0.46 °F were included in the final prediction equation. Supporting SAS analysis output is included in Appendix E.

Prediction equation

The final effective subcooling prediction equation is given in Equation 5.4 below, and includes effects greater than 0.46 °F.

$$\begin{aligned} EFFsc_{pred}(F) = {} & 37.6 + 0.206(Lhx-50) - 0.443(Ts1-13.1) + 0.270(Tcond-110) \\ & - 0.314(DTsc-9.85) + 0.0043(Lhx-50)(Tcond-110) \\ & - 25.0(ds-0.260) + 0.0116(Tcond-110)(Ts1-13.1) \end{aligned} \qquad (5.4)$$

In using Equation 5.4, variable units must be consistent with the units specified in the nomenclature listing.

In comparing Equation 5.4 with its preliminary form, Equation 5.3, the Linlet variable has been eliminated from the final equation because it failed the test for significance.

A plot of measured versus predicted effective subcooling using Equation 5.3 is given in Figure 5.4, and shows good agreement. The 95% confidence interval for Equation 5.3 is ±1.5 °F, and the 95% prediction interval (shown in Figure 5.4) is ±2.8 °F.

Analysis of variable effects

There were no surprises with the trends in the calculated effects. The effects of Tcond, DTsc, and Ts1 on EFFsc were significant because these variables define EFFsc, as was discussed in Chapter 4. The variable Lhx and ds effect the heat transfer rate between flow streams, and thus, EFFsc, as was also the case for HFC-134a. The differences in the HFC-152a and HFC-134a calculated effects of Tcond and Lhx are mainly due to differences in variable ranges tested. Other smaller differences are associated with differences in refrigerant thermodynamic and thermophysical properties. An evaluation of the effects of properties on effective subcooling is presented in Chapter 7 as part of the development of the general effective subcooling prediction procedure.

Performance prediction verification

The HFC-152a performance prediction equations were checked for the possibility of nonlinear variable effects on the response variables. Five mid-range level test points were defined for different combinations of the most significant variables affecting heat exchanger performance. These test points were run using production heat exchanger assemblies supplied by a refrigerator manufacturer.

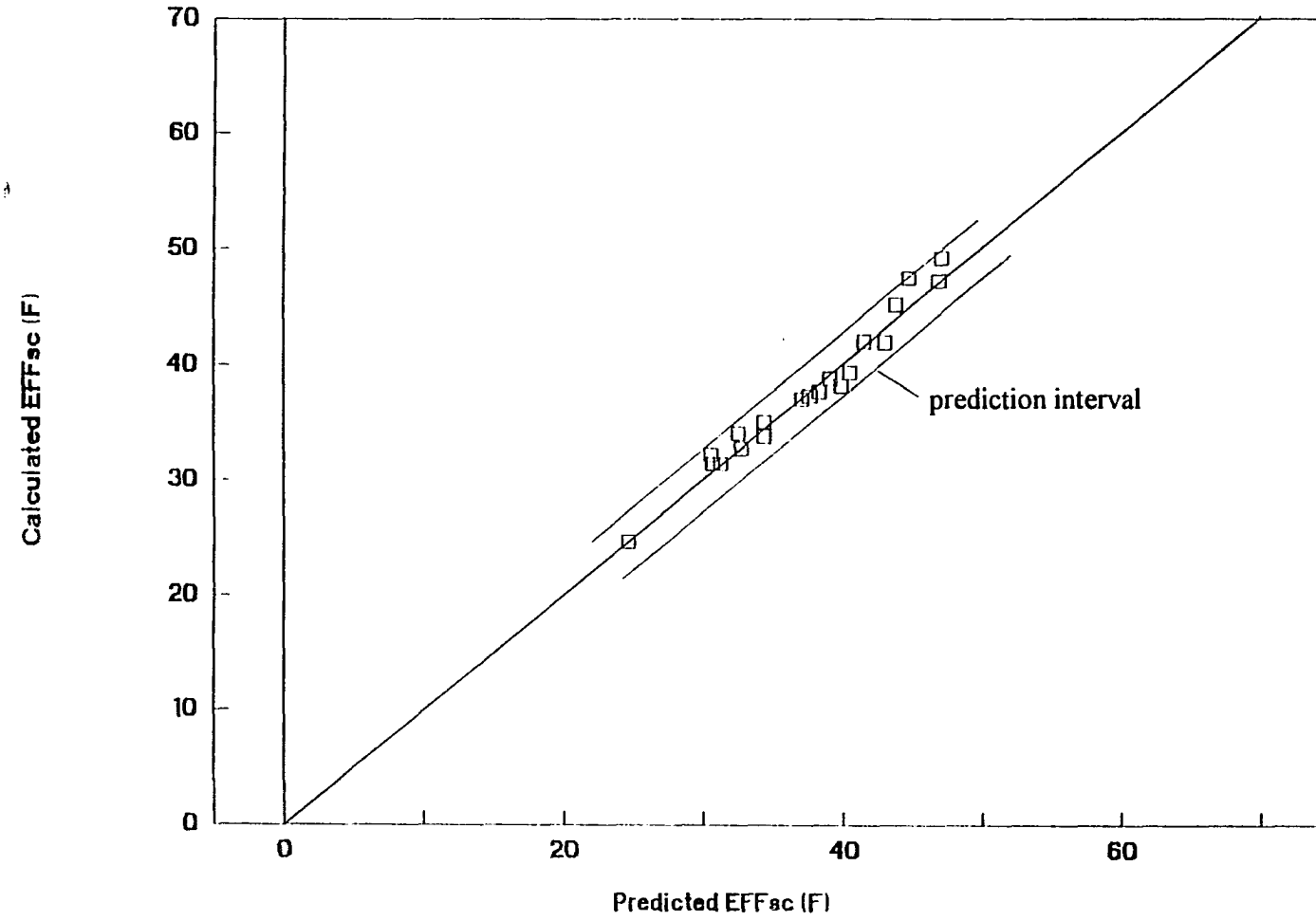

Figure 5.4: HFC-152a measured versus predicted EFFsc (Equation 5.4)

In Figure 5.5, measured mass flow rate is compared to predictions using Equation 5.2. All data falls within the 95% prediction interval. Likewise, in Figure 5.6, measured effective subcooling is compared to predictions using Equation 5.4. Again, all data falls within the 95% prediction interval.

The final conclusion was that there were no significant nonlinear effects on mass flow rate and effective subcooling for the range of variable levels tested.

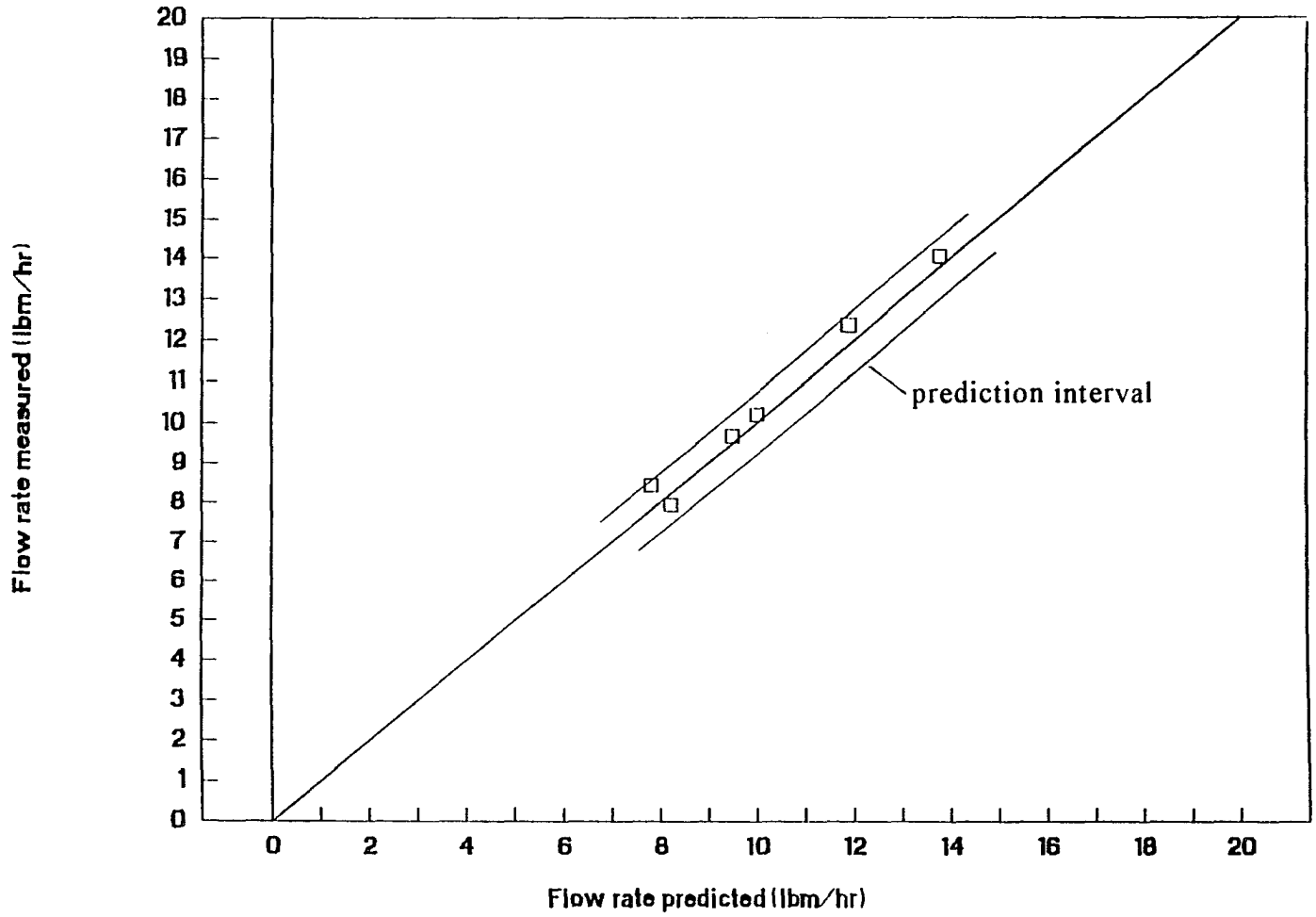

Figure 5.5: HFC-152a mid-range level test points, measured versus predicted mass flow rate (Equation 5.2)

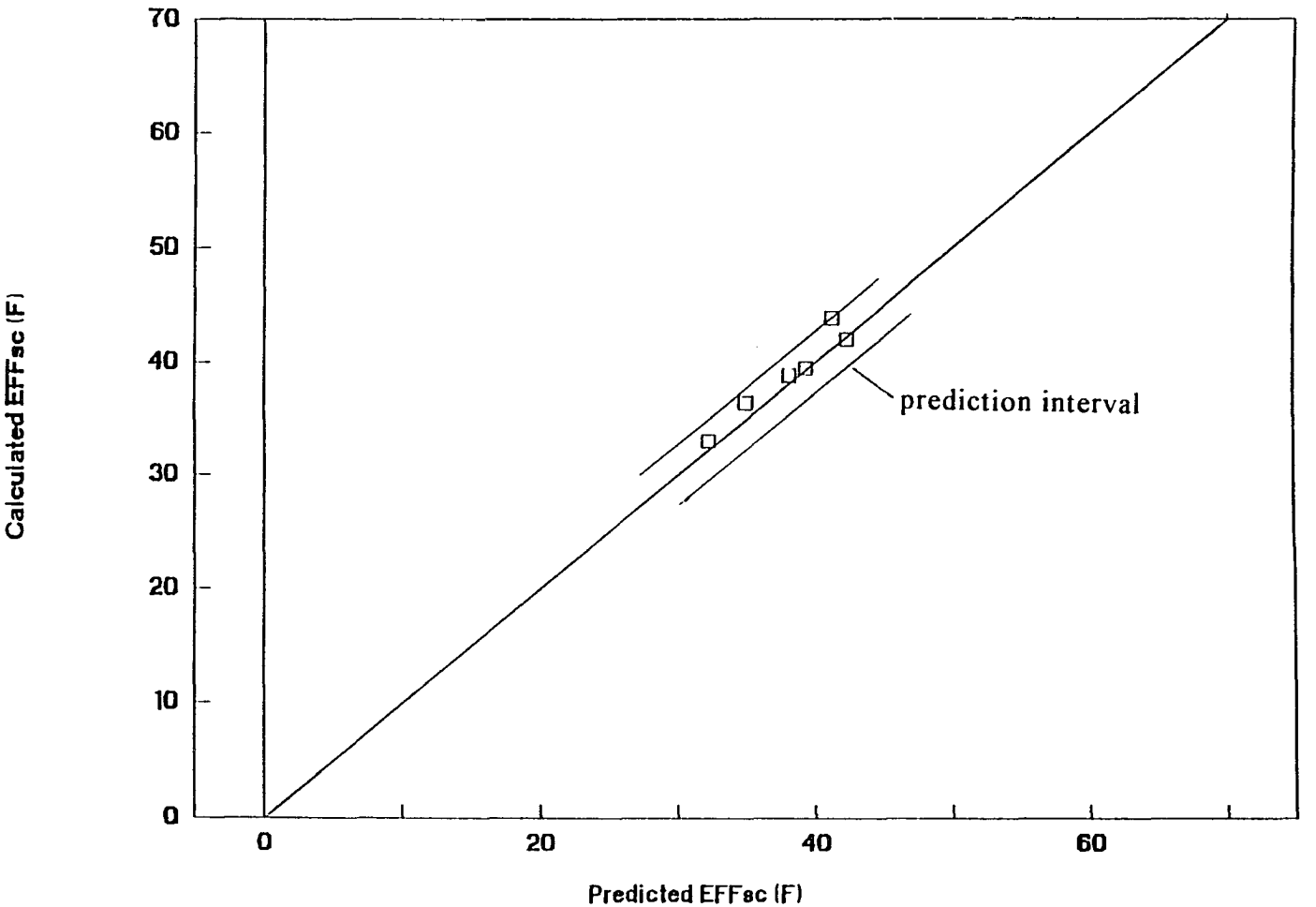

Figure 5.6: HFC-152a mid-range level test points, measured versus predicted EFFsc (Equation 5.2)

CHAPTER 6. EXPERIMENTAL RESULTS FOR CFC-12

CFC-12 has been the predominant refrigerant in household refrigerators for 50 years. Since equipment design practices throughout the industry have been developed from experience with CFC-12, performance analyses comparisons between CFC-12 and alternative refrigerants are helpful. The experimental evaluation of CFC-12 reported in this chapter was relatively limited in scope. However, the testing encompassed a range of performance that was comparable to the more extensive HFC-134a and HFC-152a testing, and thus, provided an appropriate benchmark for comparison.

The primary intent of the CFC-12 testing was to obtain test data for comparison to the predicted performance for HFC-134a and HFC-152a. Therefore, no performance prediction equations have been developed for CFC-12.

As an extension of the CFC-12 experimental evaluation, measured performance for all test points were compared to predictions using the ASHRAE prediction method. These results are also included in this chapter.

Test Matrix

The CFC-12 test matrix was a 1/2 fraction of a full two level factorial design with only four independent design variables, including condenser temperature (Tcond), capillary tube diameter (dc) and length (Lc), and heat exchanger length (Lhx). Based on testing with HFC-134a and HFC-152a, these variables have the strongest effect on performance. The low (-) and high (+) test levels for each variable are given in Table 6.1.

Table 6.1: CFC-12 variables and test ranges

Variable	"-" level	"+" level
Tcond	100 F	120 F
dc	0.026 in	0.031 in
ds	0.201 in	0.319 in
Lc	96 in	130 in
Lhx	30 in	70 in

Test points were run at a fixed inlet subcool level of 10 °F, a fixed suction line inlet temperature of 15 °F, and a fixed evaporator pressure corresponding to 0 °F saturation temperature. Consistent with previous testing with HFC-134a and HFC-152a, the eight test points were run with eight different heat exchanger assemblies, in random order. The complete test matrix with all variable settings is given in Table 6.2.

Table 6.2: CFC-12 test matrix ("-" and "+" levels are given in Table 6.1)

Test point	Tcond	dc	Lc	Lhx
1	+	-	-	+
2	+	+	+	+
3	+	-	+	-
4	-	-	-	-
5	-	-	+	+
6	+	+	-	-
7	-	+	-	+
8	-	+	+	-

Measured performance compared to ASHRAE predictions

The *1988 ASHRAE Equipment Handbook*, Chapter 19, describes the most recent ASHRAE design procedures for predicting capillary tube performance with CFC-12. Currently, there are no ASHRAE procedures for predicting capillary tube performance with alternative refrigerants.

The ASHRAE procedures incorporate charts that directly predict adiabatic mass flow rate as a function of inlet conditions and capillary tube geometry. However, in using the charts for predicting the mass flow rate for a capillary tube-suction line heat exchanger, the procedures are slightly more involved. Effective subcooling level (EFFsc) is calculated first using a chart based on simple counter flow heat exchange, and assuming single phase flow. Next, the effective subcooling level is subtracted from the capillary tube actual inlet subcool level, which results in an adiabatic equivalent inlet subcool level. The predicted capillary tube flow rate with heat exchange is then taken to be the predicted flow rate for an adiabatic capillary tube at the adiabatic equivalent inlet subcool level.

The measured CFC-12 heat exchanger performance was compared to predicted performance using the ASHRAE procedures, the results are plotted in Figures 6.1 and 6.2. In Figure 6.1, most of the mass flow rate data points fall within 5% of prediction, and all data falls within 10% of prediction (as shown). In Figure 6.2, most of the data falls within +/- 3 °F.

Based on the results presented thus far for HFC-134a and HFC-152a, mass flow rate prediction equations developed specifically for the heat exchanger configuration are more accurate. In comparison to the ASHRAE method, the

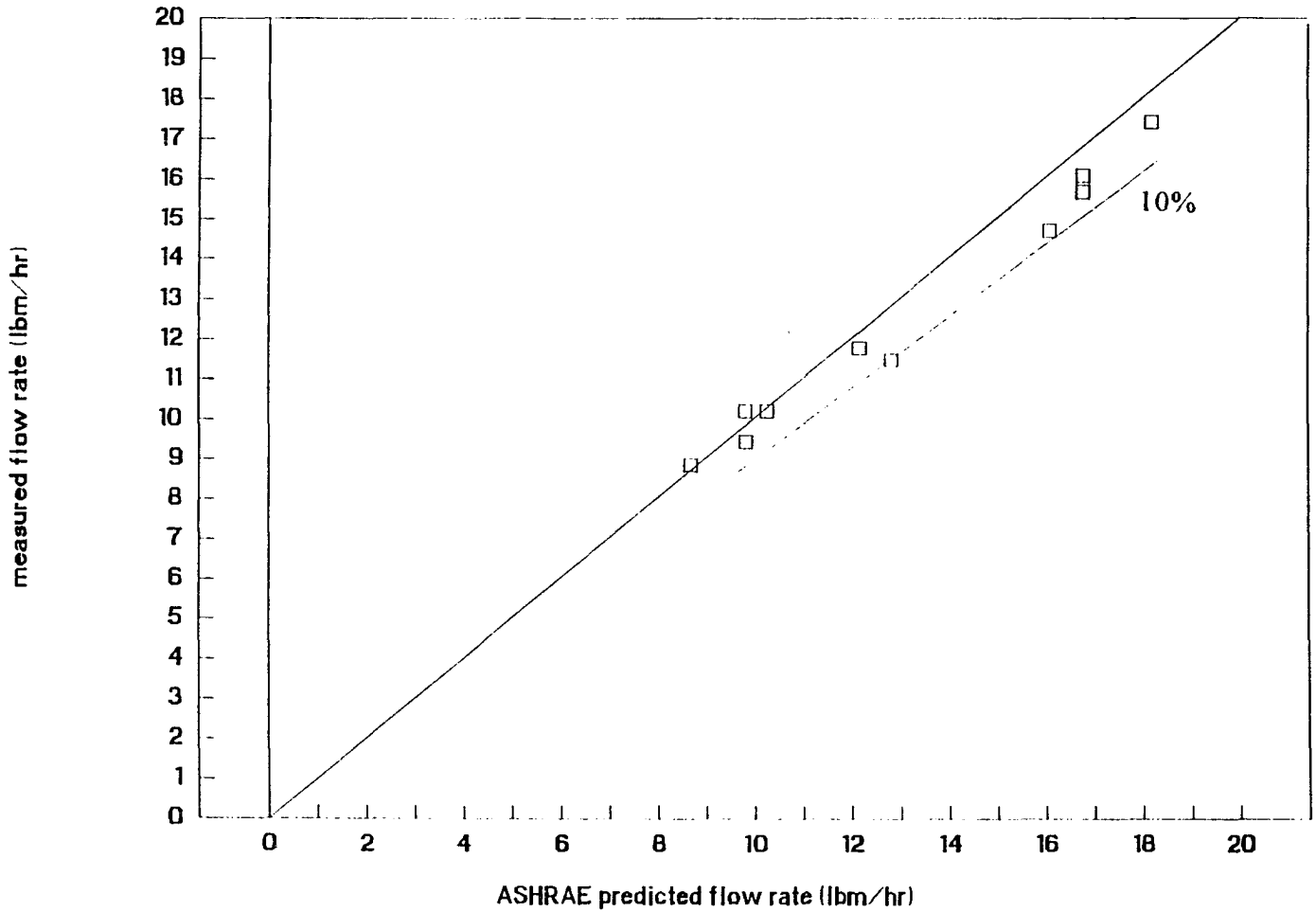

Figure 6.1: CFC-12 measured versus predicted flow rate (ASHRAE method)

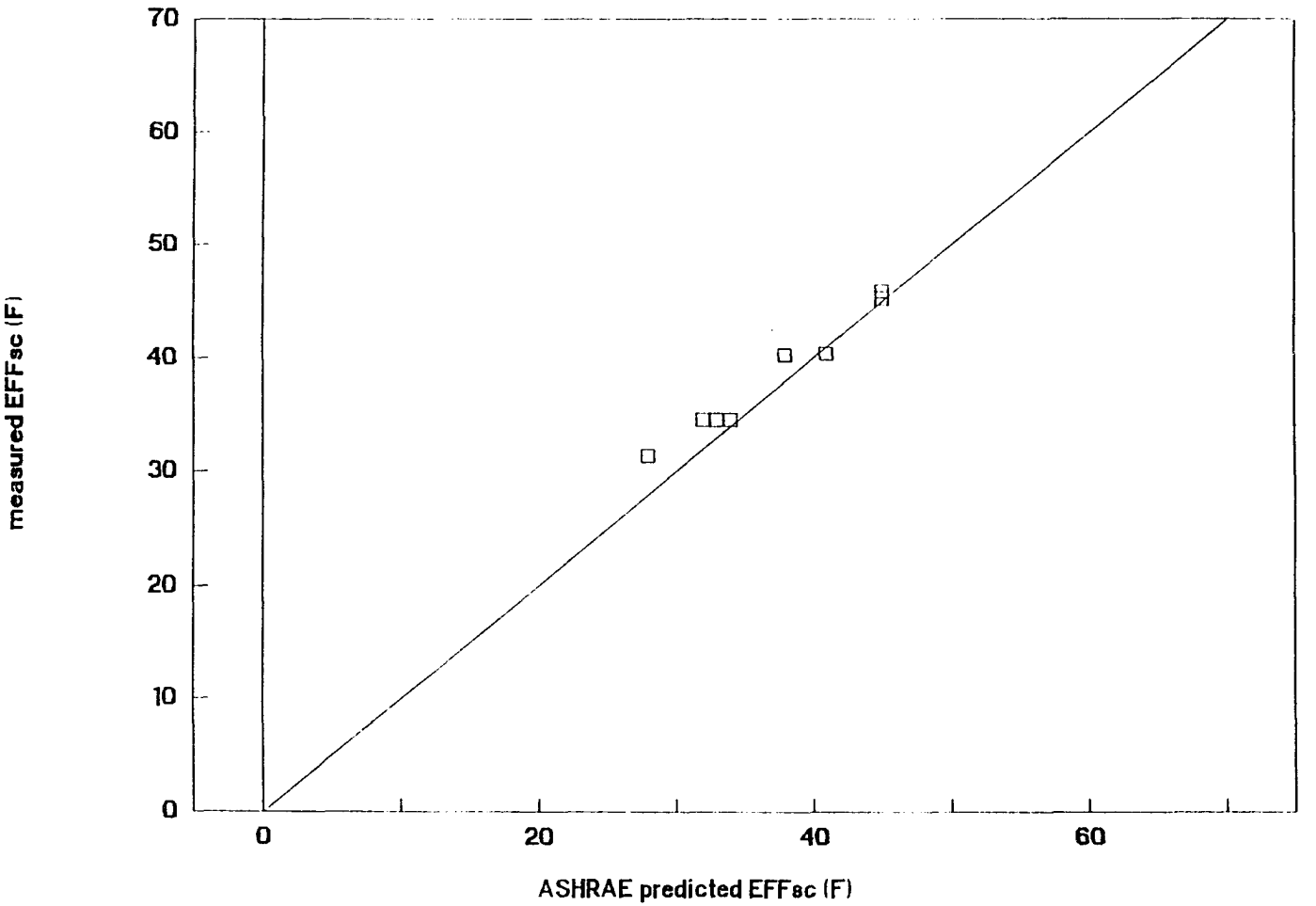

Figure 6.2: CFC-12 measured versus predicted EFFsc (ASHRAE method)

mass flow rate prediction equations are accurate to within ±5%. At ±3 °F, the effective subcooling predictions using the ASHRAE method appear to be as accurate as the prediction equations.

CHAPTER 7. GENERAL PERFORMANCE PREDICTION PROCEDURES

In Chapters 4 and 5, performance prediction equations were developed that are specific to refrigerants HFC-134a and HFC-152a. In this chapter, general performance prediction procedures are developed for a subcooled inlet condition applicable to HFC-134a, HFC-152a, and CFC-12. The approach to developing the procedures is based on fundamental processes affecting the response variables mass flow rate and effective subcooling. In the case of mass flow rate, the capillary tube flow was treated as simple turbulent pipe flow that is influenced by inlet conditions, tube geometry, and fluid properties. In the case of effective subcooling, an effectiveness-NTU analysis for a counter-flow heat exchanger was applicable. The details of the development of the procedures are presented in the following chapter sections.

For comparison, Table 7.1 presents thermodynamic and thermophysical properties for HFC-134a, HFC-152a, and CFC-12 at common operating conditions, and include the properties that influence the heat exchanger performance for each refrigerant.

Mass flow rate

Prediction procedure development

For a subcooled inlet condition, the heat exchanger mass flow rate is influenced primarily by the capillary tube inlet pressure (through the condenser temperature), and the capillary tube diameter and length (dc and Lc). Although

Table 7.1: Properties of HFC-134a, HFC-152a, and CFC-12

	HFC-134a	CFC-12	HFC-152a
T_{sat}(F) / P_{sat}(psia)	0 / 21.2	0 / 23.9	0 / 19.8
	100 / 138.8	100 / 131.7	100 / 124.6
	120 / 185.8	120 / 172.0	120 / 166.7
Liquid density, ρ @70 F (lbm/ft^3)	76.3	82.7	56.7
Vapor thermal conductivity, k @40 F (Btu/hr-ft-F)	.0065	0.0049	0.0069
Vapor specific heat, Cp_g @40 F (Btu/lbm-F)	0.194	0.147	0.246
Vapor viscosity, μ @40F (lbm/ft-hr)	0.0267	0.0278	0.0229
Liquid specific heat, Cp_f @100 F (Btu/lbm-F)	0.35	0.24	0.434
h_{fg} @0 F (Btu/lbm)	90.1	88.9	135.6

refrigerant flow through the capillary tube is complex due to the two-phase characteristics, the flow behavior can be approximated by simple turbulent pipe flow. With this approach, mass flow rate is related to inlet pressure (P), density (ρ), viscosity (μ), tube geometry (dc and Lc), and the tube's inner surface roughness through the familiar Moody diagram (Moody, 1944). The Moody diagram, which is empirically based, graphically presents the relationship between friction factor, f, and flow Reynolds number, Re_{dc}, where

$$f = \frac{(\Delta P/\rho)(dc/Lc)}{(\overline{V}^2/2)} \tag{7.1}$$

and

$$Re_{dc} = \frac{\rho \overline{V} dc}{\mu} \tag{7.2}$$

To use the Moody diagram, the capillary tube inner surface roughness must be known. Moody (1944) included a chart for estimating the surface roughness for common engineering materials. However, for drawn tubing, the chart's range of tube diameters is much larger than typical capillary tube diameters, and a reasonable estimation of surface roughness was not possible.

The alternative to using the Moody diagram directly was to develop a friction factor and Reynolds number relationship specifically applicable to the capillary tubes tested. Using the HFC-134a subcooled inlet mass flow database, friction factors and Reynolds numbers were calculated for each test point at the

corresponding inlet conditions (Figure 7.1). A functional relationship between friction factor and Reynolds number was determined by first plotting log(f) versus $\log(Re_{dc})$ (Figure 7.2). A simple linear regression through the data gives

$$\log(f) = 0.7 - (0.486)\log(Re_{dc}) \tag{7.3}$$

An explicit expression for f was developed as shown in the following steps.

$$\log(f) = \log(5.01) - (0.486)\log(Re_{dc}) \tag{7.4}$$

$$\log(f) = \log(5.01) + \log(Re_{dc})^{-0.486} \tag{7.5}$$

$$\log(f) = \log[(5.01)Re_{dc}^{-0.486}] \tag{7.6}$$

$$f = 5.01Re_{dc}^{-0.486} \tag{7.7}$$

Using Equations 7.1, 7.2 and 7.7, along with the following continuity equation

$$\dot{m} = \rho \overline{V} A, \tag{7.8}$$

the functional relationship between mass flow rate, refrigerant properties, and inlet conditions can be determined. First, substituting for f using Equation 7.7 into Equation 7.1 and rearranging results in

$$\overline{V}^2 = \frac{(0.4)(\Delta P/\rho)(dc/Lc)}{Re_{dc}^{-0.486}} \tag{7.9}$$

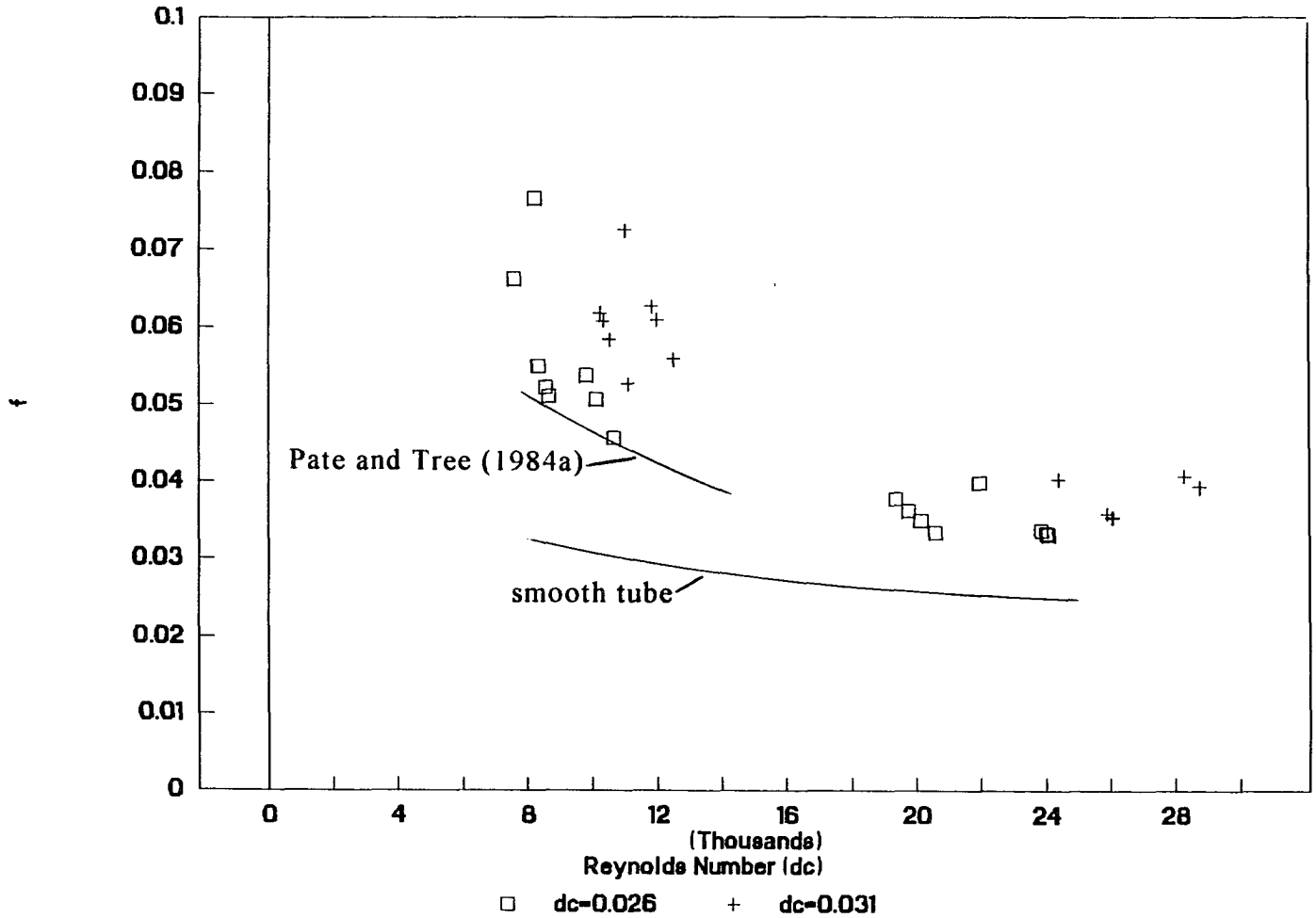

Figure 7.1: Friction factor (f) versus Reynolds numbers for the HFC-134a Phase 1 test points

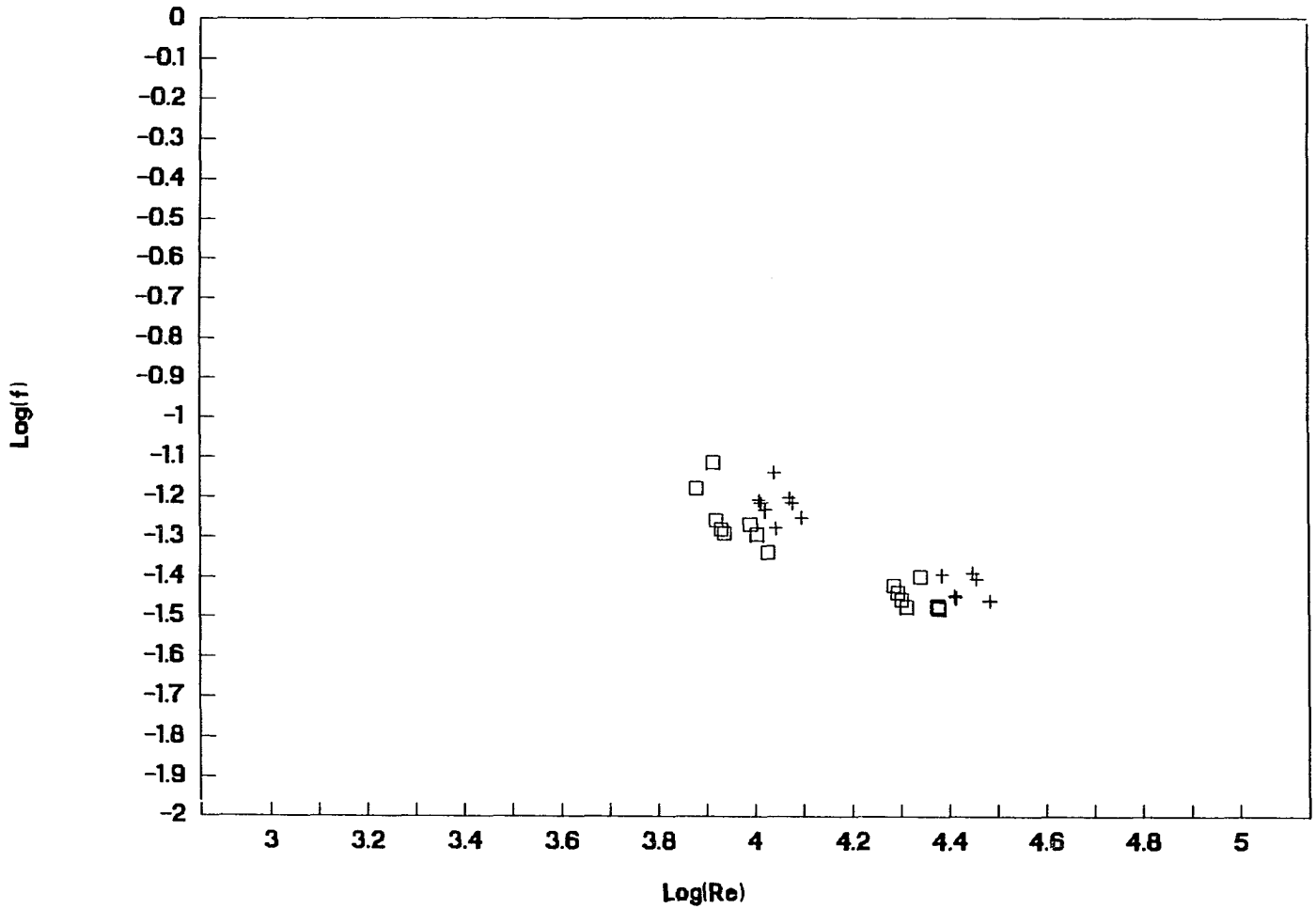

Figure 7.2: Log(f) versus log(Re_{ds}) for the HFC-134a Phase 1 test points

Substituting for Re_{dc} using Equation 7.2 gives

$$\overline{V}^2 = (0.4)(\Delta P/\rho)(dc/Lc)[(\rho \overline{V} dc)/\mu]^{0.486}, \qquad (7.10)$$

and solving explicitly for $\overline{V}$ results in

$$\overline{V} = [(0.4)(dc/Lc)\Delta P]^{0.66}(\rho)^{-0.34}(dc/\mu)^{0.32} \qquad (7.11)$$

Finally, substituting $\overline{V}$ from Equation 7.11 into the continuity equation, Equation 7.8, gives

$$\dot{m} = [(0.42)(Lc)^{-0.66}(dc)^{2.98}]\Delta P^{0.66}(\rho)^{0.66}(\mu)^{-0.32} \qquad (7.12)$$

For a fixed tube diameter and length, the functional relationship between mass flow rate, refrigerant properties, and inlet condition is

$$\dot{m} = f[(P)^{0.66}(\rho)^{0.66}(\mu)^{-0.32}] \qquad (7.13)$$

In Equation 7.13, ΔP has been replaced by P, which is the capillary tube inlet pressure. This can be done since the flow is choked and the exiting pressure has no effect on mass flow rate, for the test points reported within this study. The density, ρ, and viscosity, μ, are the refrigerant liquid properties corresponding to the inlet temperature.

The mass flow rate functional relationship given in Equation 7.13 is used to define a scaling factor, SF, to be applied to the HFC-134a subcooled inlet

equation, Equation 4.2. The HFC-134a equation was used as the reference prediction equation since its development was based on the most extensive testing for this study. The scaling factor is defined as

$$SF = \left[\left(\frac{P}{P_{ref}}\right)^{0.66}\left(\frac{\rho}{\rho_{ref}}\right)^{0.66}\left(\frac{\mu}{\mu_{ref}}\right)^{-0.32}\right] \qquad (7.14)$$

The properties subscripted "ref" refer to HFC-134a properties, while the properties subscripted "x" refer to any refrigerant "x" properties. Once again, the pressure, P, is the capillary tube inlet pressure, and the density and viscosity values are liquid properties corresponding to the inlet temperature.

A final general mass flow rate prediction equation, applicable to refrigerant "x", was obtained by simply multiplying the predicted mass flow rate for HFC-134a (Equation 4.2) by the scaling factor, SF.

$$\dot{m}_{pred,\,x} = \left(\dot{m}_{pred,\,HFC\text{-}134a}\right)(SF) \qquad (7.15)$$

Prediction procedure verification

The general mass flow rate prediction procedure was verified by comparing measured mass flow rate data for HFC-152a and CFC-12 to predictions using Equation 7.15. Figure 7.3 is a plot of measured flow rate for HFC-152a versus predicted flow rate using the HFC-134a prediction equation directly, prior to applying the scaling factor. As can be seen, the HFC-134a prediction equation overpredicts the HFC-152a measured mass flows by roughly 20%. Figure 7.4

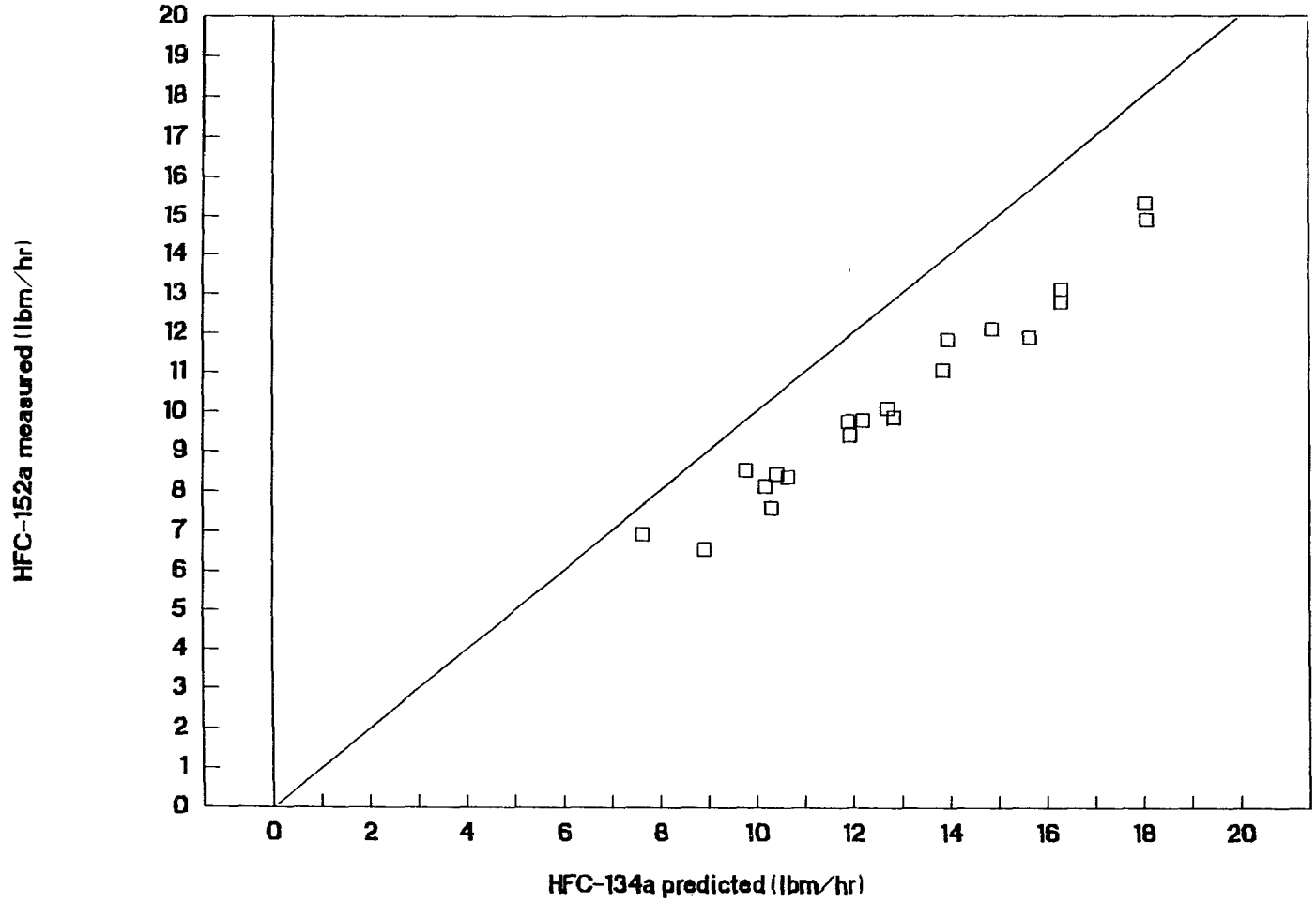

Figure 7.3: HFC-152a measured mass flow rate versus HFC-134a predicted mass flow rate (Equation 4.2)

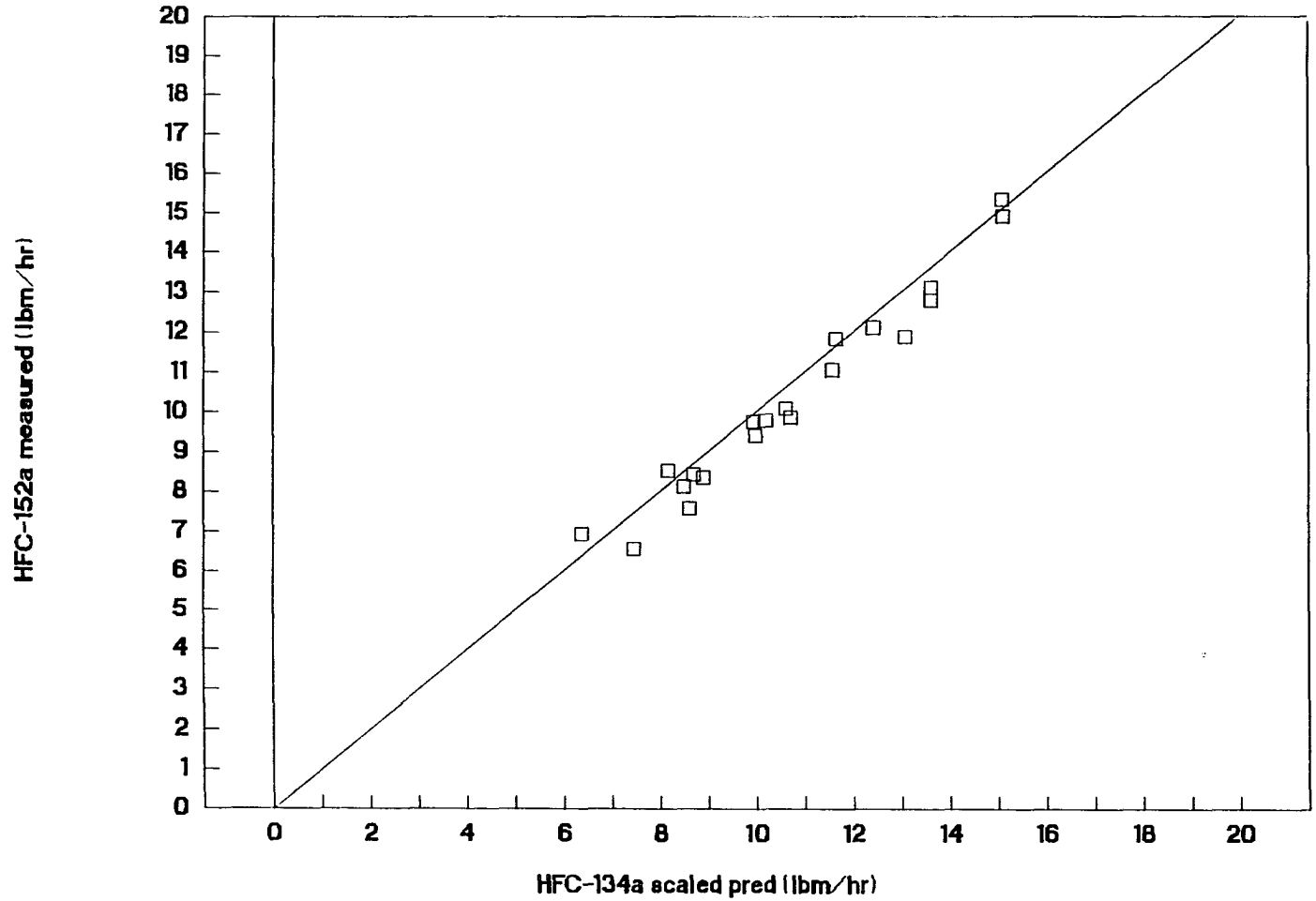

Figure 7.4: HFC-152a measured mass flow rate versus scaled predicted mass flow rate (Equation 7.15)

shows the results after applying the scaling factor to the HFC-134a prediction equation. While there is significant improvement in the predictions, the procedure still tends to slightly overpredict the HFC-152a flow rates by roughly 5%. This suggests that there is a greater resistance to flow with HFC-152a beyond that which is accounted for in the scaling factor, and most likely is associated with the two-phase flow phenomenon.

In Figure 7.5, the measured CFC-12 mass flow rates are compared to predicted flow rate using the HFC-134a prediction equation directly. With the exception of one data point, all measured CFC-12 data fall within the 95% prediction interval for the HFC-134a prediction equation. The application of the scaling factor to the HFC-134a prediction equation resulted in only a negligible correction to the predicted CFC-12 flow rates (Figure 7.6), which means that the scaling factor is near unity.

Effective Subcooling

Prediction procedure development

The general effective subcooling prediction procedures are based on applying a concentric counter-flow heat exchanger analysis to the capillary tube-suction line heat exchanger. By definition, the capillary tube-suction line heat exchanger effectiveness, ε, is given by

$$\varepsilon = \left(\frac{T_{s2} - T_{s1}}{T_{c1} - T_{s1}}\right) \tag{7.16}$$

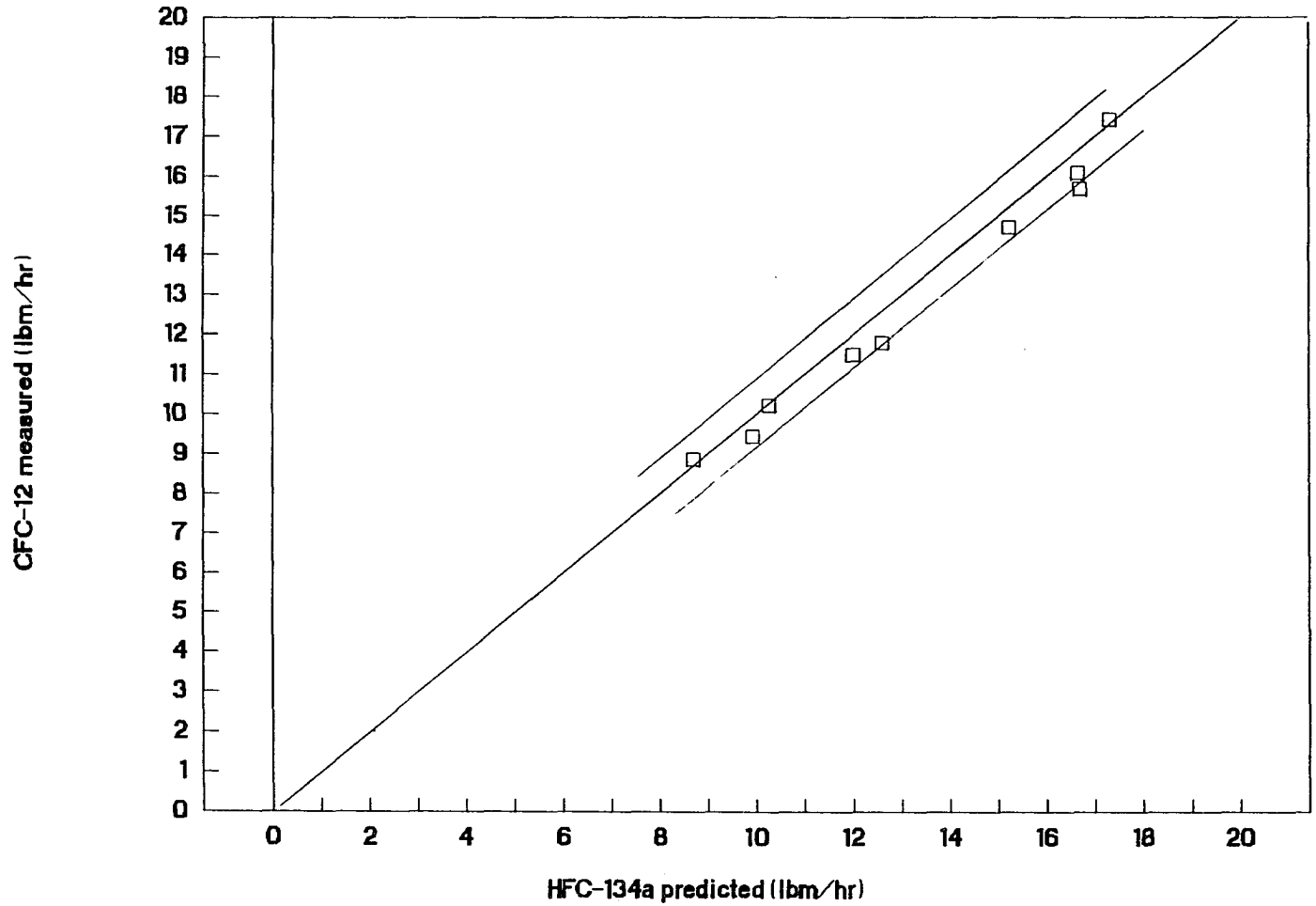

Figure 7.5: CFC-12 measured mass flow rate versus HFC-134a predicted mass flow rate (Equation 4.2)

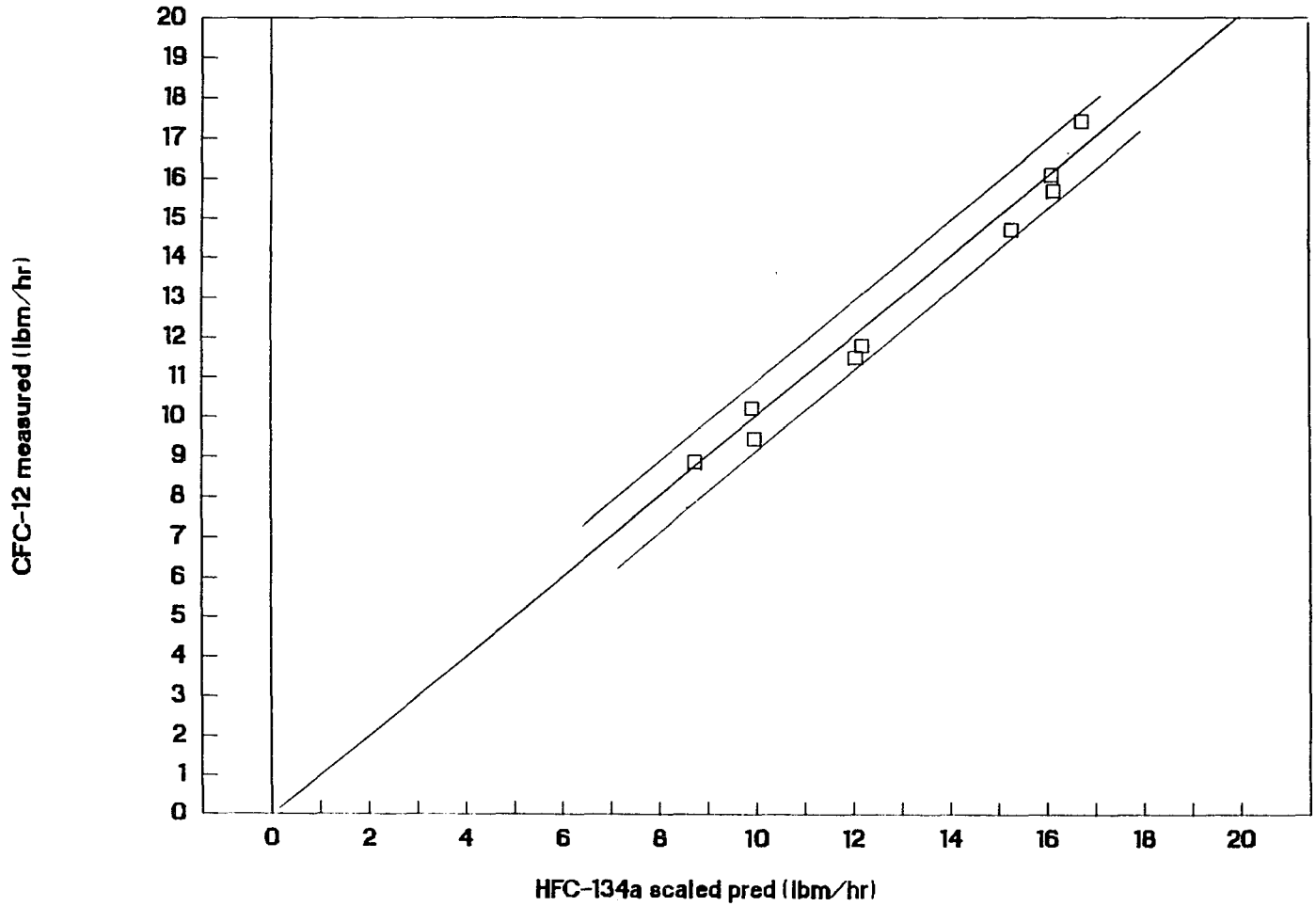

Figure 7.6: CFC-12 measured mass flow rate versus scaled predicted mass flow rate (Equation 7.15)

where T_{s2} and T_{s1} are the suction line exit and inlet temperatures, respectively, and T_{c1} is the capillary tube inlet temperature. Using Equation 7.16, the effective subcooling, EFFsc, can be expressed in terms of effectiveness, ε.

$$EFFsc = \frac{Cp_{gs}\,(T_{s2} - T_{s1})}{Cp_{fc}} \tag{7.17}$$

$$EFFsc = \frac{\varepsilon\, Cp_{gs}\,(T_{c1} - T_{s1})}{Cp_{fc}} \tag{7.18}$$

In Equations 7.17 and 7.18, Cp_{fc} is the capillary tube flow liquid specific heat, and Cp_{gs} is the suction line vapor specific heat. Equation 7.18 can be rearranged to give an expression for effectiveness, ε.

$$\varepsilon = \frac{EFFsc\; Cp_{fc}}{Cp_{gs}\,(T_{c1} - T_{s1})} \tag{7.19}$$

Effectiveness, ε, can be written in terms of another dimensionless parameter, NTU, which is commonly used in heat exchanger analysis. By definition,

$$NTU = \frac{(UA)}{(\dot{m}Cp_{gs})} \tag{7.20}$$

where U is the overall heat transfer coefficient between the capillary tube and suction line flow streams, and A is the common heat transfer area. The ε and NTU relationship for concentric tube counter flow heat exchangers is given by Kays and London (1984) as

$$\varepsilon = \frac{1 - \exp[-NTU(1 - C_r)]}{1 - C_r \exp[-NTU(1 - C_r)]} \tag{7.21}$$

and, conversely, as

$$NTU = \frac{1}{(C_r - 1)} \ln\left[\frac{\varepsilon - 1}{(\varepsilon C_r - 1)}\right] \tag{7.22}$$

In Equations 7.21 and 7.22, the C_r value is the ratio of specific heats for the two flow streams, $Cp_{g,s}/Cp_{fc}$.

The general effective subcooling prediction procedure involves simply scaling the HFC-134a predicted EFFsc value through the EFFsc, ε, and NTU relationships given in Equations 7.18 through 7.22. As was done for mass flow rate, the HFC-134a effective subcooling prediction equation was used as the reference prediction equation since its development was based on the most extensive testing. It should be noted that for the scaling procedure all suction line vapor properties should be evaluated at the suction inlet temperature, T_{s1}, and the capillary tube liquid specific heat should be evaluated at the capillary tube inlet temperature, T_{c1}, since these are the known operating conditions.

The predicted EFFsc value for a refrigerant "x" begins by calculating a reference effective subcooling value, $EFFsc_{ref}$, using the HFC-134a prediction

equation, Equation 4.4, for a specified operating condition and heat exchanger geometry. The specified condition includes knowledge of the suction line inlet temperature, T_{s1}, and the capillary tube inlet temperature, T_{c1}. The reference heat exchanger effectiveness, ε_{ref}, is then calculated using Equation 7.19, followed by the reference NTU value, NTU_{ref}, using Equation 7.22.

The NTU value for refrigerant "x" can be calculated by scaling the NTU_{ref} value through refrigerant property values. Based on the definition of NTU (Equation 7.20), NTU_x can be expressed as

$$NTU_x = NTU_{ref} \left(\frac{\dot{m}Cp_{gs}}{UA}\right)_{ref} * \left(\frac{UA}{\dot{m}Cp_{gs}}\right)_x \qquad (7.23)$$

The overall heat transfer coefficient, U, is dominated by the suction line heat transfer coefficient, h_s. This allows a substitution of the U value by the suction line h_s value, which is calculated using the Colburn equation,

$$h_s = 0.023 \left(\frac{k_s}{ds}\right) Re_{ds}^{0.8} Pr_s^{0.33} \qquad (7.24)$$

where k_s and Pr_s are the thermal conductivity and Prandtl number, respectively, for the suction line vapor. After substituting h_s for U, and for a fixed heat exchanger geometry, Equation 7.23 can be written as

$$NTU_x = NTU_{ref} \left(\frac{\dot{m}_{ref}}{\dot{m}_x}\right) \left(\frac{h_{s\text{-}x}}{h_{s\text{-}ref}}\right) \left(\frac{Cp_{g\text{-}ref}}{Cp_{g\text{-}x}}\right) \qquad (7.25)$$

Expanding the h ratio using Equation 7.24, results in

$$NTU_X = NTU_{ref} \left(\frac{\dot{m}_{ref}}{\dot{m}_X}\right) \left(\frac{Cp_{g\text{-}ref}}{Cp_{g\text{-}x}}\right) \left(\frac{Re_{ds\text{-}x}}{Re_{ds\text{-}ref}}\right)^{0.8} \left(\frac{Pr_{s\text{-}x}}{Pr_{s\text{-}ref}}\right)^{0.33} \left(\frac{k_{s\text{-}x}}{k_{s\text{-}ref}}\right) \quad (7.26)$$

Finally, expanding Reynolds and Prandl numbers in terms of their definitions gives

$$NTU_X = NTU_{ref} \left(\frac{\dot{m}_{ref}}{\dot{m}_X}\right)^{0.2} \left(\frac{Cp_{g\text{-}ref}}{Cp_{g\text{-}x}}\right)^{0.67} \left(\frac{\mu_{s\text{-}ref}}{\mu_{s\text{-}x}}\right)^{0.46} \left(\frac{k_{s\text{-}x}}{k_{s\text{-}ref}}\right)^{0.67} \quad (7.27)$$

where μ_s is the viscosity of the suction line vapor.

With the NTU_X calculated from Equation 7.27, the ε_X value can now be determined using Equation 7.21, and the $EFFsc_X$ value can then be calculated using Equation 7.18.

Prediction procedure verification

Effective subcooling levels for the HFC-152a test points are predicted using the HFC-134a prediction equation, Equation 4.4, and plotted versus measured values in Figure 7.7. As can be seen, the predicted effective subcooling levels for the HFC-152a are 1 to 5 °F greater than measured. After applying the scaling procedure to the HFC-134a predictions, most data points are within 1 °F of prediction (Figure 7.8).

Similarly, effective subcool values are predicted for the CFC-12 test points using the HFC-134a equation directly, and plotted in Figure 7.9. These predictions are consistently less than the measured CFC-12 effective subcooling

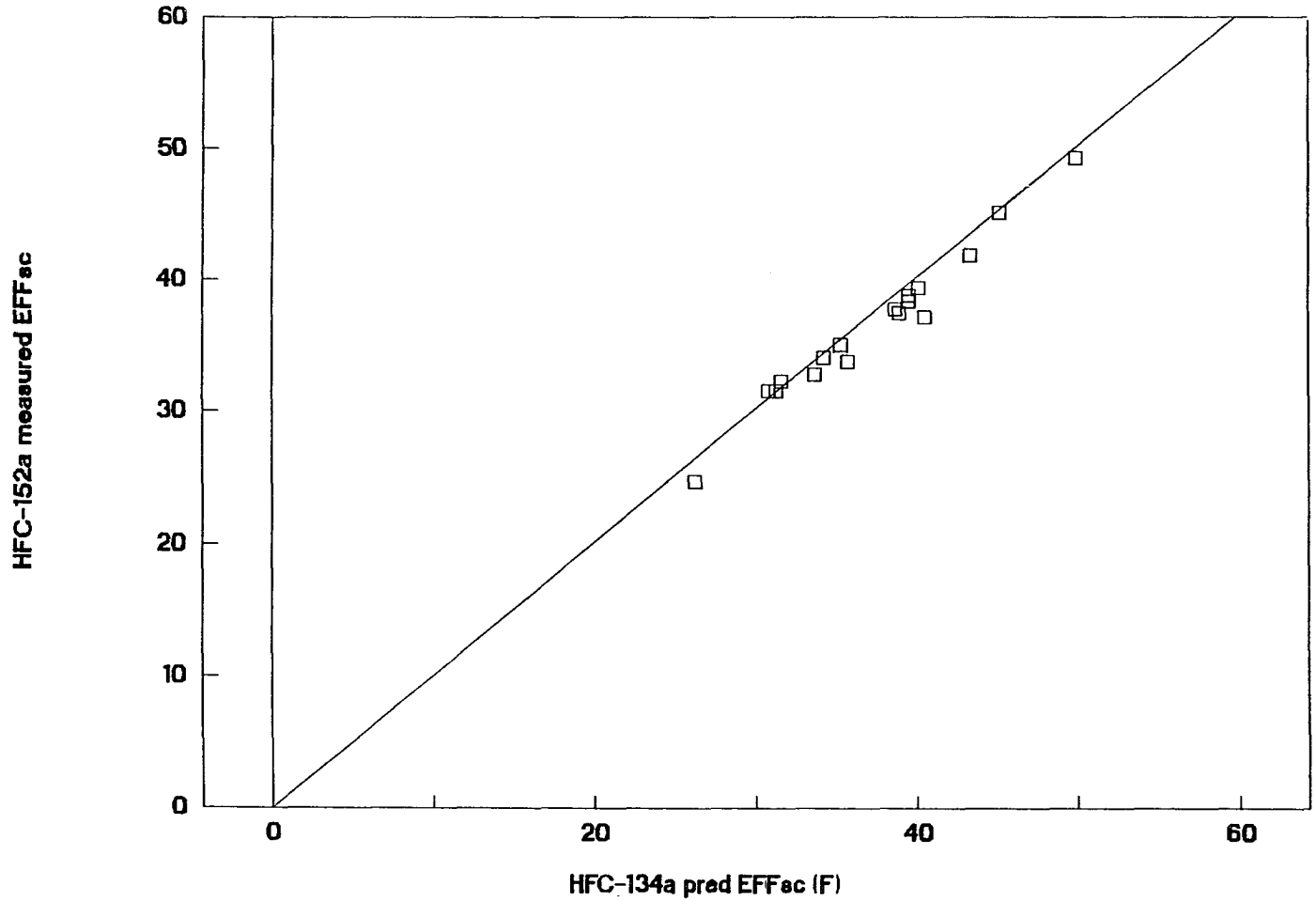

Figure 7.7: HFC-152a measured EFFsc versus HFC-134a predicted EFFsc (Equation 4.4)

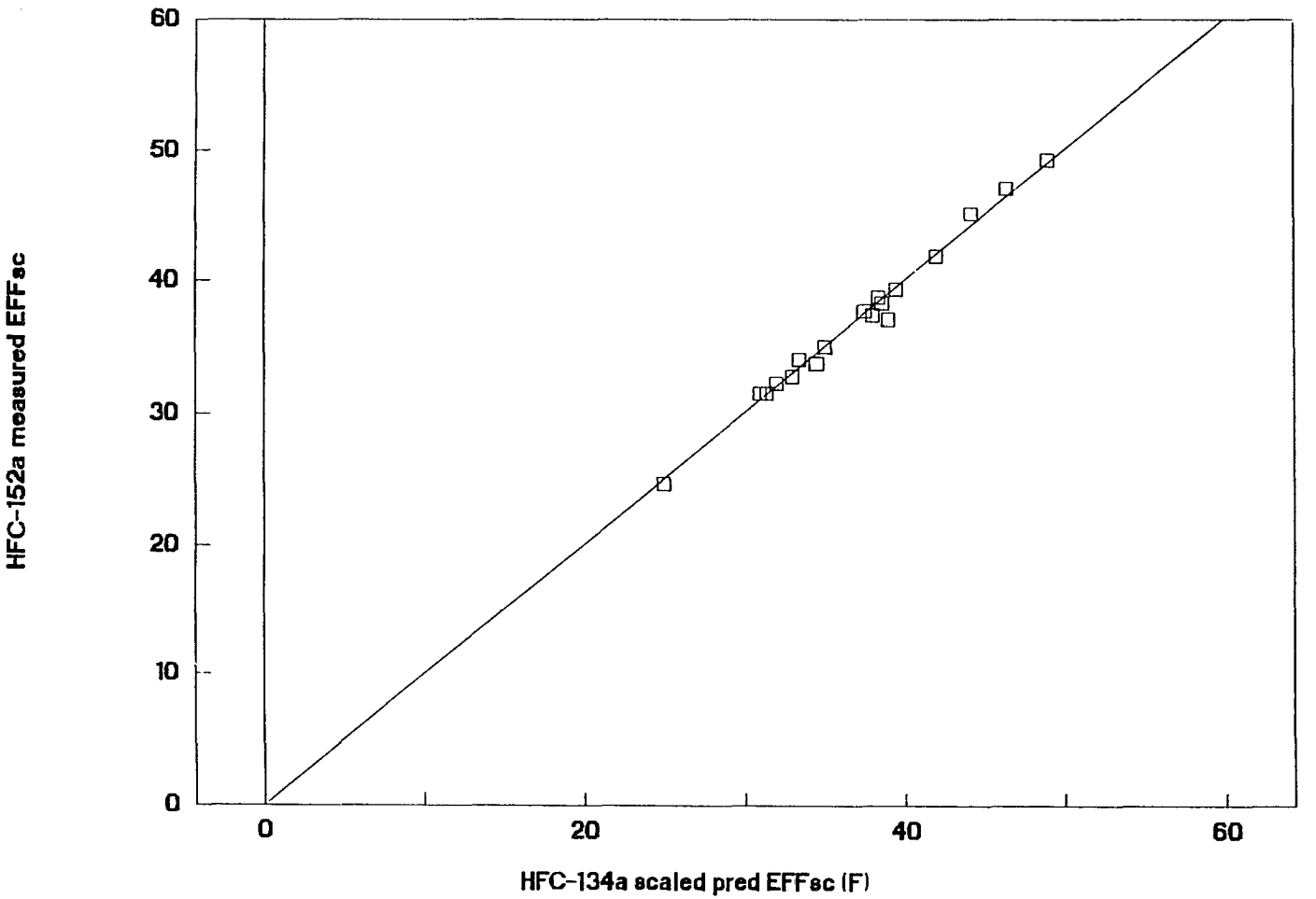

Figure 7.8: HFC-152a measured EFFsc versus scaled predicted EFFsc

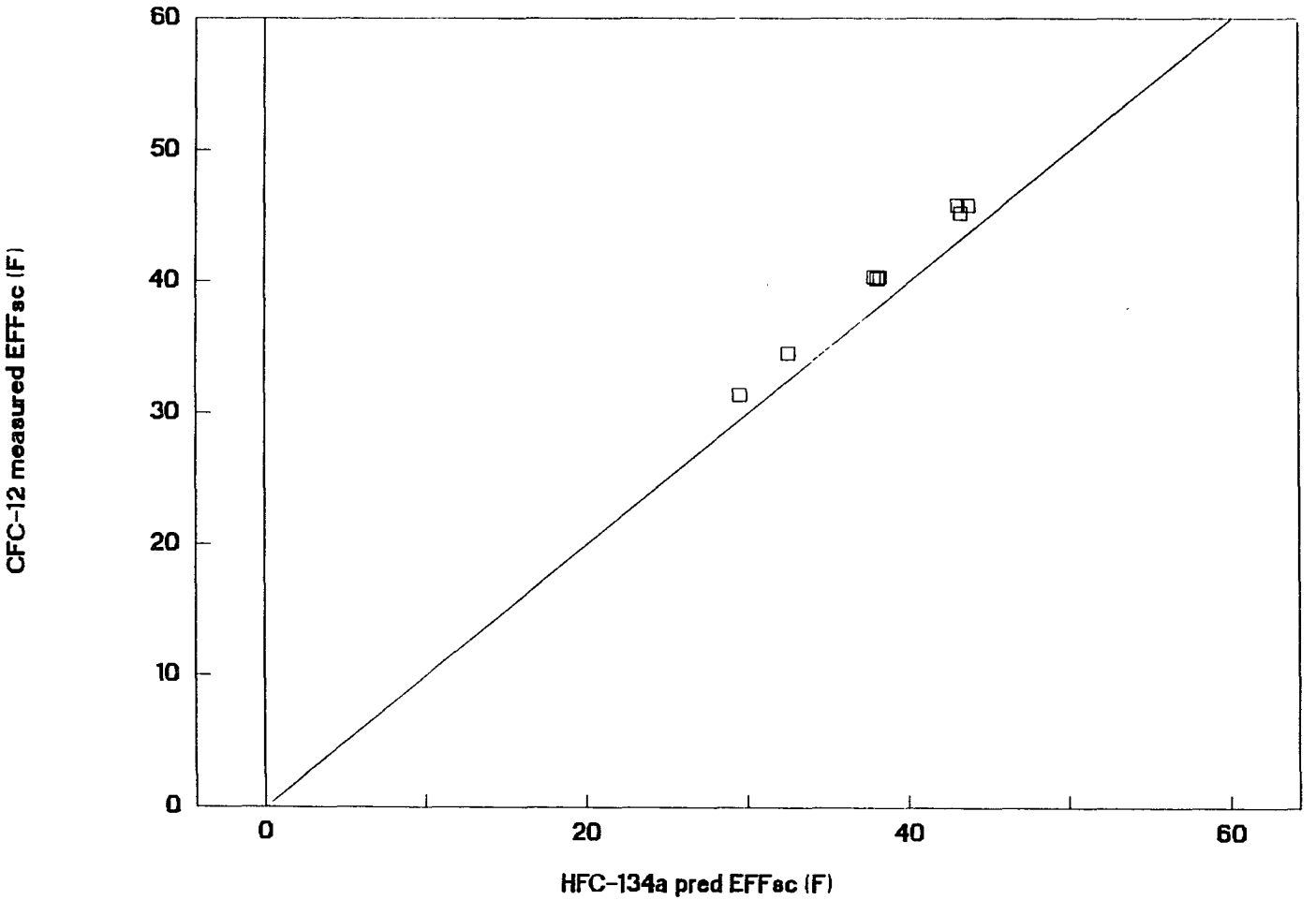

Figure 7.9: CFC-12 measured EFFsc versus HFC-134a predicted EFFsc (Equation 4.4)

values by 2 to 3 °F. Again, after applying the scaling procedure to the HFC-134a predictions, the agreement is within 1 °F (Figure 7.10).

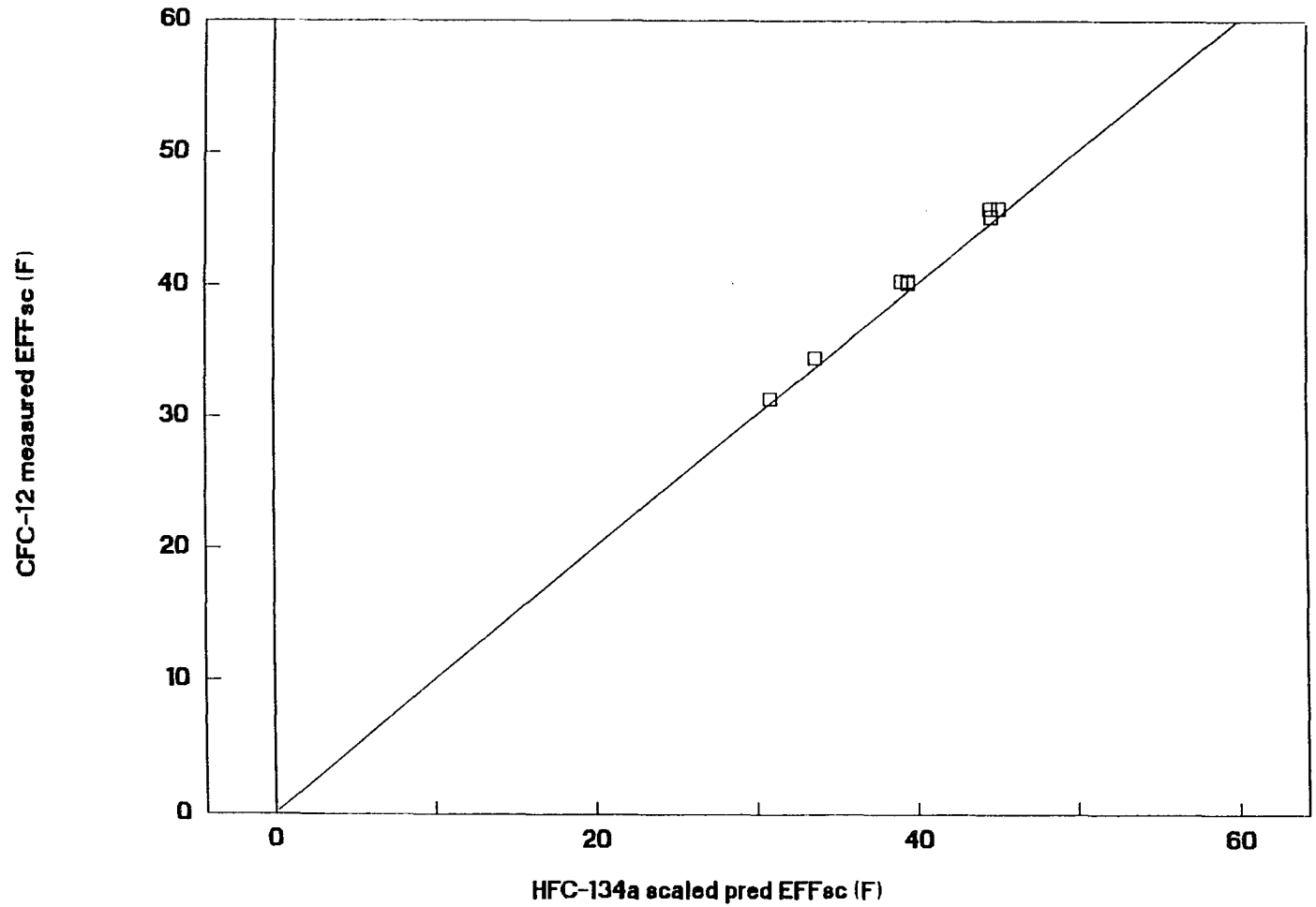

Figure 7.10: CFC-12 measured EFFsc versus scaled predicted EFFsc

CHAPTER 8. CONCLUSIONS AND RECOMMENDATIONS

Conclusions

The primary objective of this study was to experimentally evaluate the capillary tube-suction line heat exchanger performance with alternative refrigerants HFC-134a and HFC-152a. Since capillary tube-suction line heat exchangers are used mainly in household refrigerators, a test facility was first constructed simulating this application. A database, which incorporated the effects on performance of ten different heat exchanger design variables, was then obtained for each alternative refrigerant. This experimental effort greatly exceeded the scope of any previously reported study.

The results of the experimental evaluation showed that the design variables having the greatest effect on mass flow rate included condenser temperature, capillary tube diameter and length, and capillary tube inlet quality levels. The design variables having the greatest effect on effective subcooling included condenser temperature, heat exchanger length, suction line diameter, and suction line inlet temperature. The measured effects on performance of all significant variables were shown to be consistent with the trends in previously reported studies and analyses.

Heat exchanger performance prediction equations were developed for the two alternative refrigerants, based on their respective databases. These equations are design tools that are readily usable by engineers, and that are much more accurate than what have been used in the past.

General heat exchanger performance prediction procedures have also been presented that enable performance predictions to be made for other pure HFC and CFC refrigerants. The procedures were developed based on consideration of the fundamental processes influencing mass flow rate and effective subcooling, and involve scaling the predicted performance for HFC-134a through thermodynamic and thermophysical properties. Verification of the procedures were made by successfully predicting the HFC-152a and CFC-12 measured heat exchanger performance.

As an underlying focus of this study, statistical methods were incorporated into all aspects of the experimental evaluation. Specifically, statistical methods were used in designing the experimental test plans and evaluating test data, while more broadly, in developing the experimental procedures and methodology. Statistical methods provided a thorough coverage of all ten variable effects with a minimum of experimental test points. Final proof of the value of the application of statistical methods to the experimental process was found in the overall quality and consistency of the measured data.

Overall, this study has broadened the understanding of capillary tube-suction line heat exchanger performance, and further, has extended the knowledge base to alternative refrigerants. Due to the relatively low cost and high reliability of capillary tubes, this information will not only be applicable to the first generation of household refrigerators using alternative refrigerants, but to future generations of refrigerators as well.

Recommendations

Several recommendations can be made for future studies.

1. The obvious extension to this work is to develop a capillary tube-suction line heat exchanger computer model. There has been only one previously reported heat exchanger model (Pate and Tree, 1984b), and its experimental verification was limited to CFC-12 and to one capillary tube geometry. The databases reported in the current study will be valuable to the verification of a computer model.
2. New refrigerant blends and mixtures are continuously being developed and need to be experimentally evaluated for use with capillary tubes.
3. The experimental evaluation procedures and methodology described for this study could easily be extended to adiabatic capillary tubes, as well as the short tube restriction devices used in heat pumps.

BIBLIOGRAPHY

ASHRAE Standard. 1988. Method of Testing Flow Capacity of Refrigerant Capillary Tubes. ANSI/ASHRAE 28-1988.

ASHRAE. 1988. *1988 ASHRAE handbook - Equipment.* American Society of Heating, Refrigerating, and Air-Conditioning Engineers, Inc., Atlanta: 19.21.

ASHRAE. 1989. *1989 ASHRAE handbook - Fundamentals.* American Society of Heating, Refrigerating, and Air-Conditioning Engineers, Inc., Atlanta: 17.4.

Bolstad, M.M., and Jordan, R.C. 1948. Theory and use of the capillary tube expansion device. *Refrigerating Engineering*, Dec.: 519.

Bolstad, M.M., and Jordan, R.C. 1949. Theory and use of the capillary tube expansion device, part II, nonadiabatic flow. *Refrigerating Engineering*, June: 577.

Box, G.E.P, Hunter, W.G., and Hunter, J.S. 1978. *Statistics for Experimenters.* John Wiley and Sons, Inc., New York.

Chen, Z.H., Li, R.Y., Lin, S., and Chen, A.Y. 1990. A correlation for metastable flow of R-12 through capillary tubes. *ASHRAE Transactions* 96 (1): 550-554.

Christensen, L.B., and Jorgensen, H.P. 1967. Flow resistance of a capillary tube heat exchanger. *Proceedings of the XII International Congress of Refrigeration*: 1069.

Cooper, L., Chu, C.K., and Brisken, W.R. 1957. Simple selection method for capillaries derived from physical flow conditions. *Refrigerating Engineering*, July: 37.

Hopkins, N.E. 1950. Rating the restrictor tube. *Refrigeration Engineering*, Nov.: 1087.

Kays, W.M., and London, A.L. 1984. *Compact Heat Exchangers*, 3rd ed., McGraw-Hill, New York.

Kline,S.J., and McClintock,F.A. 1953. Describing uncertainties in single sample experiments. *Mechanical Engineering* 75: 3-8.

Koizumi, H., and Yokoyama, K. 1980. Characteristics of refrigerant flow in a capillary tube. *ASHRAE Transactions* 86 (2): 19-27.

Kuehl, S.J., and Goldschmidt, V.W. 1990. Steady flows of R-22 through capillary tubes: test data. *ASHRAE Transactions* 96 (1): 719-728.

Kuehl, S.J., and Goldschmidt, V.W. 1991. Modeling of steady flows of R-22 through capillary tubes. *ASHRAE Transactions* 97 (1): 139-148.

Kuijpers, L.J.M., and Janssen, M.J.P. 1983. Influence of thermal non-equalibrium on capillary tube mass flow. *Proceedings of the XVIth International Congress of Refrigeration*, Commission B2, Paris, p.307-316.

Li, R.Y., Lin, S., Chen, Z.Y., and Chen, Z.H. 1990. Metastable flow of R-12 through capillary tubes. *International Journal of Refrigeration* 13 (3), May: 181-186.

Mikol, E.P. 1963. Adiabatic single and two-phase flow in small bore tubes. *ASHRAE Journal* 5 (11): 75-86.

Moody, L. F. 1944. Friction factors for pipe flow. *Transactions of ASME* (66): 671-684.

National Institute of Standards and Technology Thermodynamic Properties of Refrigerants and Refrigerant Mixtures, NIST Standard Reference Database 23, Version 3.03.

Pannock, J., Radermacher, R., Liu, Z., and Yu, K. 1994. Evaluation of R-134a and R-152a as working fluids in a domestic refrigerator/freezer. *ASHRAE Transactions* 100 (1): No. 94-20-2.

Pate, M.B., and Tree, D.R. 1984a. An analysis of pressure and temperature measurements along a capillary tube-suction line heat exchanger. *ASHRAE Transactions* 90 (2): 291-301.

Pate, M.B., and Tree, D.R. 1984b. A linear quality model for capillary tube-suction line heat exchangers. *ASHRAE Transactions* 90 (2): 3-17.

SAS statistical analysis program, release 6.06, licensed to Iowa State University, copyright 1989, SAS Institute Inc., Cary, NC.

Staebler, L.A. 1948. Theory and use of a capillary tube for liquid refrigerant control. *Refrigerating Engineering*, Jan.: 55.

Stoecker, W. F. 1958. *Refrigeration and Air Conditioning*. McGraw-Hill, New York.

Swart, R.H. 1946. Capillary tube heat exchangers. *Refrigerating Engineering*, Sept.: 221.

United Nations Environment Programme. 1987. Montreal Protocol on substances that deplete the ozone layer. Final Act. Montreal, 17.9.

Wijaya, H. 1991. An experimental evaluation of adiabatic capillary tube performance for HFC-134a and CFC-12. *International CFC and Halon Alternatives Conference Proceedings*, Dec.: 474-483.

Whitesel, H.A.1957. Capillary two-phase flow. *Refrigerating Engineering*, Apr.: 42.

Whitesel, H.A. 1957. Capillary two-phase flow, Part II. *Refrigerating Engineering*, Sept.: 35.

APPENDIX A. REFRIGERANT PROPERTIES

The refrigerant property data used for this study were obtained from the National Institute of Standards and Technology (NIST) Thermodynamic Properties of Refrigerants and Refrigerant Mixtures, Standard reference database 23 (NIST, 1993). For comparison purposes, Tables A.1, A.2, and A.3 provide sample listings of properties.

Table A.1: HFC-134a properties

Tsat (F)	Psat (psia)
80.00	101.3
85.00	109.9
90.00	119.0
95.00	128.6
100.00	138.9
105.00	149.7
110.00	161.2
115.00	173.3
120.00	186.0
125.00	199.5
130.00	213.7
135.00	228.6

T (F)	Cpg (Btu/lb.F)	Therm Cond (w/m.K)	Viscosity (micropoise)
-10.00	.1814	.9328E-02	99.03
-5.00	.1826	.9508E-02	100.2
.00	.1838	.9689E-02	101.3
5.00	.1849	.9870E-02	102.4
10.00	.1861	.1005E-01	103.5
15.00	.1872	.1024E-01	104.7
20.00	.1884	.1042E-01	105.8
25.00	.1895	.1060E-01	106.9
30.00	.1907	.1079E-01	108.0

T (F)	Cpf (Btu/lb-F)	Density (lb/ft3)	Viscosity (micropoise)
90.00	.3415	73.71	1953.
95.00	.3449	72.99	1889.
100.00	.3486	72.26	1828.
105.00	.3525	71.51	1769.
110.00	.3566	70.73	1711.
115.00	.3610	69.94	1654.
120.00	.3658	69.13	1598.

Table A.2: HFC-152a properties

Tsat (F)	Psat (psia)
80.00	90.84
85.00	98.47
90.00	106.6
95.00	115.2
100.00	124.3
105.00	133.9
110.00	144.1
115.00	154.9
120.00	166.2
125.00	178.2
130.00	190.8
135.00	204.1

T (F)	Cpg (Btu/lb.F)	Therm Cond (w/m.K)	Viscosity (micropoise)
-10.00	.2239	.9997E-02	85.59
-5.00	.2253	.1018E-01	86.52
.00	.2268	.1036E-01	87.44
5.00	.2282	.1054E-01	88.37
10.00	.2296	.1073E-01	89.29
15.00	.2310	.1091E-01	90.22
20.00	.2324	.1110E-01	91.14
25.00	.2339	.1129E-01	92.06
30.00	.2353	.1148E-01	92.98

T (F)	Cpf (Btu/lb-F)	Density (lb/ft3)	Viscosity (micropoise)
90.00	.4309	55.02	1364.
95.00	.4350	54.54	1321.
100.00	.4392	54.06	1279.
105.00	.4437	53.57	1239.
110.00	.4484	53.06	1199.
115.00	.4535	52.55	1160.
120.00	.4588	52.02	1122.

Table A.3: CFC-12 properties

Tsat (F)	Psat (psia)
85.00	106.4
90.00	114.4
95.00	122.9
100.00	131.8
105.00	141.2
110.00	151.0
115.00	161.4
120.00	172.3
125.00	183.6
130.00	195.6
135.00	208.1

T (F)	Cpg (Btu/lb.F)	Therm Cond (w/m.K)	Viscosity (micropoise)
-10.00	.1338	.7203E-02	103.4
-5.00	.1345	.7329E-02	104.5
.00	.1352	.7456E-02	105.7
5.00	.1359	.7583E-02	106.8
10.00	.1365	.7711E-02	107.9
15.00	.1372	.7839E-02	109.1
20.00	.1379	.7968E-02	110.2
25.00	.1385	.8097E-02	111.3
30.00	.1392	.8226E-02	112.5

T (F)	Cpf (Btu/lb-F)	Density (lb/ft3)	Viscosity (micropoise)
90.00	.2388	80.21	1898.
95.00	.2406	79.52	1843.
100.00	.2426	78.82	1789.
105.00	.2447	78.10	1738.
110.00	.2470	77.36	1687.
115.00	.2494	76.60	1638.
120.00	.2520	75.83	1591.

APPENDIX B. TEST DATA

This appendix includes all test data collected for this study (Tables B.1 through B.8). In addition, an example of real time test data for one of the HFC-134a test points is presented in Figures B.1 through B.3. All test points were run in the same manner as described in Chapter 3 of the text.

Table B.1: HFC-134a Phase 1 test points

Run (HX)	dc (in)	Lc (in)	Lhx (in)	ds (in)	Linlet (in)	Tcond (°F)	LP (psia)	DTsc (°F)	DTsh (°F)	T_{s2} (°F)	Meas. Flow (lbm/hr)	Meas. EFFsc (°F)
1	0.026	96	70	0.319	6	85.0	23.9	10	20	69	6.87	26.2
2	0.031	130	40	0.201	20	132.5	23.7	5	8	94	16.83	45.4
3	0.031	96	40	0.201	20	85.0	23.9	10	20	65	10.96	24.3
4	0.026	130	50	0.319	6	132.5	23.0	6	5	96	11.66	47.8
5	0.031	96	40	0.201	6	132.2	19.1	12	22	91	19.84	42.0
6	0.031	130	40	0.201	6	85.1	18.8	5	6	65	10.29	37.8
7	0.026	130	70	0.319	20	85.3	17.2	6	5	66	7.15	38.8
8	0.026	96	70	0.319	20	132.2	18.9	12	19	98	13.90	47.4
9	0.031	96	40	0.319	6	132.2	24.5	6	17	88	19.50	36.3
10	0.031	130	40	0.319	6	85.1	23.9	10	5	60	11.05	29.3
11	0.026	130	70	0.201	20	85.0	23.5	9	5	70	6.97	35.8
12	0.026	96	70	0.201	20	132.3	24.5	6	21	110	12.71	47.6
13	0.026	130	40	0.319	6	132.3	18.3	6	19	89	11.21	41.2
14	0.031	96	70	0.201	20	85.1	18.1	11	5	67	12.48	39.9
15	0.031	130	70	0.201	20	132.3	19.1	6	21	107	18.00	51.8
16	0.026	96	40	0.319	6	85.0	18.6	10	5	58	8.90	33.8
17	0.026	96	40	0.201	6	85.1	23.7	5	5	67	8.45	33.4
18	0.031	96	70	0.319	20	85.0	24.2	5	7	69	11.96	33.8
19	0.026	130	40	0.201	6	132.2	25.0	11	18	95	11.44	40.1
20	0.031	130	70	0.319	20	132.2	25.2	10	20	100	17.88	42.7

Table B.1: (continued)

Run (HX)	dc (in)	Lc (in)	Lhx (in)	ds (in)	Liniet (in)	Tcond (°F)	LP (psia)	DTsc (°F)	DTsh (°F)	T_{s2} (°F)	Meas. Flow (lbm/hr)	Meas. EFFsc (°F)
21	0.026	130	40	0.319	20	85.0	24.1	6	21	66	6.35	24.0
22	0.026	96	40	0.319	20	132.2	24.0	12	6	83	13.93	40.1
23	0.031	96	70	0.201	6	132.1	25.4	12	6	102	21.11	51.8
24	0.031	130	70	0.201	6	85.0	23.6	6	21	73	10.20	27.5
25	0.026	130	70	0.201	6	132.2	18.6	11	6	104	11.92	59.0
26	0.026	96	70	0.201	6	85.0	18.5	5	22	74	8.20	34.3
27	0.031	130	40	0.319	20	132.2	18.8	11	7	83	17.99	44.7
28	0.031	96	40	0.319	20	85.1	18.7	6	19	61	11.79	27.8
29	0.026	96	40	0.201	20	132.4	18.9	6	6	95	13.82	52.6
30	0.031	96	70	0.319	6	132.2	18.8	6	6	100	21.14	55.5
31	0.031	130	70	0.319	6	85.1	18.8	10	20	66	10.50	30.5
32	0.026	130	40	0.201	20	85.0	18.7	11	20	66	7.23	30.5

Table B.2: HFC-134a Phase 1 replicate test points

Run	HX	dc (in)	Lc (in)	Lhx (in)	ds (in)	Linlet (in)	Tcond (°F)	LP (psia)	DTsc (°F)	DTsh (°F)	T_{s2} (°F)	Meas. Flow (lbm/hr)	Meas. EFFsc (°F)
1	12	0.026	96	70	0.201	20	132.2	25.1	7	19.6	106	12.86	46.5
2	1	0.026	96	70	0.319	6	85.1	24.3	8	20.1	71	6.85	27.5
3	3	0.031	96	40	0.201	20	85.0	24.6	11	18.7	64	11.19	24.0
4	9	0.031	96	40	0.319	6	132.2	24.8	6	18.4	89	19.85	35.9
5	21	0.026	130	40	0.319	20	85.3	23.5	6	20.4	68	6.40	24.9
6	20	0.031	130	70	0.319	20	132.2	24.3	12	18.8	98	17.57	42.3
7	19	0.026	130	40	0.201	6	132.2	24.2	11	19.3	93	11.35	38.7
8	24	0.031	130	70	0.201	6	85.0	24.3	5	20.3	73	10.43	28.1

Table B.3: HFC-134a Phase 1 mid-range level test points

Run	dc (in)	Lc (in)	Lhx (in)	ds (in)	Linlet (in)	Tcond (°F)	LP (psia)	DTsc (°F)	DTsh (°F)	T_{s2} (°F)	Meas. Flow (lbm/hr)	Meas EFFsc (°F)
1 (HX17)	0.026	96	40	0.201	6	105.1	18.4	7	15	78	10.36	40.3
1B[a]	0.026	96	40	0.201	6	105.1	18.8	6	13	77	10.54	40.5
2[a]	0.026	113	40	0.201	6	85.0	18.4	4	18	72	7.08	35.5
3[a]	0.028	96	40	0.201	6	85.0	18.6	6	16	64	10.40	32.2
4 (HX20)	0.031	130	70	0.319	20	105.1	25.0	9	11	81	13.29	37.0
4B[ab]	0.031	130	70	0.347	20	105.1	24.3	9	11	80	14.36	36.6
5[ab]	0.031	113	70	0.347	20	132.2	23.7	12	13	100	20.27	46.9
6[ab]	0.028	130	70	0.347	20	132.2	24.0	11	13	102	14.67	48.5
7[a]	0.028	113	55	0.260	13	105.1	20.8	8	10	77	12.10	39.8

a - production stock capillary tube
b - enhanced inner surface suction line

Table B.4: HFC-134a Phase 2 test points

Run	HX	dc (in)	Lc (in)	Lhx (in)	ds (in)	Linlet (in)	Tcond (°F)	LP (psia)	Q (%)	DTsh (°F)	T_{s2} (°F)	Meas. Flow (lbm/hr)	Meas DTSC (°F)
1	7	0.026	130	70	0.319	20	95.7	16.0	5.2	19	80	6.00	41.7
2	7	0.026	130	70	0.319	20	115.8	15.6	0	19	90	9.80	47.4
3	7	0.026	130	70	0.319	20	95.6	25.9	0	15	80	7.32	33.1
4	7	0.026	130	70	0.319	20	115.7	25.7	3.4	15	95	8.37	41.9
5	30	0.031	96	70	0.319	6	115.7	26.3	5.9	15	94	13.60	40.2
6	30	0.031	96	70	0.319	6	95.6	26.1	0	15	79	13.52	32.4
7	30	0.031	96	70	0.319	6	95.6	16.9	3.0	14	80	11.80	44.2
8	30	0.031	96	70	0.319	6	115.7	17.0	0	13	90	17.70	49.8
9	8	0.026	96	70	0.319	20	95.7	25.7	3.6	15	81	6.50	33.6
10	8	0.026	96	70	0.319	20	115.7	26.0	0	14	94	11.73	41.0
11	8	0.026	96	70	0.319	20	95.6	15.8	0	15	79	9.51	44.0
12	8	0.026	96	70	0.319	20	115.7	16.1	3.7	19	92	9.12	48.7
13	31	0.031	130	70	0.319	6	95.6	25.5	5.0	17	83	8.10	33.0
14	31	0.031	130	70	0.319	6	115.7	26.0	0	14	93	14.79	40.3
15	31	0.031	130	70	0.319	6	115.8	15.9	5.0	16	95	12.1	51.0
16	31	0.031	130	70	0.319	6	95.6	16.5	0	14	79	12.51	44.0

Table B.5: HFC-134a Phase 3 test points

Run	HX	dc (in)	Lc (in)	Lhx (in)	ds (in)	Linlet (in)	Tcond (°F)	LP (psia)	DTsc (°F)	DTsh (°F)	T_{s2} (°F)	Oil (%)	Meas. Flow (lbm/hr)	Meas EFFsc (°F)
1	31	0.031	130	70	0.319	6	95.6	19.7	5	7	74	0.2	12.28	41.4
2	31	0.031	130	70	0.319	6	115.7	19.5	1	6	90	0.2	15.48	49.9
3	7	0.026	130	70	0.319	20	115.7	19.1	6	9	87	0.2	10.39	47.7
4	7	0.026	130	70	0.319	20	95.6	18.7	0	8	78	0.2	8.02	44.0
5	30	0.031	96	70	0.319	6	115.7	19.7	5	6	87	0.2	17.98	48.1
6	30	0.031	96	70	0.319	6	95.7	19.6	1	6	77	0.2	14.54	43.6
7	8	0.026	96	70	0.319	20	95.6	19.3	5	9	76	0.2	9.98	41.7
8	8	0.026	96	70	0.319	20	115.7	19.3	1	6	90	0.2	12.60	50.5
9	7	0.026	130	70	0.319	20	95.8	19.0	5	9	77	2.9	8.28	43.2
10	7	0.026	130	70	0.319	20	115.7	19.4	0	7	92	2.9	10.00	51.1
11	8	0.026	96	70	0.319	20	115.7	19.4	6	7	88	2.9	12.43	49.0
12	8	0.026	96	70	0.319	20	95.7	19.1	1	10	79	2.9	10.00	43.5
13	30	0.031	96	70	0.319	6	115.7	19.7	1	6	92	2.9	18.15	51.4
14	30	0.031	96	70	0.319	6	95.6	19.5	5	7	77	2.9	15.15	43.2
15	31	0.031	130	70	0.319	6	115.7	19.4	6	7	90	2.9	16.21	49.6
16	31	0.031	130	70	0.319	6	95.6	20.0	0	8	80	2.9	12.94	44.2

a - constant parameter levels

Table B.6: HFC-152a test points

Run	Tcond (°F)	dc (in)	Lc (in)	DTsc (°F)	Lhx (in)	T_{s1} (°F)	T_{s2} (°F)	ds (in)	Linlet (in)	Meas Flow (lbm/hr)	Meas EFFsc (°F)
1	120	0.026	96	7	30	19	78	0.319	20	9.79	32.8
2	120	0.026	130	15	70	7	93	0.201	20	8.35	49.2
3	120	0.031	130	6	30	5	73	0.319	6	11.89	37.4
4	100	0.026	130	3	70	21	82	0.319	6	6.92	35.1
5	100	0.026	96	14	70	20	78	0.201	20	8.54	33.8
6	100	0.026	130	14	30	10	66	0.319	20	6.55	32.3
7A	100	0.031	130	5	30	20	75	0.201	20	9.76	31.5
7B	100	0.031	130	5	30	19	74	0.201	20	9.40	31.5
8	100	0.031	96	4	70	7	80	0.319	20	12.11	42.0
9A	120	0.026	96	14	70	5	88	0.319	6	9.86	47.4
9B	120	0.026	96	15	70	8	87	0.319	6	10.08	45.1
10A	120	0.031	130	14	70	19	88	0.319	20	12.79	39.4
10B	120	0.031	130	15	70	20	87	0.319	20	13.13	38.3
11A	100	0.026	96	5	30	5	73	0.201	6	7.59	38.8
11B	100	0.026	96	4	30	7	73	0.201	6	8.14	37.7
12	100	0.031	130	14	70	4	76	0.201	6	11.05	41.9
13	120	0.026	130	15	30	21	81	0.201	6	8.45	34.1
14	120	0.031	96	5	70	17	100	0.201	6	15.34	47.1
15	100	0.031	96	14	30	20	63	0.319	6	11.84	24.7
16	120	0.031	96	15	30	7	73	0.201	20	14.90	37.1

Table B.7: HFC-152a mid-range level test points

Run	Tcond (°F)	dc (in)	Lc (in)	DTsc (°F)	Lhx (in)	T_{s1} (°F)	T_{s2} (°F)	ds (in)	Liniet (in)	Meas Flow (lbm/hr)	Meas EFFsc (°F)
17	110	0.026	130	10	70	15	84	0.319	6	8.44	39.5
18	110	0.031	96	10	70	15	88	0.201	6	14.05	42.0
19	100	0.028	96	9	30	18	75	0.201	6	9.69	33.0
20	120	0.028	96	11	30	6	84	0.201	6	12.37	43.9
21	110	0.026	113	10	30	18	82	0.201	6	7.92	36.5
22	110	0.028	113	10	55	14	82	0.260	13	10.22	38.9

Table B.8: CFC-12 test points

Run	Tcond (°F)	dc (in)	Lc (in)	DTsc (°F)	Lhx (in)	T_{s1} (°F)	T_{s2} (°F)	ds (in)	Liniet (in)	Meas Flow (lbm/hr)	Meas EFFsc (°F)
1	120	0.026	96	11	70	14	90	0.319	6	11.80	45.8
2A	120	0.031	130	10	70	14	89	0.319	20	16.09	45.2
2B	120	0.031	130	10	70	13	89	0.319	20	15.69	45.8
3	120	0.026	130	11	30	14	81	0.201	6	10.21	40.4
4A	100	0.026	96	11	30	15	71	0.201	6	9.43	34.6
4B	100	0.026	96	11	30	13	69	0.201	6	10.22	34.6
5	100	0.026	130	10	70	11	76	0.319	6	8.86	40.3
6	120	0.031	96	10	30	14	72	0.319	6	17.40	34.5
7	100	0.031	96	9	70	11	76	0.319	20	14.70	40.2
8	100	0.031	130	9	30	16	67	0.319	6	11.49	31.4

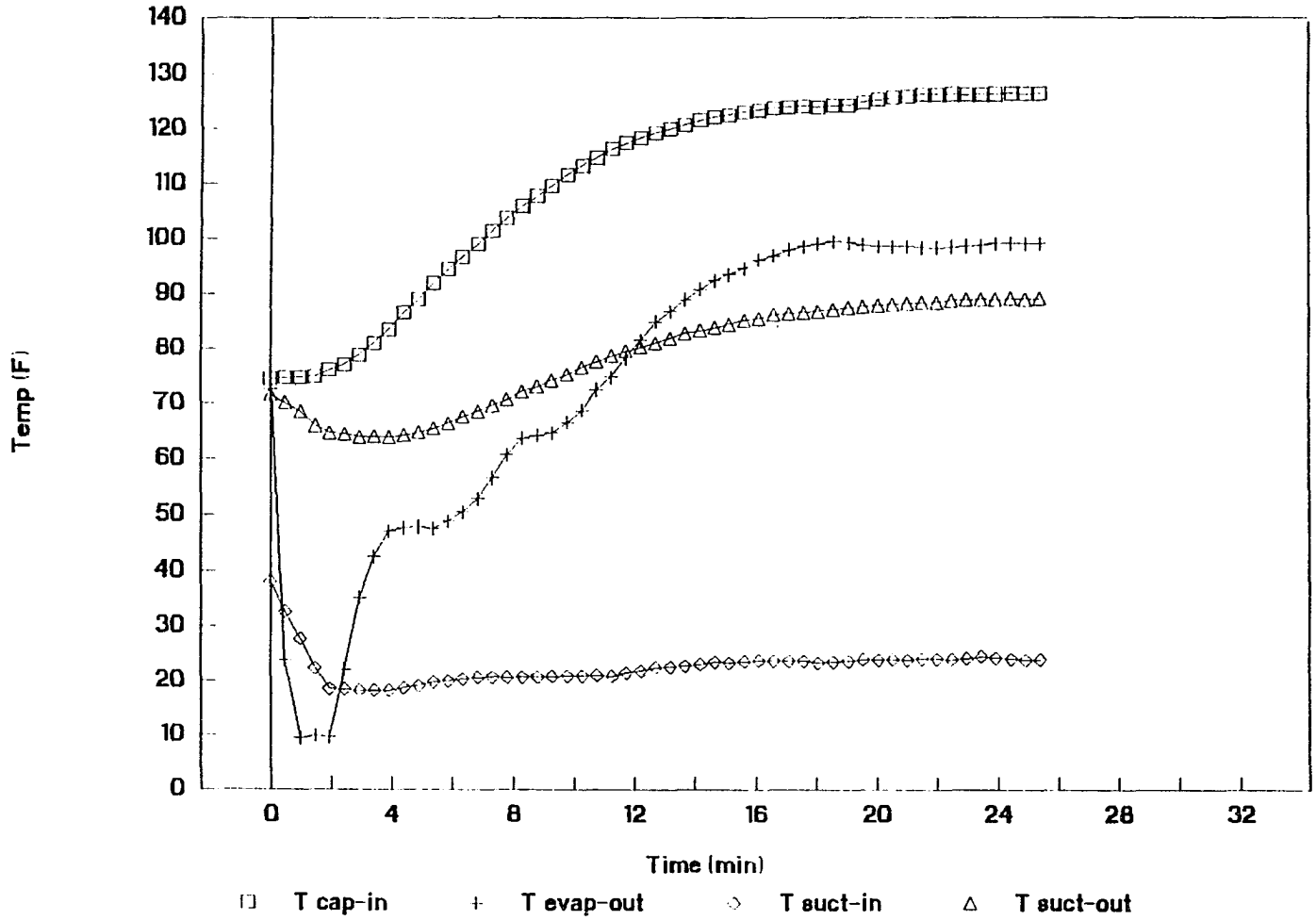

Figure B.1: Temperature versus time test data for HFC-134a replicate test point 4

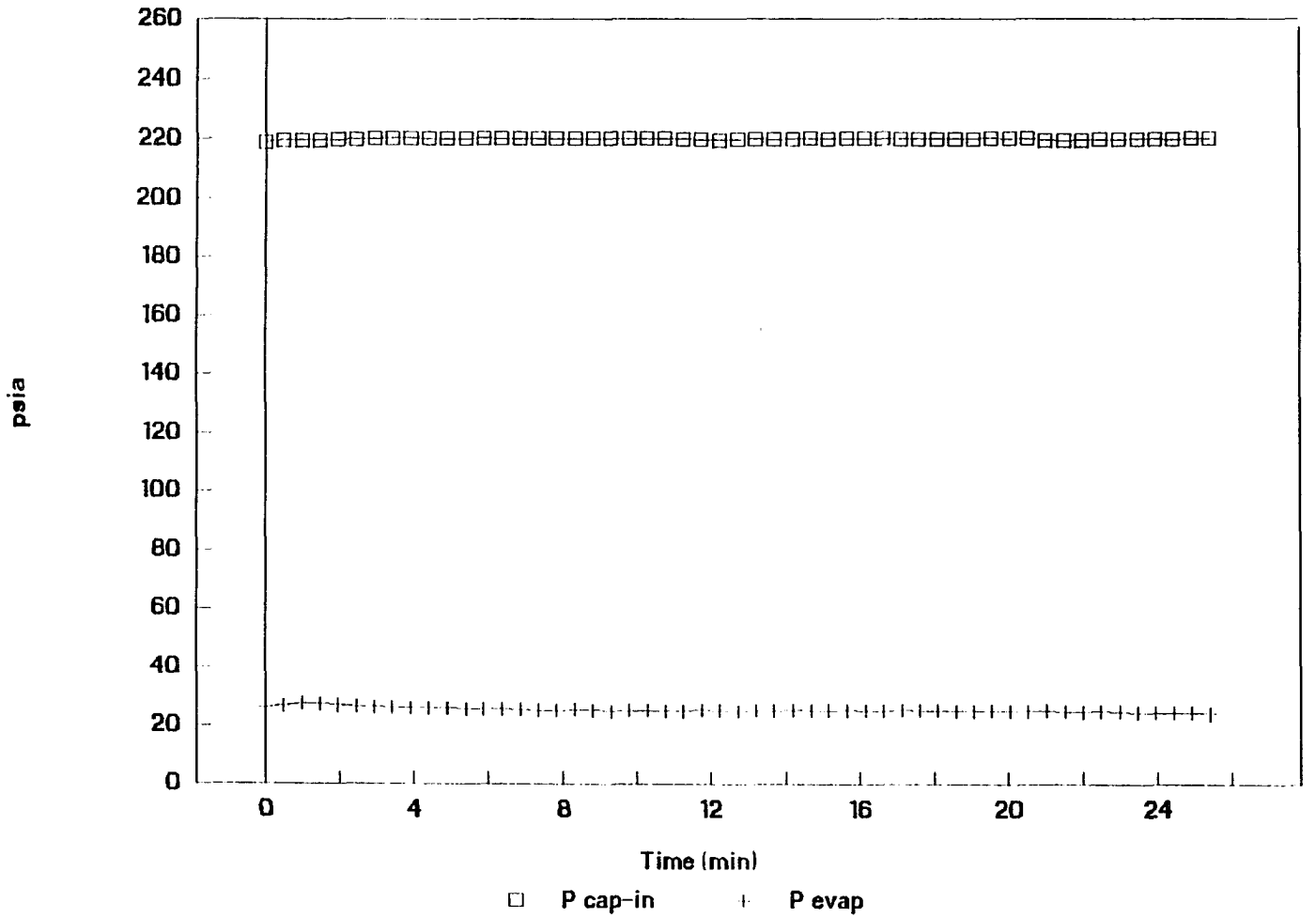

Figure B.2: Pressure versus time test data for HFC-134a replicate test point 4

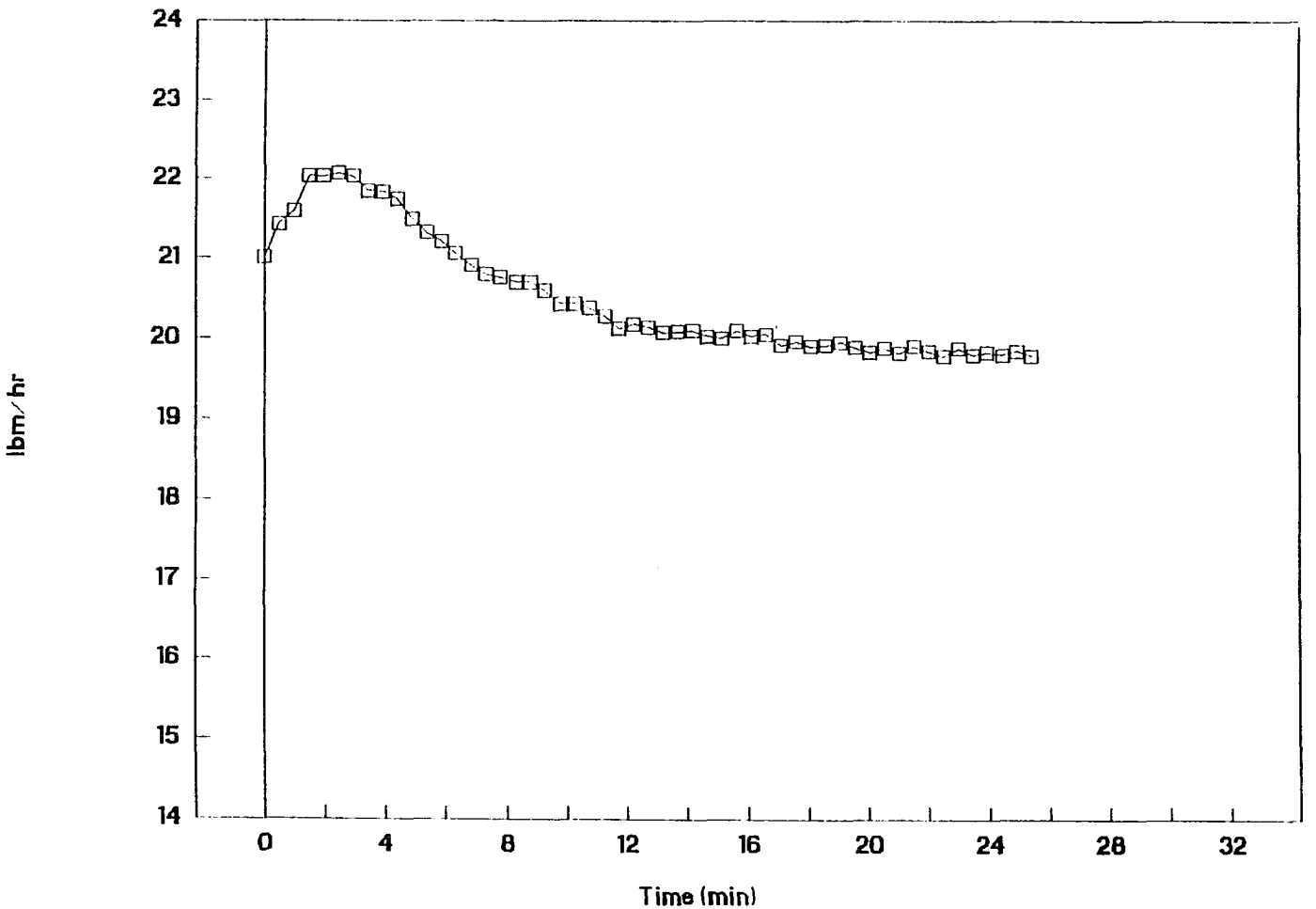

Figure B.3: Mass flow rate versus time test data for HFC-134a replicate test point 4

APPENDIX C. UNCERTAINTY ANALYSIS

The prediction equations presented in Chapter 4 for HFC-134a were developed from test data using 32 different heat exchanger assemblies. Similarly, the prediction equations presented in Chapter 5 for HFC-152a were developed from test data using 16 different heat exchanger assemblies. The scatter in the data surrounding a predicted value is due to: (1) variability in the geometry variables, (2) random error in the measured dependent and independent variables that contribute to experimental error, and (3) insignificant effects not included in the final prediction equations. The overall uncertainty in a predicted mean value of mass flow rate or effective subcooling is, therefore, best quantified by the calculated confidence and prediction intervals based on the statistical assessment of the data scatter.

The contributions to data scatter from geometry variability and measurement error in the independent variables can be quantified by an uncertainty analysis applied to each prediction equation. This appendix section presents a sample uncertainty analysis for each performance equation. The classic Kline and McClintock (1953) propagation of error uncertainty analysis is used to establish the uncertainties, which accounts for the individual uncertainties in all independent variables. The general equation for uncertainty is given by

$$\Delta W = [(\partial W/\partial x_1 * \Delta x_1)^2 + (\partial W/\partial x_2 * \Delta x_2)^2 + \ldots + (\partial W/\partial x_n * \Delta x_n)^2]^{1/2} \quad (C.1)$$

where

$W = f(x_1, x_2, \ldots x_n)$,

ΔW is the uncertainty in W, and

$\Delta x_1, \ldots \Delta x_n$ are uncertainties in $x_1, \ldots x_n$.

HFC-134a prediction equations

Measured effective subcooling

The uncertainty in the calculated effective subcooling value, EFFsc, for Phase 1 test point 5 follows, and is applicable to all test points to a close approximation.

The effective subcooling is given by

$$EFFsc = (Cp_{gs}/Cp_{fc})(T_{s2} - T_{s1}) \qquad (C.2)$$

The uncertainty in calculated EFFsc is given by

$$\Delta EFFsc = [(\partial EFFsc/\partial Cp_{gs} * \Delta Cp_{gs})^2 + (\partial EFFsc/\partial Cp_{fc} * \Delta Cp_{fc})^2 + (\partial EFFsc/\partial T_{s2} * \Delta T_{s2})^2 + (\partial EFFsc/\partial T_{s1} * \Delta T_{s1})^2]^{1/2} \qquad (C.3)$$

Phase 1 test point 5 data:

$T_{s2} = 91$ °F, $T_{s1} = 17$ °F

$Cp_{gs} = 0.198$ at $T_{s\text{-}avg} = 54°$ F

$Cp_{fc} = 0.364$ at $T_{c1} = 120$ °F

The individual term contributions to the overall uncertainty are given below. It is assumed that the specific heat values are known to 1%, and the measured temperature values are accurate to ± 0.5 °F.

$$(\partial EFFsc/\partial Cp_{gs})\Delta Cp_{gs} = (T_{s2} - T_{s1})/Cp_{fc}*\Delta Cp_{gs}$$
$$= (91-17)/.364*(.01*.198) = 0.40 \qquad (C.4)$$

$$(\partial EFFsc/\partial Cp_{fc})\Delta Cp_{fc} = -Cp_g(T_{s2} - T_{s1})/Cp_{fc}^{2}*\Delta Cp_{fc}$$
$$= -(91-17)*.198/(.3642)^2*(.01*.364)$$
$$= 0.40 \qquad (C.5)$$

$$(\partial EFFsc/\partial T_{s2})\Delta T_{s2} = Cp_{gs}/Cp_{fc}*\Delta T_{s2}$$
$$= .198/.364*0.5 = 0.27 \qquad (C.6)$$

$$(\partial EFFsc/\partial T_{s1})\Delta T_{s1} = -Cp_{gs}/Cp_{fc}*\Delta T_{s1}$$
$$= -.198/.364*0.5 = -0.27 \qquad (C.7)$$

The overall uncertainty in calculated EFFsc for Phase 1 test point 5 is therefore,

$$\Delta EFFsc = [(0.40)^2+(0.40)^2+(0.27)^2+(0.27)^2]^{1/2}$$
$$= \pm 0.68\ °F \qquad (C.8)$$

Effective subcooling prediction

The uncertainty in the predicted effective subcooling value due to geometry variability and measurement error for Phase 1 test point 5 follows, and is applicable to all test points to a close approximation.

The effective subcooling prediction equation is given by

$$\begin{aligned} EFFsc_{pred}(F) = {} & 39.2 + 0.3156(Tcond-108.6) - 0.4735(DTsh-12.85) \\ & + 0.1815(Lhx-55 - 0.9262(LP-21.4) - 28.54(ds-0.260) \\ & - 0.2188(DTsc-8.2) - 143.6(dc-0.0285) \\ & + 3.116\times10^{-3}(Lhx-55)(Tcond-108.6) \\ & - 0.343(Tcond-108.6)(ds-0.260) \\ & + 0.756(ds-0.260)(DTsh-12.85) \\ & + 1.829\times10^{-3}(Tcond-108.5)(DTsh-12.85) \end{aligned} \qquad (C.9)$$

The uncertainty in predicted EFFsc is given by

$$\begin{aligned} \Delta EFFsc = {} & [(\partial EFFsc/\partial Tcond*\Delta Tcond)^2 + (\partial EFFsc/\partial LP*\Delta LP)^2 \\ & + (\partial EFFsc/\partial DTsh*\Delta DTsh)^2 + (\partial EFFsc/\partial ds*\Delta ds)^2 \\ & + (\partial EFFsc/\partial Lhx*\Delta Lhx)^2 + (\partial EFFsc/\partial DTsc*\Delta DTsc)^2 \\ & + (\partial EFFsc/\partial dc*\Delta dc)^2]^{1/2} \end{aligned} \qquad (C.10)$$

Phase 1 test point 5 data:

Tcond = 132 °F, DTsc = 12 °F,

LP = 19.1 psia, Lhx = 40 in,

DTsh = 22 F, ds = .201 in, dc = .031 in

Individual uncertainties:

ΔTcond = 0.11 °F, ΔDTsc = 0.5 °F,

ΔLP = 0.1 psia, ΔLhx = 0.25 in,

ΔDTsh = 0.5 °F, Δds = 0.01 in, Δdc = 0.0001 in

The individual term contributions are given below.

$$(\partial EFFsc/\partial Tcond)\Delta Tcond = [0.3156 + 3.116*10^{-3}(Lhx-55) - 0.343(ds-0.260) + 1.829 \times 10^{-3}(DTsh - 12.85)]*0.11 = 0.034 \quad (C.11)$$

$$(\partial EFFsc/\partial LP)\Delta LP = -0.9262*0.10 = -0.093 \quad (C.12)$$

$$(\partial EFFsc/\partial DTsh)\Delta DTsh = [-0.4735 + 0.756(ds - 0.260) + 1.829 \times 10\text{-}3(Tcond - 108.5)]*0.5 = -0.238 \quad (C.13)$$

$$(\partial EFFsc/\partial ds)\Delta ds = [-28.54 - 0.343(Tcond-108.6) + 0.756(DTsh - 12.85)]*0.01 = -0.296 \quad (C.14)$$

$$(\partial EFFsc/\partial Lhx)\Delta Lhx = [0.1815 + 3.116*10^{-3}(Tcond-108.6)]*0.25 = 0.064 \quad (C.15)$$

$$(\partial EFFsc/\partial DTsc)\Delta DTsc = -0.2188*0.5 = -0.11 \qquad (C.16)$$

$$(\partial EFFsc/\partial dc)\Delta dc = -143.6*0.0001 = -0.014 \qquad (C.17)$$

The overall uncertainty in predicted EFFsc for Phase 1 test point 5 is therefore,

$$\Delta EFFsc = [(0.034)^2 + (-0.093)^2 + (-0.238)^2 + (-0.296)^2 + (0.064)^2 + (-0.11)^2 + (-0.014)^2]^{1/2}$$
$$= \pm 0.41\ ^\circ F \qquad (C.18)$$

Subcooled inlet mass flow rate prediction

The uncertainty in the subcooled inlet predicted mass flow rate due to geometry variability and measurement error for Phase 1 test point 5 follows, and is applicable to all test points to a close approximation.

The subcooled inlet mass flow rate prediction equation is given by

$$\dot{m}_{pred}(lbm/hr) = 12.57 + 0.1373(Tcond-108.6) + 1010(dc-.0285) - 0.0531(Lc-113) - 0.04078(DTsh-12.85) - 0.0737(LP-21.4) + 0.0464(DTsc-8.2) + 0.0064(Lhx-55) + 12.034(dc-.0285)(Tcond-108.6) - 7.228x10^{-4}(Tcond-108.6)(Lc-113) + 5.867(dc-.0285)(Lhx-55) \qquad (C.19)$$

The uncertainty in predicted mass flow rate is given by

$$\Delta\dot{m} = [(\partial\dot{m}/\partial dc*\Delta dc)^2 + (\partial\dot{m}/\partial Tcond*\Delta Tcond)^2 + (\partial\dot{m}/\partial Lc*\Delta Lc)^2 + (\partial\dot{m}/\partial DTsh*\Delta DTsh)^2 + (\partial\dot{m}/\partial LP*\Delta LP)^2 + (\partial\dot{m}/\partial DTsc*\Delta DTsc)^2 + (\partial\dot{m}/\partial Lhx*\Delta Lhx)^2\ ]^{1/2} \quad (C.20)$$

Phase 1 test point 5 data:

Tcond = 132 °F, DTsc = 12 °F,

LP = 19.1 psia, Lhx = 40 in,

DTsh = 22 F, Lc = 96 in, dc = 0.031 in

Individual uncertainties:

ΔTcond = 0.11 °F, ΔDTsc = 0.5 °F,

ΔLP = 0.1 psia, ΔLhx = 0.25 in,

ΔDTsh = 0.5 °F, ΔLc = 0.25 in, Δdc = 0.0001 in

Individual term contributions are given below.

$$(\partial\dot{m}/\partial dc)\Delta dc = [1010 + 12.034(Tcond-108.6) + 5.867(Lhx - 55)]*0.0001 = 0.120 \quad (C.21)$$

$$(\partial\dot{m}/\partial Tcond)\Delta Tcond = [0.1373 + 12.034(dc-0.0285) - 7.228*10^{-4}(Lc-113)]*0.11 = 0.020 \quad (C.22)$$

$$(\partial\dot{m}/\partial Lc)\Delta Lc = [-0.0531 - 7.228*10^{-4}(Tcond-108.6)]*0.25$$

$$= -0.018 \qquad \text{(C.23)}$$

$$(\partial\dot{m}/\partial DTsh)\Delta DTsh = -0.04078*0.5 = -0.020 \qquad \text{(C.24)}$$

$$(\partial\dot{m}/\partial LP)\Delta LP = -0.0737*0.1 = -0.0074 \qquad \text{(C.25)}$$

$$(\partial\dot{m}/\partial DTsc)\Delta DTsc = 0.0464*0.5 = 0.023 \qquad \text{(C.26)}$$

$$(\partial\dot{m}/\partial Lhx)\Delta Lhx = [0.0064 + 5.867(dc - .0285)]*0.25$$
$$= 0.005 \qquad \text{(C.27)}$$

The overall uncertainty in predicted mass flow rate for Phase 1 test point 5 is therefore,

$$\Delta\dot{m} = [(0.120)^2 + (0.020)^2 + (-0.018)^2 + (-0.020)^2 + (-0.0074)^2 + (0.023)^2 + (0.005)^2]^{1/2}$$
$$= \pm 0.125 \text{ lbm/hr} \qquad \text{(C.28)}$$

Quality inlet mass flow rate prediction

The uncertainty in the predicted mass flow rate due to geometry variability and measurement error for Phase 2 test point 15 follows, and is applicable to all quality inlet test points (Q > 0%) to a close approximation.

The quality inlet mass flow rate prediction equation is given by

$$\dot{m}_{qual}(lbm/hr) = 10.78 + 894.4(dc-.0285) + 0.1368(Tcond-105.7) - 0.605(Q-2.2) - 0.0533(Lc-113) - 0.0576(LP-21) - 51.64(Q-2.2)(dc-.0285) + 0.00515(LP-21)(Tcond-105.7) - 5.506(dc-0.0285)(Lc-113) - 17.92(LP-21)(dc-0.0285) + 6.408(dc-0.0285)(Tcond-105.7) \quad (C.29)$$

The uncertainty in predicted mass flow rate is given by

$$\Delta\dot{m} = [(\partial\dot{m}/\partial dc*\Delta dc)^2 + (\partial\dot{m}/\partial Tcond*\Delta Tcond)^2 + (\partial\dot{m}/\partial Q*\Delta Q)^2 + (\partial\dot{m}/\partial Lc*\Delta Lc)^2 + (\partial\dot{m}/\partial LP*\Delta LP)^2]^{1/2} \quad (C.30)$$

Since the quality, Q(%), is a calculated value based on measured parameter levels, the ΔQ is also based on a propagation of error analysis. Quality was calculated based on an energy balance between the refrigerant flow and the preheater power requirement.

$$\dot{q}_{net} = \dot{m}xh_{fg} + \dot{m}Cp_f(T_{sat} - T_{prehtr\text{-}in}) \quad (C.31)$$

Solving for x gives,

$$x = [\dot{q}_{net} - \dot{m}Cp_f(T_{sat} - T_{prehtr\text{-}in})]/(\dot{m}h_{fg}) \quad (C.32)$$

where x is the thermodynamic equilibrium quality. The uncertainty in thermodynamic equilibrium quality is given by

$$\Delta x = [(\partial x/\partial q_{net}*\Delta q_{net})^2 + (\partial x/\partial \dot{m}*\Delta \dot{m})^2 + (\partial x/\partial h_{fg}*\Delta h_{fg})^2 + (\partial x/\partial Cp_f*\Delta Cp_f)^2 + (\partial x/\partial T_{sat}*\Delta T_{sat})^2 + (\partial x/\partial T_{in}*\Delta T_{in})^2]^{1/2} \quad (C.33)$$

Phase 2 test point 15 data:

Tcond = 115.7 °F, Q = 5.0%, $\dot{m}$ = 11.62 lbm/hr,

LP = 15.9 psia, q_{net} = 67 W, Lc = 130 in

dc = 0.031 in, h_{fg} = 66.8 Btu/lbm,

T_{sat} = 115.7 °F, $T_{prehtr\text{-}in}$ = 72 °F

Cp_f = 0.343 Btu/lbm-F

Individual uncertainties:

ΔTcond = 0.11 °F, $\Delta\dot{m}$ = 0.50 lbm/hr,

ΔLP = 0.1 psia, Δq_{net} = 2% = 1.34 W, ΔLc = 0.25 in,

Δdc = 0.0001 in, Δh_{fg} = 1%, ΔCp_f = 1%,

ΔT_{sat} = 0.11 °F, $\Delta T_{prehtr\text{-}in}$ = 0.5 F

Individual term contributions to the quality uncertainty are given below.

$$(\partial x/\partial q_{net})\Delta q_{net} = [1/(\dot{m}h_{fg})]*1.34$$
$$= 1/(11.62*66.8)*1.34*3.412$$
$$= 0.0059 \quad (C.34)$$

$$(\partial x/\partial \dot{m})\Delta \dot{m} = (-q_{net}/(\dot{m}^2 h_{fg})*0.50$$
$$= -67/(11.62^2*66.8)*0.25*3.412$$
$$= -0.0126 \quad (C.35)$$

$$(\partial x/\partial h_{fg})\Delta h_{fg} = [-q_{net}/(\dot{m}h_{fg}^2) + Cp_f(T_{sat}-T_{in})]*0.668$$
$$= [-67/11.62*3.412 + 0.343(115.7-72)]\ /66.8^2*0.668$$
$$= -0.00070 \qquad (C.36)$$

$$(\partial x/\partial Cp_f)\Delta Cp_f = -(T_{sat}-T_{in})/h_{fg}*0.00343$$
$$= -(115.7-72)/66.8*0.00343$$
$$= -0.00224 \qquad (C.37)$$

$$(\partial x/\partial T_{sat})\Delta T_{sat} = -Cp_f/h_{fg}*0.5$$
$$= -0.343/66.8*0.5 = -0.00257 \qquad (C.38)$$

$$(\partial x/\partial T_{in})\Delta T_{in} = Cp_f/h_{fg}*0.5$$
$$= 0.343/66.8*0.5 = 0.00257 \qquad (C.39)$$

The uncertainty in thermodynamic equilibrium quality is,

$$\Delta x = [(0.0059)^2 + (-0.0126)^2 + (-0.0007)^2 + (-0.00224)^2 +$$
$$(-0.00257)^2 + (0.00257)^2]^{1/2}$$
$$= \pm 0.0146 \qquad (C.40)$$

Therefore,

$$\Delta Q = \pm 1.46\% \qquad (C.41)$$

The uncertainty in predicted mass flow rate can now be determined. Beginning with Equation C.30,

$$\Delta\dot{m} = [(\partial\dot{m}/\partial dc*\Delta dc)^2 + (\partial\dot{m}/\partial Tcond*\Delta Tcond)^2 + (\partial\dot{m}/\partial Q*\Delta Q)^2 + (\partial\dot{m}/\partial Lc*\Delta Lc)^2 + (\partial\dot{m}/\partial LP*\Delta LP)^2]^{1/2} \quad (C.30)$$

The individual term contributions are given below.

$$(\partial\dot{m}/\partial dc)\Delta dc = [894.4 - 17.92(LP-21) + 6.408(Tcond-105.7) - 5.506(Lc-113) - 51.64(Q-2.2)]*0.0001 = 0.0812 \quad (C.42)$$

$$(\partial\dot{m}/\partial Tcond)\Delta Tcond = [0.1368 + 6.408(dc-0.0285) + 0.00515(LP-21)]*0.11 = 0.0139 \quad (C.43)$$

$$(\partial\dot{m}/\partial Q)\Delta Q = [-0.605 - 51.64(dc-0.0285)]*1.46 = -1.071 \quad (C.44)$$

$$(\partial\dot{m}/\partial Lc)\Delta Lc = [-0.0533 - 5.506(dc-0.0285)]*0.25 = -0.0167 \quad (C.45)$$

$$(\partial\dot{m}/\partial LP)\Delta LP = [-0.0576 - 17.92(dc-0.0285) + 0.00515(Tcond-105.7)]*0.1 = -0.005 \quad (C.46)$$

The overall uncertainty in predicted mass flow rate for Phase 2 test point 15 is therefore,

$$\Delta\dot{m} = [(0.0812)^2 + (0.0139)^2 + (-1.071)^2 + (-0.0167)^2 + (-0.005)^2]^{1/2}$$
$$= \pm 1.07 \text{ lbm/hr} \qquad \text{(C.47)}$$

Overall uncertainty is the more conservative quantification of the "confidence" in using the quality inlet mass flow prediction equation. The dominant factor contributing to overall uncertainty is the uncertainty in measured mass flow rate (assumed ±0.5 lbm/hr) used in calculating quality, Q. This is a result of the inherent instability of the two-phase flow regime. The inclusion of replication points in the Phase 2 test matrix would have resulted in a more reliable statistical assessment of the results.

HFC-152a prediction equations

Measured effective subcooling

The uncertainty in the calculated effective subcooling value, EFFsc, for test point 8 follows, and is applicable to all test points to a close approximation.

The effective subcooling is given by

$$EFFsc = (Cp_{gs}/Cp_{fc})(T_{s2} - T_{s1}) \qquad \text{(C.2)}$$

The uncertainty in calculated EFFsc is given by

$$\Delta EFFsc = [(\partial EFFsc/\partial Cp_{gs}*\Delta Cp_{gs})^2 + (\partial EFFsc/\partial Cp_{fc}*\Delta Cp_{fc})^2 + (\partial EFFsc/\partial T_{s2}*\Delta T_{s2})^2 + (\partial EFFsc/\partial T_{s1}*\Delta T_{s1})^2]^{1/2} \quad (C.48)$$

Test point 8 data:

$T_{s2} = 80\ °F$, $T_{s1} = 7°\ F$

$Cp_{gs} = 0.241$ at $T_{s\text{-}avg} = 44\ °F$

$Cp_{fc} = 0.434$ at $T_{c1} = 95\ °F$

The individual term contributions to the overall uncertainty are given below. It is assumed that the specific heat values are known to 1%, and the measured temperature values are accurate to ± 0.5 °F.

$$(\partial EFFsc/\partial Cp_{gs})\Delta Cp_{gs} = (T_{s2} - T_{s1})/Cp_{fc}*\Delta Cp_{gs} = (80-7)/.434*(.01*.241) = 0.41 \quad (C.49)$$

$$(\partial EFFsc/\partial Cp_{fc})\Delta Cp_{fc} = -Cp_{gs}(T_{s2} - T_{s1})/Cp_{fc}^2*\Delta Cp_{fc} = -(80-7)*.241/(.434)^2*(.01*.434) = 0.41 \quad (C.50)$$

$$(\partial EFFsc/\partial T_{s2})\Delta T_{s2} = Cp_g/Cp_f*\Delta T_{s2} = .241/.434*0.5 = 0.28 \quad (C.51)$$

$$(\partial EFFsc/\partial T_{s1})\Delta T_{s1} = -Cp_g/Cp_f*\Delta T_{s1} = -.241/.434*0.5 = -0.28 \quad (C.52)$$

The overall uncertainty in calculated EFFsc for test point 8 is therefore,

$$\Delta EFFsc = [(0.41)^2+(0.41)^2+(0.28)^2+(0.28)^2]^{1/2}$$
$$= \pm 0.69\ ^\circ F \qquad (C.53)$$

Effective subcooling prediction

The uncertainty in the predicted effective subcooling value due to geometry variability and measurement error for test point 8 follows, and is applicable to all test points to a close approximation.

The effective subcooling prediction equation is given by

$$EFFsc_{pred}(F) = 37.6 + 0.206(Lhx-50) - 0.443(Ts1-13.1) + 0.270(Tcond-110)$$
$$- 0.314(DTsc-9.85) + 0.0043(Lhx-50)(Tcond-110)$$
$$- 25.0(ds-0.260) + 0.0116(Tcond-110)(Ts1-13.1) \qquad (C.54)$$

The uncertainty in predicted EFFsc is given by

$$\Delta EFFsc = [(\partial EFFsc/\partial Tcond*\Delta Tcond)^2$$
$$+ (\partial EFFsc/\partial Ts1*\Delta Ts1)^2 + (\partial EFFsc/\partial ds*\Delta ds)^2$$
$$+ (\partial EFFsc/\partial Lhx*\Delta Lhx)^2 + (\partial EFFsc/\partial DTsc*\Delta DTsc)^2]^{1/2} \qquad (C.55)$$

Test point 8 data:

Tcond = 100 °F, DTsc = 5 °F,

Lhx = 70 in, ds = .319 in,

Ts1 = 7 °F

Individual uncertainties:

ΔTcond = 0.10 °F, ΔDTsc = 0.5 °F,

ΔLhx = 0.25 in, Δds = 0.01 in,

ΔTs1 = 0.5 °F

The individual term contributions are given below.

$$(\partial EFFsc/\partial Tcond)\Delta Tcond = [0.270 + 0.0043(Lhx-50) - 0.0116(Ts1-13.1)]*0.10$$
$$= 0.029 \qquad (C.56)$$

$$EFFsc/\partial Ts1)\Delta Ts1 = [-0.443 + 0.0116(Tcond-110)]*0.5$$
$$= -0.280 \qquad (C.57)$$

$$(\partial EFFsc/\partial ds)\Delta ds = -25*0.01 = -0.25 \qquad (C.58)$$

$$(\partial EFFsc/\partial Lhx)\Delta Lhx = [0.206 + 0.0043(Tcond-110)]*0.25$$
$$= 0.041 \qquad (C.59)$$

$$(\partial EFFsc/\partial DTsc)\Delta DTsc = -0.314*0.5 = -0.157 \qquad (C.60)$$

The overall uncertainty in predicted EFFsc for test point 8 is therefore,

$$\Delta EFFsc = [(0.041)^2 + (-0.280)^2 + (0.029)^2 + (-0.157)^2 + (-0.25)^2]^{1/2}$$
$$= \pm 0.41\ °F \qquad (C.61)$$

Subcooled inlet mass flow rate prediction

The uncertainty in the subcooled inlet predicted mass flow rate due to geometry variability and measurement error for test point 8 follows, and is applicable to all test points to a close approximation.

The subcooled inlet mass flow rate prediction equation is given by

$$\dot{m}_{pred}(lbm/hr) = 10.39 + 828.8(dc-.0285) + 0.1079(Tcond-110)$$
$$- 0.054(Lc-113) + 0.0134(Lhx-50)$$
$$+ 0.030(DTsc-9.85) + 9.36(dc-.0285)(Tcond-110)$$
$$- 4.024(dc-.0285)(Lc-113) \qquad (C.62)$$

The uncertainty in predicted mass flow rate is given by

$$\Delta\dot{m} = [(\partial\dot{m}/\partial dc*\Delta dc)^2 + (\partial\dot{m}/\partial Tcond*\Delta Tcond)^2 + (\partial\dot{m}/\partial Lc*\Delta Lc)^2$$
$$+ (\partial\dot{m}/\partial DTsc*\Delta DTsc)^2 + (\partial\dot{m}/\partial Lhx*\Delta Lhx)^2\ ]^{1/2} \qquad (C.63)$$

Test point 8 data:

Tcond = 100 °F, DTsc = 5 °F,

Lhx = 70 in, Lc = 96 in,

dc = 0.031 in

Individual uncertainties:

$\Delta Tcond = 0.10\ °F$, $\Delta DTsc = 0.5\ °F$,

$\Delta Lhx = 0.25$ in, $\Delta Lc = 0.25$ in

$\Delta dc = 0.0001$ in

Individual term contributions are given below.

$$(\partial \dot{m}/\partial dc)\Delta dc = [828.8 + 9.36(Tcond-110) - 4.024(Lc-113)]*0.0001$$
$$= 0.080 \qquad (C.64)$$

$$(\partial \dot{m}/\partial Tcond)\Delta Tcond = [0.1079 + 9.36(dc-.0285)]*0.10$$
$$= 0.013 \qquad (C.65)$$

$$(\partial \dot{m}/\partial Lc)\Delta Lc = [-0.054 - 4.024(dc-.0285)]*0.25$$
$$= -0.016 \qquad (C.66)$$

$$(\partial \dot{m}/\partial DTsc)\Delta DTsc = 0.0301*0.5 = 0.015 \qquad (C.67)$$

$$(\partial \dot{m}/\partial Lhx)\Delta Lhx = 0.0134*0.25$$
$$= 0.0034 \qquad (C.68)$$

The overall uncertainty in predicted mass flow rate for test point 8 is therefore,

$$\Delta\dot{m} = [(0.013)^2 + (0.0804)^2 + (-0.016)^2 + (0.0034)^2 + (0.015)^2]^{1/2}$$

$$= \pm 0.084 \text{ lbm/hr} \qquad \text{(C.69)}$$

APPENDIX D. TEST MATRIX CONFOUNDING PATTERNS

This appendix presents the confounding patterns associated with the development of the HFC-134a, HFC-152a, and CFC-12 test matrices. Confounding between main effects and interaction effects exist with fractional designs, as were used for this study.

HFC-134a test matrix - Phase 1

The HFC-134a Phase 1 test matrix was a 1/16 fraction of a 2^9 factorial design with resolution IV, designated 2_{IV}^{9-4}. For simplicity, the nine variables (main effects) are redefined as follows.

dc - A
ds - B
Lhx - C
Tcond - D
LP - E
Lc - F
DTsc - G
DTsh - H
Linlet - J

For the 2_{IV}^{9-4} design, the following identities are defined initially (Box, et. al., 1978).

$$F = BCDE$$

$$G = ACDE$$

$$H = ABDE$$

$$J = ABCE$$

Multiplying both sides of each of these four identities by F,G,H, and J, respectively, provides the four generating relations

$$I = BCDEF$$

$$I = ACDEG$$

$$I = ABDEH$$

$$I = ABCEJ$$

where I is referred to as a defining relation. The complete set of defining relations included these four "words", plus all other combinations of words. Multiplying two at a time gives

$$I = ABFG = ACFH = ADFJ = BCGH = BDGJ = CDHJ.$$

Multiplying three at a time gives

$$I = DEFGH = CEFGJ = AEGHJ = BEFHJ.$$

Multiplying four at a time gives

I = ABCDFGHJ.

The complete set of defining relations is, therefore,

I = BCDEF = ACDEG = ABDEH = ABCEJ
= ABFG = ACFH = ADFJ = BCGH = BDGJ = CDHJ
= DEFGH = CEFGJ = AEGHJ = BEFHJ = ABCDFGHJ.

All main effects are confounded with four factor and higher interactions, and all three factor and higher interactions were assumed to be insignificant. With a resolution IV design, two factor interactions are confounded with other two factor interactions. In many instances, two factor interactions can be of significance. The two factor confounding patterns follow.

AB = FG	AJ = DF
AF = BG = CH = DJ	BC = GH
AG = BF	BH = CG
AC = FH	BD = GJ
AH = CF	BJ = DG
AD = FJ	CD = HJ
AF = DJ	CJ = DH

HFC-134a test matrix - Phase 2

The Phase 2 test matrix was a 1/2 fraction of a 2^5 factorial design with resolution V, designated 2_V^{5-1}. For simplicity, the five variables (main effects) are redefined as follows.

Q - A

LP - B

dc - C

Lc - D

Tcond - E

For the 2_V^{5-1} design, the following identity is defined (Box, et. al., 1978).

$$E = ABCD$$

The generator, or defining relation for this design, is ABDCE alone. For a resolution V design, main effects are confounded with four factor and higher interactions, and two factor interaction are confounded with three factor interactions. All three factor and higher interactions were assumed to be insignificant. The confounding patterns follow.

A = BCDE	AB = CDE	BD = ACE
B = ACDE	AC = BDE	BE = ACD
C = ABDE	AD = BCE	CD = ABE
D = ABCE	AE = BCD	CE = ABD
E = ABCD	BC = ADE	DE = ABC

HFC-134a test matrix - Phase 3

The Phase 3 test matrix was a 1/2 fraction of a 2^5 factorial design with resolution V, designated 2_V^{5-1}. For simplicity, the five variables (main effects) are redefined as follows.

Tcond - A
dc - B
Lc - C
%oil - D
DTsc - E

The confounding patterns were the same as presented for the Phase 2 test matrix, since both test matrices are 2_V^{5-1}.

HFC-152a test matrix

The HFC-152a test matrix was a 1/16 fraction of a 2^8 factorial design with resolution IV, designated 2_{IV}^{8-4}. For simplicity, the eight variables (main effects) are redefined as follows.

Tcond - A
dc - B
Lc - C
DTsc - D
Lhx - E
Ts1 - F
ds - G
Linlet - H

For the 2_{IV}^{8-4} design, the following identities are defined initially (Box, et. al., 1978).

$$E = BCD$$
$$F = ACD$$
$$G = ABC$$
$$H = ABD$$

Multiplying both sides of each of these four identities by E,F,G, and H, respectively, provides the four generating relations

$$I = BCDE$$

$$I = ACDF$$

$$I = ABCG$$

$$I = ABDH$$

where I is referred to as a defining relation. The complete set of defining relations included these four "words", plus all other combinations of words. Multiplying two at a time gives

$$I = ABEF = ADEG = ACEH = BDFG = BCFH = CDGH.$$

Multiplying three at a time gives

$$I = CEFG = DEFH = AFGH = BEHG.$$

Multiplying four at a time gives

$$I = ABCDEFGH.$$

The complete set of defining relations is, therefore,

$$I = BCDE = ACDF = ABCG = ABDH$$
$$= ABEF = ADEG = ACEH = BDFG = BCFH = CDGH$$
$$= CEFG = DEFH = AFGH = BEHG$$
$$= ABCDEFGH.$$

All main effects are confounded with four factor and higher interactions, and all three factor and higher interactions were assumed to be insignificant. With a resolution IV design, two factor interactions are confounded with other two factor interactions. The two factor confounding patterns follow.

$$AB = CG = DH = EF$$
$$AC = DF = BG = EH$$
$$AD = CF = BH = EG$$
$$AE = BF = DG = CH$$
$$AF = GH = CD = BE$$
$$AG = BC = DE = FH$$
$$AH = BD = CE = FG$$

CFC-12 test matrix

The CFC-12 test matrix was a 1/2 fraction of a 2^4 factorial design with resolution IV, designated 2_{IV}^{4-1}. For simplicity, the four variables (main effects) are redefined as follows.

Tcond - A

dc - B

Lc - C

Lhx - D

For the 2_{IV}^{4-1} design, the following identity is defined (Box, et. al., 1978).

$$D = ABCD$$

The generator, or defining relation for this design, is ABDC alone. For a resolution IV design, main effects are confounded with three factor and higher interactions, and two factor interaction are confounded with other two factor interactions. All three factor and higher interactions were assumed to be insignificant. The confounding patterns follow.

A = BCD	AB = CD
B = ACD	AC = BD
C = ABD	AD = BC
D = ABC	

APPENDIX E. SAS OUTPUT

Appendix E presents the results from the SAS analysis in the following tables for each of the HFC-134a test phases, and the HFC-152a testing. Appendix D includes the variable definitions used in the SAS analysis.

Table E.1: HFC-134a Phase 1 calculated variable effects on mass flow rate

Parameter	Estimate
INTERCEPT	12.56968750
A	2.52531250
B	0.04156250
A*B	0.08968750
C	0.09593750
A*C	0.21781250
B*C	-0.07468750
A*B*C	-0.09531250
D	3.23531250
A*D	0.70593750
B*D	0.05468750
A*B*D	-0.09468750
C*D	0.13906250
A*C*D	0.04343750
B*C*D	0.08343750
A*B*C*D	-0.02718750
E	-0.20281250
A*E	0.04406250
B*E	-0.00843750
A*B*E	0.03843750
C*E	-0.04281250
A*C*E	0.08031250
B*C*E	-0.28593750
A*B*C*E	-0.07281250
D*E	0.03031250
A*D*E	-0.07781250
B*D*E	0.02218750
A*B*D*E	-0.28343750
C*D*E	0.01531250
A*C*D*E	0.11593750
B*C*D*E	-0.90281250
A*B*C*D*E	-0.09968750

Table E.2: Analysis of HFC-134a Phase 1 mass flow rate prediction using Equation 4.2, including the eight replicate test points

Analysis of Variance

Source	DF	Sum of Squares	Mean Square	F Value	Prob>F
Model	10	745.51793	74.55179	562.585	0.0001
Error	29	3.84298	0.13252		
C Total	39	749.36091			

Root MSE	0.36403	R-square	0.9949
Dep Mean	12.45350	Adj R-sq	0.9931
C.V.	2.92310		

Parameter Estimates

Variable	DF	Parameter Estimate	Standard Error	T for H0: Parameter=0	Prob > |T|
INTERCEP	1	12.556161	0.05957809	210.751	0.0001
A	1	2.549500	0.05755791	44.295	0.0001
C	1	0.062000	0.05755791	1.077	0.2903
D	1	3.267000	0.05755791	56.760	0.0001
E	1	-0.216339	0.05957809	-3.631	0.0011
BCDE	1	-0.875521	0.05874479	-14.904	0.0001
ACDE	1	0.110729	0.05874479	1.885	0.0695
ABDE	1	-0.296964	0.05957809	-4.984	0.0001
AD	1	0.697000	0.05755791	12.110	0.0001
BCE	1	-0.291146	0.05874479	-4.956	0.0001
AC	1	0.245104	0.05874479	4.172	0.0003

$$\text{significance limit} = \pm t_{\alpha=.05,\ df_{error}=29} * (\text{std err})$$

$$= \pm 2.045 * 0.058 = \pm 0.119 \text{ lbm/hr}$$

std err pred = 0.185

Table E.3: HFC-134a Phase 1 calculated variable effects on EFFsc

Parameter	Estimate
INTERCEPT	39.17812500
A	-0.35937500
B	-1.68437500
A*B	0.44062500
C	2.72187500
A*C	0.14687500
B*C	0.12187500
A*B*C	0.05937500
D	7.44687500
A*D	0.00937500
B*D	-0.47812500
A*B*D	0.24687500
C*D	1.10312500
A*C*D	0.20312500
B*C*D	-0.05937500
A*B*C*D	0.00312500
E	-2.54687500
A*E	0.11562500
B*E	0.07812500
A*B*E	0.30312500
C*E	-0.20312500
A*C*E	-0.10312500
B*C*E	-0.04062500
A*B*C*E	0.02187500
D*E	-0.10312500
A*D*E	0.30937500
B*D*E	-0.16562500
A*B*D*E	-3.29062500
C*D*E	-0.12187500
A*C*D*E	-0.54687500
B*C*D*E	0.00312500
A*B*C*D*E	-0.10937500

Table E.4: Analysis of HFC-134a Phase 1 EFFsc prediction using Equation 4.4, including the eight replicate test points

Analysis of Variance

Source	DF	Sum of Squares	Mean Square	F Value	Prob>F
Model	11	3519.40753	319.94614	515.197	0.0001
Error	28	17.38847	0.62102		
C Total	39	3536.79600			

Root MSE	0.78805	R-square	0.9951
Dep Mean	38.06000	Adj R-sq	0.9932
C.V.	2.07054		

Parameter Estimates

Variable	DF	Parameter Estimate	Standard Error	T for HO: Parameter=0	Prob > |T|
INTERCEP	1	39.213393	0.12897433	304.040	0.0001
A	1	-0.367708	0.12717041	-2.891	0.0073
B	1	-1.669792	0.12717041	-13.130	0.0001
C	1	2.660000	0.12460104	21.348	0.0001
D	1	7.503125	0.12717041	59.001	0.0001
E	1	-2.511607	0.12897433	-19.474	0.0001
ACDE	1	-0.490000	0.12460104	-3.933	0.0005
ABDE	1	-3.255357	0.12897433	-25.240	0.0001
BD	1	-0.486458	0.12717041	-3.825	0.0007
ADE	1	0.323958	0.12717041	2.547	0.0166
CD	1	1.095000	0.12460104	8.788	0.0001
ABE	1	0.359375	0.12717041	2.826	0.0086

$$\text{significance limit} = \pm t_{\alpha=.05,\ df_{error}=28} * (\text{std err})$$

$$= \pm 2.048 * 0.126 = \pm 0.26 \text{ F}$$

$$\text{std err pred} = 0.185$$

Table E.5: HFC-134a Phase 2 calculated variable effects on mass flow rate

Parameter	Estimate
INTERCEPT	10.77937500
A	1.33062500
B	-0.28812500
A*B	0.01812500
C	2.23562500
A*C	0.28437500
B*C	-0.22437500
A*B*C	0.01937500
D	-0.90562500
A*D	-0.09937500
B*D	0.05937500
A*B*D	0.16062500
C*D	-0.23437500
A*C*D	0.25937500
B*C*D	0.02312500
A*B*C*D	1.37187500

Table E.6: Analysis of HFC-134a, Phase 2 mass flow rate prediction using Equation 4.11

Analysis of Variance

Source	DF	Sum of Squares	Mean Square	F Value	Prob>F
Model	10	157.32826	15.73283	335.840	0.0001
Error	5	0.23423	0.04685		
C Total	15	157.56249			

MSE

Root MSE	0.21644	R-square	0.9985
Dep Mean	10.77938	Adj R-sq	0.9955
C.V.	2.00791		

Parameter Estimates

Variable	DF	Parameter Estimate	Standard Error	T for H0: Parameter=0	Prob > |T|
INTERCEP	1	10.779375	0.05410999	199.212	0.0001
C	1	2.235625	0.05410999	41.316	0.0001
ABCD	1	1.371875	0.05410999	25.353	0.0001
A	1	1.330625	0.05410999	24.591	0.0001
D	1	-0.905625	0.05410999	-16.737	0.0001
B	1	-0.288125	0.05410999	-5.325	0.0031
AC	1	0.284375	0.05410999	5.255	0.0033
BC	1	-0.224375	0.05410999	-4.147	0.0089
ABD	1	0.160625	0.05410999	2.968	0.0312
CD	1	-0.234375	0.05410999	-4.331	0.0075
ACD	1	0.259375	0.05410999	4.793	0.0049

Note: Phase 2 did not include replicate test points. The statistical significance of the calculated effects were determined by using the Phase 1 significance limit of 0.12 lbm/hr.

Table E.7: HFC-134a Phase 3 calculated variable effects on mass flow rate

Parameter	Estimate
INTERCEPT	12.77687500
A	1.37812500
B	2.56437500
A*B	0.23562500
C	-1.07687500
A*C	-0.05812500
B*C	-0.03687500
A*B*C	0.06187500
D	0.11812500
A*D	-0.07562500
B*D	0.15312500
A*B*D	0.02937500
C*D	0.03937500
A*C*D	0.00312500
B*C*D	0.03687500
A*B*C*D	-0.06062500

Table E.8: Analysis of HFC-134a Phase 3 mass flow rate to establish the significance of the oil effect

Analysis of Variance

Source	DF	Sum of Squares	Mean Square	F Value	Prob>F
Model	4	155.04682	38.76171	450.566	0.0001
Error	11	0.94632	0.08603		
C Total	15	155.99314			

Root MSE	0.29331	R-square	0.9939
Dep Mean	12.77688	Adj R-sq	0.9917
C.V.	2.29561		

Parameter Estimates

Variable	DF	Parameter Estimate	Standard Error	T for H0: Parameter=0	Prob > |T|
INTERCEP	1	12.776875	0.07332674	174.246	0.0001
A	1	1.378125	0.07332674	18.794	0.0001
B	1	2.564375	0.07332674	34.972	0.0001
C	1	-1.076875	0.07332674	-14.686	0.0001
AB	1	0.235625	0.07332674	3.213	0.0083

$$\text{significance limit} = \pm t_{\alpha=.05}{}^{*}(\text{std err})$$

$$df_{error}=11$$

$$= \pm 2.201 * 0.073 = \pm 0.161 \text{ lbm/hr}$$

Table E.9: HFC-134a Phase 3 calculated variable effects on EFFsc

Parameter	Estimate
INTERCEPT	48.47875000
A	3.54125000
B	0.07875000
A*B	0.11625000
C	0.04125000
A*C	-0.07125000
B*C	-0.20875000
A*B*C	0.20375000
D	0.52125000
A*D	0.13375000
B*D	0.17125000
A*B*D	-0.04125000
C*D	0.05875000
A*C*D	0.04625000
B*C*D	-0.19125000
A*B*C*D	-1.17875000

Table E.10: Analysis of HFC-134a Phase 3 effective subcooling to establish the significance of the oil effect

Analysis of Variance

Source	DF	Sum of Squares	Mean Square	F Value	Prob>F
Model	5	227.35213	45.47043	145.914	0.0001
Error	10	3.11625	0.31163		
C Total	15	230.46838			

Root MSE	0.55823	R-square	0.9865
Dep Mean	48.47875	Adj R-sq	0.9797
C.V.	1.15150		

Parameter Estimates

Variable	DF	Parameter Estimate	Standard Error	T for HO: Parameter=0	Prob > |T|
INTERCEP	1	48.478750	0.13955846	347.372	0.0001
A	1	3.541250	0.13955846	25.375	0.0001
B	1	0.078750	0.13955846	0.564	0.5850
C	1	0.041250	0.13955846	0.296	0.7736
D	1	0.521250	0.13955846	3.735	0.0039
ABCD	1	-1.178750	0.13955846	-8.446	0.0001

$$\text{significance limit} = \pm t_{\alpha=.05,\ df_{error}=10} * (\text{std err})$$

$$= \pm 2.228 * 0.14 = \pm 0.31 \text{ F}$$

Table E.11: HFC-152a calculated variable effects on mass flow rate

Parameter	Estimate
INTERCEPT	10.38687500
A	1.07937500
B	2.07187500
A*B	0.23437500
C	-0.91812500
A*C	-0.13562500
B*C	-0.17062500
A*B*C	-0.12312500
D	0.14562500
A*D	-0.04187500
B*D	0.08312500
A*B*D	-0.02937500
C*D	0.13812500
A*C*D	0.05062500
B*C*D	0.26812500
A*B*C*D	-0.07937500

Table E.12: Analysis of HFC-152a mass flow rate prediction using Equation 5.2, including the replicate test points

Analysis of Variance

Source	DF	Sum of Squares	Mean Square	F Value	Prob>F
Model	7	117.25878	16.75125	162.782	0.0001
Error	12	1.23487	0.10291		
C Total	19	118.49366			

Root MSE	0.32079	R-square	0.9896
Dep Mean	10.32850	Adj R-sq	0.9835
C.V.	3.10587		

Parameter Estimates

Variable	DF	Parameter Estimate	Standard Error	T for H0: Parameter=0	Prob > |T|
INTERCEP	1	10.366667	0.07320984	141.602	0.0001
A	1	1.061786	0.07424833	14.300	0.0001
B	1	2.075417	0.07320984	28.349	0.0001
C	1	-0.914583	0.07320984	-12.493	0.0001
D	1	0.128036	0.07424833	1.724	0.1103
AB	1	0.251500	0.07173070	3.506	0.0043
BC	1	-0.190833	0.07320984	-2.607	0.0229
BCD	1	0.250536	0.07424833	3.374	0.0055

$$\text{significance limit} = \pm t_{\alpha=.05}\text{*(std err)}$$

$$df_{error}=12$$

$$= \pm 2.179*0.073 = \pm 0.159 \text{ lbm/hr}$$

Table E.13: HFC-152a calculated variable effects on EFFsc

Parameter	Estimate
INTERCEPT	37.63750000
A	2.70000000
B	-0.07500000
A*B	-0.16250000
C	-0.10000000
A*C	-0.36250000
B*C	-0.06250000
A*B*C	-1.47500000
D	-1.52500000
A*D	0.23750000
B*D	-0.41250000
A*B*D	-0.45000000
C*D	0.76250000
A*C*D	-2.90000000
B*C*D	4.12500000
A*B*C*D	0.86250000

Table E.14: Analysis of HFC-152a EFFsc prediction using Equation 5.4, including the replicate test points

Analysis of Variance

Source	DF	Sum of Squares	Mean Square	F Value	Prob>F
Model	7	724.32283	103.47469	89.675	0.0001
Error	12	13.84667	1.15389		
C Total	19	738.16950			

Root MSE	1.07419	R-square	0.9812
Dep Mean	37.84500	Adj R-sq	0.9703
C.V.	2.83840		

Parameter Estimates

Variable	DF	Parameter Estimate	Standard Error	T for H0: Parameter=0	Prob > |T|
INTERCEP	1	37.666667	0.24514971	153.648	0.0001
A	1	2.700000	0.25120370	10.748	0.0001
D	1	-1.525000	0.25120370	-6.071	0.0001
ABC	1	-1.475000	0.25120370	-5.872	0.0001
ACD	1	-3.025000	0.24019668	-12.594	0.0001
BCD	1	4.125000	0.25120370	16.421	0.0001
CD	1	0.575000	0.24019668	2.394	0.0339
ABCD	1	0.891667	0.24514971	3.637	0.0034

significance limit = $\pm t_{\alpha=.05}$*(std err)

$df_{error}=12$

$= \pm 2.179*0.25 = \pm 0.545$ F